Role of Solid Wettability in Two Processes: Bubble Generation from Porous Media and Froth Treatment in Processing Oil Sands

By

Fu Chen

A thesis submitted to the Faculty of Graduate Studies and Research
of McGill University in Partial Fulfillment of the Requirement for
the degree of Doctor of Philosophy

Department of Mining and Metallurgical Engineering
McGill University
Montreal, Canada

September 2001

0-612-77431-7

To My Wife, Mrs. Yi Jin

and My daughters: Jinxi Chen and Mary Jinping Chen

Preface

This thesis contains three parts. The first part includes the thesis preface, abstract, acknowledgements, table of contents, nomenclature, glossaries, list of tables and figures. The second part, the main body of the thesis, has 8 chapters that follow the general structure: basic theory, literature review, experimental setup, results and discussion, and conclusions and suggested future work. The appendices, documenting the Kumar and Kuloor and proposed models, and the experimental and processed data, form the last part of the thesis.

For each chapter, there is an introduction (chapters 1, 2, 3 and 4) or an abstract (Chapters 5 and 6) that summarize the chapter contents. There is some repetition in the related chapters in an attempt to make each complete to aid comprehension. To further aid the reader, a table of contents for each chapter is provided.

This thesis is the study of two processes related through their dependence on solid wettability; i.e., the theory of solid wettability is common to both. The first subject is a study of wettability on the size of bubbles generated at the multiple orifices of a rigid porous sparger of the type used in a flotation column. The second is a study of the solid wettability effect on the froth treatment process in oil recovery from tar sands. The two applications reflect the situation that developed during the Ph.D. program. The initial project was the froth treatment one funded by Syncrude and directed by Prof. Z. Xu. Prof. Xu left the University in 1996 and the project was terminated by the sponsor in 1998, when funding ended. Since the work completed to that point was judged insufficient for a thesis, and no expertise resided in the department to continue, a second "wettability" related project was suggested by Prof. J. Finch who became the supervisor. The thesis is the outcome of this history.

Abstract

Solid wettability plays an important role in many industrial processes. Two examples of processes dependent on solid wettability are: Bubble generation from porous media (project one) and the bitumen froth treatment process in the recovery of oil from oil sands (project two).

Project one:

Bubble size has a profound effect on flotation efficiency controlling particle collection and froth stability. Models of bubble generation at a rigid sparger usually include a wettability effect (i.e., contact angle). The role of sparger wettability on bubble formation was examined using three rigid spargers exhibiting water contact angles of 0, 64 and >90°. The wettability was varied by heating the sparger, and the contact angle was determined by the Washburn and modified Washburn methods. By measuring permeability, it was determined that heating had no effect on sparger pore structure. The results showed no detectable wettability effect on bubble formation over the practical operating range of column flotation. The lack of wettability effect may be attributed to the highly irregular morphology of the sparger surface. The bubble size, it was shown, can be predicted by using the concept of sparger equivalent pore diameter and active pore number, which are estimated by a back-calculation routine.

Project two:

Production of oil from oil sand deposits in northern Alberta involves open pit mining, mixing the ore with water, extraction of bitumen from the slurry by a flotation-related process (Hot Water Extraction Process), removal of water and solids from the froth formed (froth treatment process), and upgrading the heavy bitumen to liquid hydrocarbons. The froth treatment process to remove fine solids and water from the bitumen froth depends on the wettability of the solids. Fine solids were extracted from samples of bitumen froth using heptane. A mixture of heptane and toluene (diluent) was used to study fine solid wettability. The contact angle (sessile drop method) and partition of the fine solids among the aqueous, diluent and interphase regions were determined. The effect of diluent composition, sample drying, and surface washing was examined. The partition of the particles correlated well with their wettability, and the results helped interpret observations from plant practice.

Résumé

La mouillabilité joue un rôle important dans plusieurs procédés industriels. Deux exemples de tels procédés sont: la production de bulles à partir de média poreux (Premier projet) et le procédé de traitement de l'écume provenant de la récupération de sols bitumineux (Second projet).

Premier projet:

La grosseur des bulles a un effet considérable sur l'efficacité de la flottation précisément au niveau de la collection des particules et de la stabilité de l'écume. La modélisation de bulles produites à partir d'un barboteur poreux rigide prend souvent compte de la mouillabilité du matériau du barboteur, par exemple, l'angle de contact de l'eau. Le rôle de la mouillabilité du barboteur dans la formation des bulles a donc été examiné en utilisant trois barboteurs rigides formants des angles de contact avec l'eau de 0, 64 et >90°. La mouillabilité a été variée en chauffant le barboteur, et l'angle de contact a été déterminé par les méthodes de Washburn et de Washburn modifiée. En vérifiant la perméabilité, l'effet possible du chauffage sur la structure des pores du barboteur fut déterminé négligeable. Les résultats démontrent qu'il n'y a aucun effet détectable de la mouillabilité du matériau du barboteur sur la formation des bulles pour toute la zone pratique d'opération de flottation en colonne. L'absence d'effet de mouillabilité peut être attribuable à la structure particulière de la surface du barboteur rigide, i.e., dimensions irrégulières et surface non-plane. La grosseur des bulles peut être estimée par les modèles à partir des concepts de diamètre de pore équivalent et de nombre de pores actifs, estimés par calcul à rebours.

Second Projet :

Le traitement des sols bitumineux du Nord de l'Alberta implique le minage à ciel ouvert, l'ajout d'eau au minerai, l'extraction du bitume de la pulpe par un procédé lié à la flottation (procédé d'extraction par eau chaude), la séparation de l'eau et des solides de l'écume ainsi formée (procédé de traitement de l'écume) et la transformation du bitume lourd en hydrocarbures liquides. Le succès du traitement de l'écume, visant la séparation de l'écume de bitume en eau et fines, dépend du contrôle de la mouillabilité des fines. Pour les besoins de cette étude, des fines ont été préparées à partir d'échantillons d'écume de bitume en utilisant la précipitation à l'heptane. Un mélange d'heptane et de toluène (diluant) a été utilisé afin d'étudier la mouillabilité des fines. La partition des fines entre les régions aqueuse, organique et les interphases, a été étudiée et l'angle de contact a été évalué par la méthode par goutte sessile. Les effets de la composition du diluant, du séchage de l'échantillon et du nettoyage de la surface ont été examinés. La partition des particules est en étroite corrélation avec leur mouillabilité, et les résultats pourraient être utilisés afin d'interpréter les observations dans la pratique de traitement de l'écume.

Acknowledgements

For their contributions, I wish to thank the following:

Dr. J. A. Finch and Dr. Z. H. Xu (University of Alberta), for the guidance provided throughout this work.

Professors Laplante and Harris, Dr. C. O. Gomez (McGill) and Dr. J. Czarnecki (Syncrude Canada Ltd., Edmonton, Alberta), for their valuable input and, in the case of Dr. Gomez, countless hours of help during this work

Dr. Z. A. Zhou, Dr. Liming Huang, Dr. S. Gelinas and Dr. Choung for their help, useful ideas and suggestions.

Syncrude Canada Ltd. and NSERC for the NSERC-Industrial Postgraduate Student Scholarship (1996-1998).

Colleagues from the mineral processing chemistry and sensor research groups, past and present, and Jessica (exchange student, University of Newcastle, Australia).

Table of Contents

CHAPTER 1: GENERAL INTRODUCTION

CHAPTER 2: THEORY OF WETTING

CHAPTER 3: TWO PROCESSES RELATED TO SOLID WETTABILITY

CHAPTER 4: CHARACTERIZATION TECHNIQUES

CHAPTER 5: ROLE OF SOLID WETTABILITY ON BUBBLE FORMATION AT POROUS RIGID SPARGER

CHAPTER 6: ROLE OF FINE SOLID WETTABILITY IN THE FROTH TREATMENT STAGE OF OIL SAND PROCESSING

CHAPTER 7: SUMMARY

CHAPTER 8: CONTRIBUTIONS TO THE ORIGINAL KNOWLEDGE AND FUTURE WORK

APPENDIX A

APPENDIX B

APPENDIX C

Nomenclature

a	Thickness of the plate or sample in Wilhelmy method
A, B, C, E	Constant in Washburn method (Chapters 5 and 6) or Kumar and Kuloor model (Chapter 6).
D	Diameter of orifice
D_b	Bubble diameter
D_e	Equivalent pore diameter
D_{10}	Number mean bubble diameter
D_{32}	Sauter mean bubble diameter
F	Force
F_s	Surface tension force
F_b	Buoyancy
F_i	Inertial force
F_{vis}	Viscous drag
g	Gravity acceleration
k	Molar absorption coefficient
k_m	Force constant
J_g	Superficial gas velocity
J_a	Air flowrate per unit area of sparger
l	Width of the plate or sample in Wilhelmy method
L_s	Length of sparger

M	Virtual mass of the bubble
P_k	Permeability
Q	Air flowrate for single orifice
q	Air flowrate for sparger
q_m	Liquid flowrate in the sparger permeability test
r_i	Inner radius of sparger
r_o	Outer radius of sparger
r_{fb}	Bubble radius of the first stage in bubble generation
R_∞	Absolute reflectance of the infinite thick layer
s	Scattering coefficient
S_b	Bubble surface area flux, the surface area of bubbles per unit time per unit cross-sectional area of flotation machine
t_F	Time for bubble develop during second stage
V	Bubble volume
V_F	Final bubble volume
V_{fb}	Bubble volume at the end of the first stage
w	Liquid weight that penetrating into the sample in Washburn method

Greek letters

Δv	Volume increase of liquid bubble phase after aeration.
ρ_g	Gas (here air) density
ρ_l	Liquid density

γ	Surface tension or interfacial tension
γ^{LW}, γ^{AB}	Lifshitz-van der Waals contribution, and acid-base contribution, respectively
γ^{+}, γ^{-}	Acid and basic component of surface tension
γ_S, γ_L	Solid and liquid surface tension
γ^{d}	Dispersion component of surface tension
ν	Rate of change of the bubble radius
μ	Dynamic viscosity
μ_m	Mass of the atoms
θ	Contact angle
φ	Adjustable parameter in surface energy equation
ϕ	Operating angle, it is the angle between the horizontal plane and the orifice plane
ω	Frequency of the vibration

Glossaries

Aliphatic	Of, relating to, or designating a group of organic chemical compounds in which the carbon atoms are linked in open chains[1].
Aromatic	An organic compound with an aroma, fragrant or sweet-smelling. The typical properties of these compounds are: one or more carbon rings composed of conjugated double bonds that cannot be easily broken; and easy substitution reaction with H in the ring.
Asphaltenes	An organic mixture of bitumen fraction that is insoluble in heptane. The exact molecular structure is not well defined.
Bitumen	Here, a black fluid that consists of organic compounds extracted from oil sands and is dissolvable in toluene or naphtha.
Biwettable	Here means that the fine solids coated with organics can be wetted by water and organic solvent, and have tendency to stay in the water/organic interface.
Bubble Surface Area Flux (S_b)	Also called bubble surface area generation rate, it is the surface area of air bubbles per unit time per cross-sectional area of a vessel (e.g., $cm^2/cm^2 \bullet s$). It cannot be measured directly, but is calculated from the Sauter mean bubble diameter (d_{32}), air flowrate q and the cross sectional area of vessel A_c

---

[1] The American Heritage Talking Dictionary, Version 4.0, SoftKey International Co., USA, 1995.

$$S_b = \frac{6q}{d_{32} A_c}$$

Chert A variety of silica that contains microcrystalline quartz, or a siliceous rock of chalcedonic or opaline silica occurring in limestone[1].

Clark's Hot Water Extraction Process (HWEP) Extraction process used by Syncrude to recover bitumen from oil sand. It was developed in the 1920's by K.A. Clark of the Alberta Research Council (Clark and Pasternak, 1932). The process consists of three steps. First, the oil sand is agitated in hot water with a small amount of caustic added to maintain the pH in the range 8.0 to 8.5. In the second step, the sand grains that have settled to the bottom of the reaction tank are removed and the oil froth that forms is recovered by skimming. Fine particulate matter, dominated by clay minerals, remains in what is called the "middling" stream. This stream is subjected to the third processing step, froth flotation, which provides incremental recovery of suspended bitumen[2].

Diluent Here, an organic liquid mixture that can dissolve bitumen, used in the bitumen recovery process to reduce density and viscosity, and hence improve the separation of bitumen from water and solids during the froth treatment process.

Emulsion Generally, a suspension of small droplets of one liquid dispersed in a second liquid (the continuous phase)[1].

---

[2] Takamura, k., Microscopic Structure of Athabasca Oil Sand, The Canadian Journal of Chemical Engineering, 60, 538-545(1982).

Feldspar	Any of a group of abundant rock-forming minerals occurring principally in igneous, plutonic, and some metamorphic rocks, and consisting of silicates of aluminum with potassium, sodium, calcium, and, rarely, barium. About 60 percent of the earth's outer crust is composed of feldspar[1].
Froth	Here, a mixture of bitumen (60% w/w), water (30% w/w) and solids (10% w/w).
Illite	Mineral with chemical formula: $(K,H_3O)(Al,Mg,Fe)_2(Si,Al)_4O_{10}\,[(OH)_2H_2O]$.
Kaolinite	Mineral with chemical formula $Al_2\,Si_2O_5(OH)_4$[1].
Microemulsion	A mixture of two mutually immiscible liquid phases, one dispersed in the other with/without the assistance of other substances (such as one or more surfactants, fine divided solids, etc.). It has a smaller droplet size (diameter<100nm) than a conventional emulsion (diameter>100nm) and is consequently, more stable.
Muscovite	A potassium aluminum silicate mineral, $KAl_2(AlSi_3O_{10})(OH)_2$, the most common form of mica, which ranges from colorless or pale yellow to gray and brown, has a pearly luster, and is used as an insulator[1].
Naphtha	A general term applied to refined, partly refined, or unrefined petroleum products. The wide range of naphtha available from crude oil refining with varying degrees of volatility offer products suitable for many uses[3]. Here the naphtha consists of mainly toluene, and is used as solvent. It also reduces the

---

[3] Mushrush, G.W. and Speight, J. G., Petroleum Products: Instability and Incompatibility, Applied Energy Technology Series, Washington, Talor & Francis, p.148, 1995.

	density of the organic phase and the viscosity of the froth in the froth treatment process thus improving the separation of the organic phase and aqueous phase.
Oil sands	Small mineral particles that coexist with bitumen in natural deposits of oil storage underground.
Paraffins	The paraffin series of hydrocarbons is characterized by the rule that the carbon atoms are connected by a single bond and the other bonds are saturated with hydrogen atoms. The general formula for paraffins is C_nH_{2n+2}. The samples used here n-pentane (C_5H_{12}) and isopentane (C_5H_{12}).
Rag Layer	Mixture of water, fine solids and a small amount of organics that forms at the interface between organic and aqueous phases during froth treatment using heptane.
Surfactant	Generally, these are chemicals which have both hydrophobic and hydrophilic groups hence they accumulate at air/water and oil/water interfaces.
Surface energy	Generally refers to surface free energy. In the case of liquid, it is the reversible work to bring molecules from the bulk to the surface to create a unit area of surface.
Surface tension	The most fundamental characteristic of liquid surfaces is that they tend to contract to the smallest surface area in order to achieve the lowest free energy. Since the molecules in the surface interact not only with the same kind of molecules inside the bulk, but also with the molecules of the contacting phase (liquid or gas), the molecules on the surface are subjected to

an asymmetric force. Consequently, they have more energy than those molecules inside the bulk. The excess energy per unit area of the liquid surface is the liquid surface tension (generally measured against air).

Interfacial tension: This refers to the surface tension between two liquids, or between liquid and solid.

Upgrade A processing method that produces commercial products from the raw material (petroleum from bitumen in this case).

van der Waals force Excluding Coulombic interactions (between ions) and metallic bonding, physical interaction between molecules including the Keesom dipole-dipole, Debye dipole-induced dipole and London dispersion forces, are collectively termed van der Waals forces. These intermolecular interactions give rise to an attractive potential varying with the inverse sixth power of the intermolecular distance[4].

Evidence shows that the London force is the main contribution. Polar forces are operative only for strongly polar and hydrogen-bonding substances such as a acetone, water, and ammonia, whereas the contribution of induction forces is small.

---

[4] Erbil, H. Y., *Interfacial interactions of liquids* in "Handbook of surface and colloid chemisrty", Ed: Birdi, K.S., Boca Raton, CRC Press, 1997.

Dipole-dipole interaction: Because of the asymmetric electric density distribution of the molecule, a dipole is formed. When two molecules approach, there is a force due to interaction of their dipoles.

Dipole induced dipole interaction: Some molecules have a large electron cloud that is easy to deform. As another molecule with a dipole approaches, the dipole will induce a dipole in the first molecule, and interaction occurs.

Dispersion force: Also called the London force, it results from the natural oscillations of the electron cloud of the molecule inducing synchronous oscillations in a neighboring molecule. The resulting temporal dipoles of the neighboring molecules produce mutual attraction.

Water-in-oil droplets Small water droplets in an oil phase. The "oil" here is a general term that denotes an organic phase immiscible with water.

Organic substance Here, the organics on the fine solid surface including aliphatic, aromatic and other organics.

Toluene insoluble organic matter Here, the organics on the fine solid surface that cannot be dissolved by toluene.

List of Tables

List of Figures

Chapter 1

General Introduction

Contents

1.1 Thesis outline

The first part of the thesis presents the thesis preface, abstract, acknowledgements, table of contents, nomenclature, glossaries, list of tables and figures.

The thesis body consists of 8 chapters. Chapter 1 gives an overview and presents the thesis structure, including a brief description of each chapter. Chapter 2 introduces the theory of wetting and solid wettability, and Chapter 3 gives an introduction and literature survey of the two engineering applications of wettability studied here: bubble generation at a rigid sparger, and removal of residual water in the froth treatment process for oil recovery from oil sands. Chapter 4 describes the characterization techniques. Chapter 5 presents the work on bubble generation, and Chapter 6 the work on the froth treatment process. Chapter 7 summarizes the conclusions, and to close, Chapter 8 outlines the contributions to knowledge and suggestions for future work.

Appendices list details of the Kumar and Kuloor and proposed models, and the experimental and processed data.

1.2 Objective

To explore the effect of solid wettability on two engineering processes: bubble generation using a stainless steel sparger and residual water removal in the froth treatment process for oil recovery from oil sands.

Chapter 2

Theory of Wetting

Contents

2.1 Introduction

Surface chemical properties are exploited in many industrial processes. These properties, for example, determine the interaction of solids with liquids, or wetting. To better understand how wetting may influence a process, some basic concepts are reviewed first.

2.2 Wettability

2.2.1 Concept

Considering a solid-liquid system, wettability is the tendency for a liquid to spread over or adhere to a solid surface[1]. The contact angle is a “scale” to measure the wettability (Figure 2.1). If the liquid tends to spread, i.e. the liquid easily wets the solid, the contact angle of the liquid on the solid surface is small. If the liquid tends to contract, i.e. the liquid does not readily wet the solid, the contact angle is large. When water is the liquid, then the solid surface in the first case is said to be hydrophilic and in the second case hydrophobic.

The contact angle is the angle of the tangent at the three phase contact line. The magnitude depends on the properties of the system. As early as the 18th century, Young[2] proposed that the contact angle of a liquid drop on an ideal surface (e.g. smooth, homogeneous and non-deformable) was related to the tensions existing along the three interfaces (see Eq. 2.1)

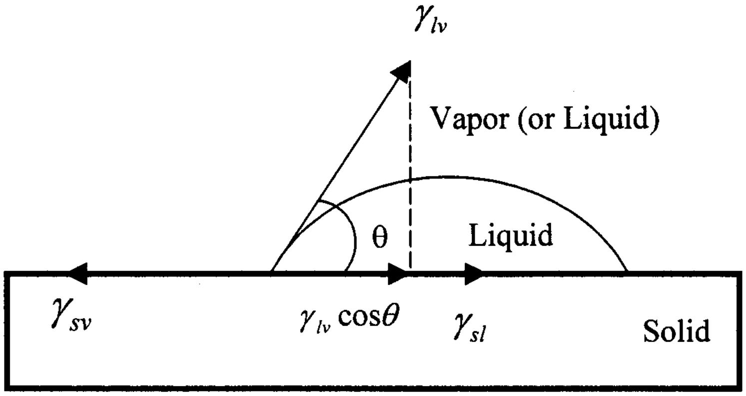

Figure 2.1: - Schematic of contact angle at gas/liquid/solid interfaces; γ_{sv} is the interfacial tension of solid/vapor, γ_{sl} the interfacial tension of solid/liquid, γ_{lv} the interfacial tension of liquid/vapor, and θ the contact angle.

$$\gamma_{lv}\cos\theta = \gamma_{sv} - \gamma_{sl} \tag{2.1}$$

where γ_{lv}, and γ_{sv} and γ_{sl} are the interfacial tension of liquid/vapor, solid/vapor and solid/liquid, respectively, and θ is the contact angle. A common situation is a water drop on a solid. In this case, the Young equation is

$$\gamma_{wv}\cos\theta = \gamma_{sv} - \gamma_{sw} \tag{2.2}$$

where γ_{wv} and γ_{sw} are the interfacial tension of water/vapor and solid/water, respectively. If the vapor is replaced by a second immiscible liquid, then Eq. (2.3) is appropriate

$$\gamma_{wl}\cos\theta = \gamma_{sl} - \gamma_{sw} \tag{2.3}$$

where γ_{wl}, γ_{sl} and γ_{sw} are the interfacial tension of water/liquid, solid/liquid and solid/water, respectively.

2.2.2 Basic theory

2.2.2.1 Interfacial free energy (interfacial tension)

The interaction of a solid surface with a liquid determines the wettability of the solid by the liquid. If the solid surface has a strong affinity for the liquid, the liquid will tend to spread on the solid surface, i.e. the liquid easily wets the solid. If the solid surface has a weak affinity for the liquid, the liquid will tend to contract. These phenomena can be interpreted knowing the interfacial free energies of the system.

The most fundamental characteristic of a liquid surface is that it tends to contract to the smallest surface area in order to achieve the lowest free energy. This contraction results in an interfacial tension[*3,4], γ, acting along a unit length of surface with units mN/m (or dyne/cm). The origin of the force can be understood on the basis of molecular theory. If the surface area of a liquid is expanded, some of the molecules inside the liquid bulk must migrate to the surface. Because a molecule inside a mass of liquid is under the influence of the surrounding like molecules while a molecule on the surface is partly surrounded by other molecules, work is required to bring molecules from the bulk to the surface. Since molecules on the surface are not surrounded only by the like molecules, they experience an asymmetric force, and have excess free energy compared to those in the bulk. Those molecules brought to the surface tend to resume their original state, and the result is a force along the surface. This force appears as tension in the surface on the direction of reducing the surface area, and when expressed as tension per unit length of a line on the surface it is called the surface tension[5].

---

[*] The term "interfacial" tension (energy) is generally used in this thesis, but it is understood that the term "surface" tension (energy) is more common in some cases, e.g. liquid/air.

Surface energy is the reversible work required to bring molecules from the bulk to the surface to create a unit area of surface (unit mJ/m^2 or erg/cm^2)[6]. It is numerically equal to the surface tension of the liquid[7], and, consequently surface tension and surface energy are often used interchangeably.

For solids, it is preferable to refer to their surface energy rather than surface tension to avoid possible confusion with surface stress. Surface tension and surface energy are, nevertheless, often used interchangeably for solids also.

Surface tension is the usual term for the case of liquid/gas or solid/gas interfaces, whereas interfacial tension generally refers to two immiscible liquids, and to the liquid/solid case. An interface is where the molecules of the two phases meet and hence the asymmetrical force is present. This force creates excess energy in the molecules at the interface - the interfacial tension (or interfacial energy). The forces across the interface can be illustrated by the case of two immiscible liquids such as oil and water (Figure 2.2)[8].

The relative magnitude of the interfacial tension (IFT) can be estimated. The IFT between two liquid is less than the surface tension of the liquid with the higher surface tension because the molecules of each liquid mutually attract each other across the interface, thus reducing the inward pull exerted by that liquid on its own molecules at the surface. As an example consider heptane-water where the surface tensions are 20.1, and 72.8 mN/m, respectively, and the interfacial tension is 50.1mN/m[9,10].

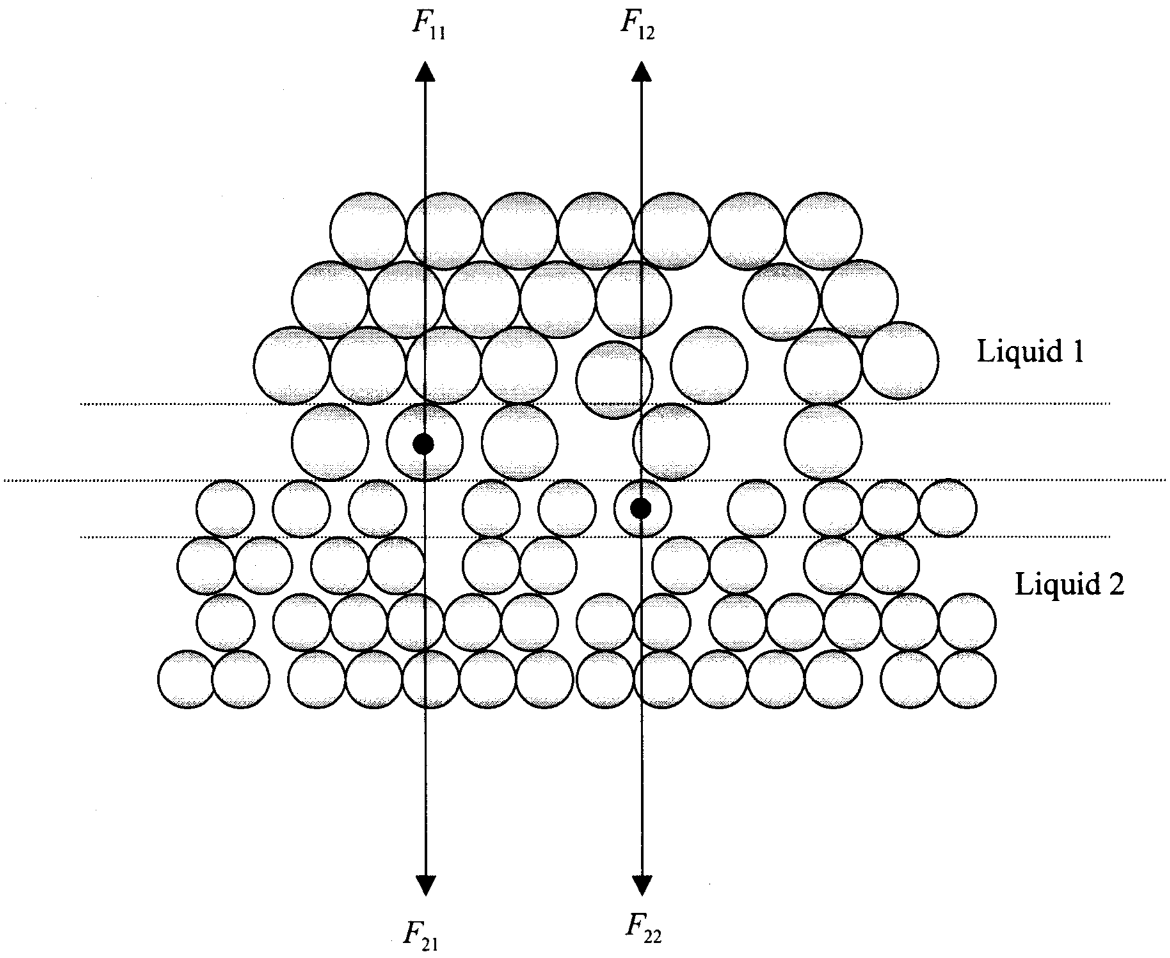

Figure 2.2: - Forces across the interface: F_{11} is the force exerted on the molecule of liquid 1 at the interface by the liquid 1 molecules; F_{12} is the force exerted on the molecule of liquid 2 by molecules of liquid 1; Similar notation are F_{21} and F_{22}.

2.2.2.2 Interaction of solid surface and liquid

Zisman and co-workers in the 1960's provided much of the impetus for all subsequent wettability studies[11]. They studied the contact angle (θ) of alkanes on low energy surfaces (e.g. plastics) and concluded that $\cos\theta$ plotted against the surface tension of the wetting liquid (the Zisman plot) was linear. The corresponding surface tension value at the intercept of this line with $\cos\theta = 1$ is called the "critical surface tension of wetting". A liquid with a surface tension lower than the critical surface tension of the solid will wet the solid.

Later it was argued that if the surface tension (surface free energy) is a result of molecular interactions only by dispersion force, then the combining rule for the surface and interfacial tensions should be similar to that for van der Waals interactions between dissimilar molecules in the gas phase. Following this argument, an equation was developed[12] based on the Bertholet relation[13] for interaction of molecules

$$\gamma_{sl} = \gamma_s + \gamma_{lv} - 2\sqrt{\gamma_s \gamma_{lv}} \qquad (2.4)$$

where γ_{sl} is solid/liquid interfacial tension, γ_s solid surface tension, γ_{lv} liquid surface tension. This equation can be applied only when the liquid phase is a saturated hydrocarbon since this ensures that only dispersion forces are operative.

A revised equation with an adjustable parameter φ was proposed[12] to allow for deviation from Eq. (2.4):

$$\gamma_{sl} = \gamma_s + \gamma_{lv} - 2\varphi\sqrt{\gamma_s \gamma_{lv}} \tag{2.5}$$

where φ differs from 1 when interactions occur within the liquid or solid phase, but not across the interface. These interactions could be caused by hydrogen bonds, metallic bonds and acid-base interactions. Neumann's surface equation of state theory represents a different approach. It relates the solid-liquid interfacial tension to the total solid and liquid surface tensions, and the interfacial tension is completely defined by the total surface tensions of the phases in contact. Based on this theory, all liquids having the same surface tension would have the same contact angle on a given solid[14].

A major advance in interpretation was made by Fowkes[15]. He recognized that the critical factors controlling wettability were interactions between the phases across the interface (Figure 2.2). He assumed these forces to be independent of each other. Owens and Went[16] and Kaelble[17] extended Fowkes' concepts and included a polar component. Further refinement[18] showed that all the interactions across an interface can be reduced to just two types: dispersion and acid-base (including hydrogen bonding). In this theory, the interactions across the solid/liquid interface are considered physical and chemical in nature[19]. The physical interactions can be described by Lifshitz-van der Waals theory, and the chemical interactions by acid-base theory, i.e.,

$$\gamma = \gamma^{LW} + \gamma^{AB} \tag{2.6}$$

where γ is the surface energy, γ^{LW} the Lifshitz-van der Waals contribution, and γ^{AB} the acid-base contribution.

The acid-base theory assumes that all interactions which are not included in the Lifshitz-van der Waals contributions are accounted for by acid-base interactions. The combination of the Lifshitz-van der Waals and acid-base interactions results in the van Oss-Chaudhury-Good equation,

$$(1+\cos\theta)\gamma_L = 2\,(\sqrt{\gamma_S^{LW}\gamma_S^{LW}} + \sqrt{\gamma_S^{+}\gamma_L^{-}} + \sqrt{\gamma_S^{-}\gamma_L^{+}}) \tag{2.7}$$

where the γ^+ and γ^- are the acid and base components of the surface energy, respectively, and subscripts S and L refer to solid and liquid, respectively. These physical and chemical interactions exist in the interface between solid and liquid, which determines the wettability of the solid.

2.2.3 Applications

Wettability concepts have been widely studied and applied to industrial processes. Two everyday examples are detergents used to enhance wetting of a solid surface by water, whereas prevention of wetting is the objective of every good car wax. More sophisticated applications are in the pharmaceutical industry. For example, drug-loaded nanoparticles are obtained by polymerization in a microemulsion produced by dispersing one liquid in another with low interfacial tension[20]. There is evidence that much of the behavior of the living cell is mediated by cell surface properties. Basic interfacial properties such as the electrical potential and the hydrophobic/hydrophilic character control cell behavior[21]. In the chemical industry, the wettability of metal and metal oxide surfaces is an issue in preparation of catalysts[22]. High temperature wetting behavior of inorganic liquids on metal and ceramic substrates influences the application of a variety of composite materials[23]. The cleanness of metal surfaces can be characterized by wettability[24]. In the mineral industry, the wettability of particles determines their recovery by flotation[25]. In the petroleum industry, oil recovery from fields nearing exhaustion requires surfactants to reduce the interfacial tension of oil and water to improve flow[26]. Wettability is involved in processing and use of polymer materials, pulp and paper, semiconductors, adhesives, cleaning fluids, etc.

In this research, the focus is on two industrial applications of wettability: bubble generation by rigid spargers used in flotation, and residual water removal in the froth treatment process in bitumen recovery.

In the first application, models of bubble production at a porous material usually include a wettability effect (i.e., contact angle). However, most researchers ignore this effect and assume the water contact angle at an orifice is zero. As far as the author can ascertain, there are no reports investigating the wettability effect of rigid porous sparger material on the size of the bubbles generated.

The issue in the second is that the fine solids tend to disperse in the oil phase in the froth treatment process. The fine solids are mainly kaolinite ($Al_2Si_2O_5(OH)_4$) and illite ($(K,H_3O)(Al,Mg,Fe)_2(Si,Al)_4O_{10}[(OH)_2, (H_2O)]$)[27] coated with organics, making them hydrophobic. The hypothesis is that these fine solids accumulate at the surface of small water droplets in the oil phase and stabilize them. The wettability of these fine solids controls the phenomenon, and is affected by the type of extracting solvent (diluent) used. To explore the mechanism, a model system was studied.

2.3 Characterization of wettability

Techniques to characterize wettability include film flotation, sedimentation, two-phase partition, contact angle, and surface/interfacial energy measurement. Each is briefly described.

In film flotation, small particles float on a liquid surface, the prerequisite for this flotation being a relatively large contact angle. Closely sized particles are sprinkled onto the surface of the wetting liquid. Depending on the wetting characteristics of the material and the surface tension of the test liquid, the particles either remain at the liquid/vapor interface or are engulfed into the liquid. The fraction sunk and floated are recovered, dried and weighed. For a given liquid (including an aqueous solution), the wettability of different solids can thus be evaluated and compared[28].

Sedimentation can be used to determine the surface tension of fine solids. In non-aqueous media, the influence of electrostatic interaction may be considered negligible. The van der Waals interaction between particles is related to surface tension[29,30]. A series of test liquids are used for the sedimentation experiments. Fine particles will have a maximum or minimum sedimentation volume when their surface tension is equal to that of the liquid, thus the surface tension of the fine solids is obtained[31,32].

Two-phase partition can be used to compare the wettability of particles or their behavior in different liquid systems[33]. Generally, the system is water-organics, and the fraction of particles in the organic and aqueous phase is determined. Hydrophobic particles tend to collect in the organic phase while the hydrophilic ones collect in aqueous phase.

Surface/interfacial energy (or tension) is a measurement of the wettability of a solid. Generally, if the surface energy is high, wettability is high. However, it is difficult to measure the surface energy of a solid directly, it is usually determined by indirect methods such as contact angle or heat immersion.

Contact angle is probably the most widely used method to characterize the wettability of a solid surface. Many methods have been developed, such as heat of immersion, captive bubble and sessile drop methods, axisymmetric drop shape analysis, Washburn and Wilhelmy methods. The heat of immersion determines the contact angle of solids based on their immersion heat in the test liquid[34,35]. It normally provides relative and semi-quantitative information. The captive bubble technique uses a gas (typically air) bubble brought into contact with a flat solid surface immersed in the test liquid[36,37]. The sessile drop method, perhaps the simplest of them all, determines the contact angle by placing a drop of test liquid on the solid surface, and measuring the contact angle at the three phase contact line. If the solid surface is smooth, homogenous and non-deformable, contact angle hysteresis can be ignored and the contact angle will be the equilibrium contact angle[12].

Axisymmetric drop shape analysis (ADSA) relates the surface tension and contact angle to the shape of the sessile drop[38] and determines the contact angle from the shape of the meniscus. It involves a complicated procedure, still in the development stage.

The Washburn and Wilhelmy methods are well established and widely used. The Washburn method is based on the imbibition of a test liquid into a porous material by capillary force[39]. It is used to determine the contact angle on powders or porous solids with contact angles less than 90° [40]. If the contact angle is larger than 90°, a modified Washburn method can be applied[41]. The Wilhelmy method is based on the capillary force applied to the sample along the meniscus formed while it is dipping into a test liquid[42]. It is generally used to determine the contact angle of a hydrophobic sample with a regular shape[43] or to study contact angle hysteresis[44].

In addition to the above, hydrophobic interaction chromatography and the salting-out aggregation test[45,46], as well as surface analysis techniques including infrared spectroscopy[47,48], are also used.

References

---

[1] Corex Co., http://www.corex.co.uk/97-019.html.

[2] Young, T., in *Miscellaneous Works*, Ed: Peacock, G., J. Murray, London, 1, 418(1855).

[3] Cotell, C. M., Sprague, J.A. and Smidt, F.A., *Surface Engineering*, ASM Hand Book, Volume 5, Materials Park, OH, ASM International, p969, 1990.

[4] Myers, D., *Surfaces, Interfaces, and Colloids, Principles and Applications*, 2nd edition, New York, Wiley-VCH, pp. 8-20, 1999.

[5] Considine, D. M. and Considine, G.D., *Van Nostrand's Scientific Encyclopedia*, 8th edition, New York, Van Nostrand Reinhold, c1995.

[6] Meyers, R.A., San Diego, *Encyclopedia of Physical Science and Technology*, 2th edition, Volume 16, Academic Press, 1992.

[7] Birdi, K.S., in *Handbook of Surface and Colloid Chemistry*, Ed: Birdi, K.S., Boca Raton, CRC Press, pp. 71-118, 1997.

[8] Fowkes, F.M., *Industrial and Engineering Chemistry*, 56(12), 40-52(1964).

[9] Van Oss, C.J., in *Interfacial Forces in Aqueous Media*, New York, Marcel Dekker, Inc., pp. 170-185, 1994.

[10] Donhue, J. and Bertell, F.E., *J. Phys. Chem.*, 56, 480(1952).

[11] Zisman, W.A., in *Advanced in Chemistry,* Series 43, Ed: Gould, R.F., Washington, American Chemical Society, p.1, 1964.

[12] (1). Johnson, R.E., Dettre, R. H., in *Wettability*, Surfactant Science Series, V. 49, Ed: Berg J. C., New York, Marcel Dekker Inc., pp. 1-73, 1993. (2) Spelt, J.K., Moy, E., Kwok, D.Y and Neumann, A.W., in *Applied Surface Thermodynamics*, Surfactant Science Series Volume 63, Ed: Neumann, A.W. and Spelt, J.K., New York, Marcel Dekker, Inc., pp. 293-332, 1996.

[13] Bertholet, D., *Compt. Rend*, 126, 1703 and 1857(1898).

[14] Neumann, A.W., *Adv. Coll. Inter. Sci.*, 4, 1(1974).

---

[15] Fowkes, F. M., in *Wetting*, SCIMonograph No. 25, London, Soc. Chemical Industry, p.3, 1967.

[16] Owens, D.K. and Wendt, R.C., *J. Appl. Polym. Sci.* 13, 1741(1969).

[17] Kaelble. D.H., *J. Ahdesion*, 2, 66(1970).

[18] Fowkes, F.M., Riddle, F.L., Pastore, W.E. and Weber, A.A., *Coll. Surf.*, 43, 367(1990).

[19] Berg J. C., in *Wettability*, Ed: J. C. Berg, Surfactant Science Series, Volume 49, New York, Marcel Dekker Inc., pp. 75-148, 1993.

[20] Yuan, Y., Cabasso, Y. and Fendler, J.H., *Chem. Mater.*, 2, 226(1990).

[21] Macrichie, F., *Chemistry at Interfaces*, San Diego, Academic Press, pp. 241-267, 1990.

[22] (1). Dodson, B.W., *Surf. Sci.*, 184, 1(1987). (2). Ruckenstein, E, in *Metal-Support Interactions in Catalysis, Sintering, and Redispersion*, New York, Van Nostrand Reinhold, 1987. (3). Ruckenstein, E, *J. Cryst. Growth*, 47, 666(1979).

[23] Zelinski, B.J.J, Cronin, J.P., Denesuk, M. and Uhlmann, R.D., in *Wettability*, Surfactant Science Series, Volume 49, Ed: Berg J. C., New York, Marcel Dekker Inc., pp. 465-524, 1993.

[24] Petermann, L.B., Baroux, B. and Fontaine M.N.B., *J. Adhes. Sci. Technol.*, 3, 221(1993).

[25] Leja, J., *Surface Chemistry of Froth Flotation*, New York, Plenum Press, 1982.

[26] Littnmann, W., in *Handbook of Surface and Colloid Chemistry*, Ed: Birdi, K.S., Boca Raton, CRC Press, pp.689-699, 1997.

[27] http://web.wt.net.

[28] Liu, Q., Ph.D. thesis, *An Innovative Approach in Magnetic Carrier Technology*, McGill University, 1996.

[29] Omenyi, S.N., Neumann, A.W. and van Oss, C.J., *J. Appl. Phys.*, 52, 789(1981).

[30] Neumann, A.W., Omenyi, S.N. and van Oss, C.J., *J. Phys. Chem.*, 86, 1267(1982).

[31] Vargha-Butler, E.I., Zubovits, T.K., Hamza, H.A. and Neumann, A.W., *J. Dispersion Sci. Technol.*, 6(3), 357(1985).

[32] Vargha-Butler, Moy, E. and Neumann, A.W., *Colloids and Surfaces*, 24, 315(1987).

[33] Weiss, E., Rosenberg, M., Judes, H. and Rosenberg, E., *Current Microbiol.* 7, 125(1982).

[34] Good, R..J. and Girifalco, J.A., *Journal of Physical Chemistry*, 62,1418-1421(1958).

---

[35] Spagnolo, D. A., Maham Y. and Chuang, K. T., Journal of Physical Chemistry, 100, 6626-6630(1996).

[36] Drelish, J., Miller, J.D. and Good, R.J., Journal of Colloid and Interface Science, 179, 37-50(1996).

[37] Grundke, K., Bogumil, T., Werner, C., Janke, A. Poschel, K. and Jacobasch, H.J., Colloids and Surfaces, A: Physicochemical and Engineering Aspects, 116, 79-91(1996).

[38] Lahooti, S., Del Rio, O.I., and Neumann, A.W. and Cheng, P., in Applied Surface Thermodynamics, Surfactant Science Series Volume 63, Ed: Neumann, A.W. and Spelt, J.K., New York, Marcel Dekker, Inc., pp. 441-508, 1996.

[39] Washburn, E.W., Physical Review, 17(3), 273-283(1921).

[40] Grundke, K., Boerner, M. and Jacobasch, H.J., Colloids and Surfaces, 58, 47-59(1991).

[41] Hansford, D.T, Grant, D.J.W. and Newton, J.M., J.C.S. Faraday I, 76, 2417-2431(1980).

[42] Wilhelmy, L., Ann. Phys., 119, 177(1863).

[43] Johnson, R.E., Dettre, R. H. and Brandreth, D.A., Journal of Colloid and Interface Science, 62(2), 205-212(1977).

[44] Decker, E.L. and Garoff, S., Langmuir, 13, 6321-6332(1997).

[45] Magnusson, K.E., Stendahl, O., Stjernstrom, I., and Edebo, L., Immunology, 36, 439(1979).

[46] Schutze, H.E., and Heremans, J.F., in Molecular Biology of Human Proteins, Volume I, Amsterdam, Elsevier, 1966.

[47] Stewart, J. E., Infrared Spectroscopy: Experimental Methods and Techniques, New York, M. Dekker, 1970.

[48] Gadsden, J. A., Infrared Spectra of Minerals and Related Inorganic Compounds, London , Butterworths, 1975.

Chapter 3

Two Processes Related to Solid Wettability

Contents

3.1 Introduction

In this thesis, two processes related to solid wettability are studied: “Bubble generation from porous media”, and “Froth treatment in processing oil sands”. The problem statement, general concepts, theory and literature review pertinent to each process are presented in this chapter.

Bubble generation is a central feature of so-called bubble column reactors such as flotation columns used in mineral separation. Column flotation is used here to illustrate the significance of bubble size and the ways bubbles are generated including the use of rigid spargers. The Kumar and Kuloor models are introduced to relate bubble size to sparger characteristics including wettability.

In the second process, the nature of bitumen deposits, the extraction process, and the need for froth treatment are presented. The wettability of fine solids and their characterization in the context of residual water removal are reviewed.

3.2 Bubble generation at a rigid sparger

Column flotation has been widely used in oil recovery[1], de-inking of recycled paper[2,3], processing of coal[4] and minerals[5], and, increasingly, in effluent treatment[6]. Bubble size or more specifically its derivative bubble surface area flux (BSAF or S_b) is an important operational parameter.

In some columns, notably in de-inking and de-oiling applications, bubbles are sometimes generated using rigid porous metal or ceramic spargers. The bubble size depends on sparger properties (as well as several operating variables). Bubble size may be affected by the wettability of the sparger material, but there appears to be no systematic work on this aspect. Rectifying this deficiency is one objective of this thesis.

3.2.1 Bubble column reactors

In a conventional flotation column, shown schematically in Figure 3.1, bubbles rise against a downward flowing slurry in the pulp (or collection) zone, collect hydrophobic particles and transport them to the froth (or cleaning) zone[7]. The froth is frequently washed by water (wash water) to counter recovery of hydrophilic particles by entrainment.

Flotation functions by separating particles according to their wettability. All particles have opportunity to collide with bubbles but only sufficiently hydrophobic ones will attach during the time of bubble-particle contact. These particles will be collected while the hydrophilic particles will remain in the pulp. Various reagents are used to modify the wettability to make the particles more or less hydrophobic and therefore control their floatability[8].

Bubble size has a profound effect on flotation efficiency both through effects in particle collection and froth stability[9]. Generally, small bubbles (<1mm diameter) are more efficient at particle collection and give higher solid recovery rate than big bubbles[10,11].

One reason, and perhaps the main, is that smaller bubbles at a given air flowrate produce a higher bubble surface area flux, which has proved to be a key parameter in defining flotation machine performance[12]. The higher the S_b, the higher the flotation rate constant and the higher the recovery rate of particles.

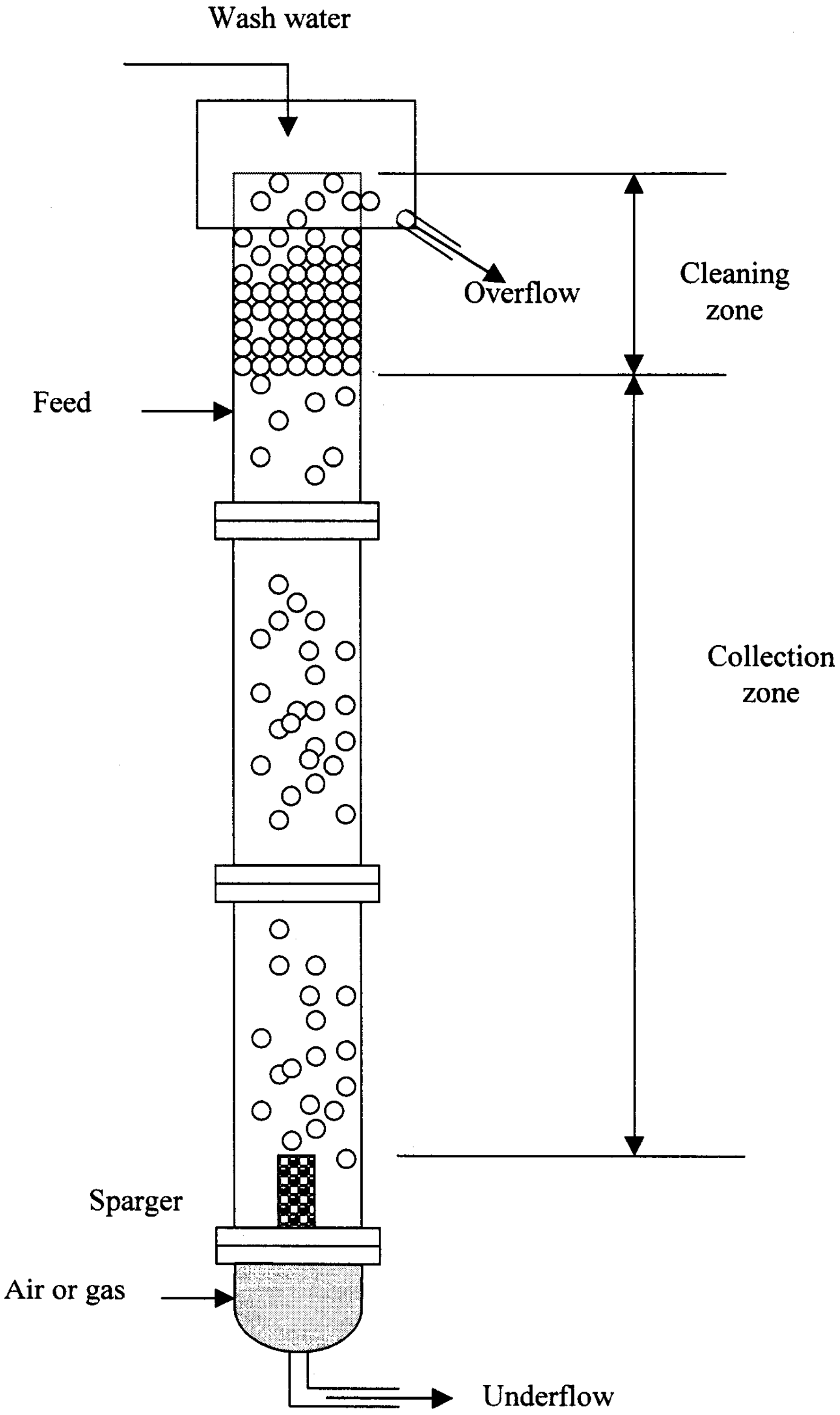

Figure 3.1: - Convention column flotation

3.2.2 Bubble generation at rigid porous media

3.2.2.1 Rigid porous sparger

The rigid porous sparger has been used extensively in laboratory flotation columns and periodically, in industrial applications. There are many kinds of porous spargers including disks, sheets, and cylinders[13]. The sparger material can be ceramic or metal, including stainless steel. A cylindrical sparger made from 316L stainless steel (SS) is used in this study (Figure 3.2). The spargers come in several grades defined by their nominal pore diameter which range from: 0.5, 2, 5, 10, 20, 40 to 100 μm.

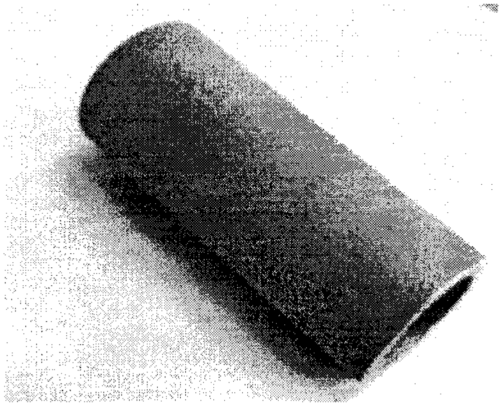

Figure 3.2: - A cylindrical stainless steel sparger

The structure of the sparger can be considered as many pores interconnecting to form so-called "capillaries". The ends of these capillaries act as "orifices" to produce bubbles as air is forced through. Orifices on the surface of a SS sparger (nominal pore size 10μm) are shown in Figure 3.3.

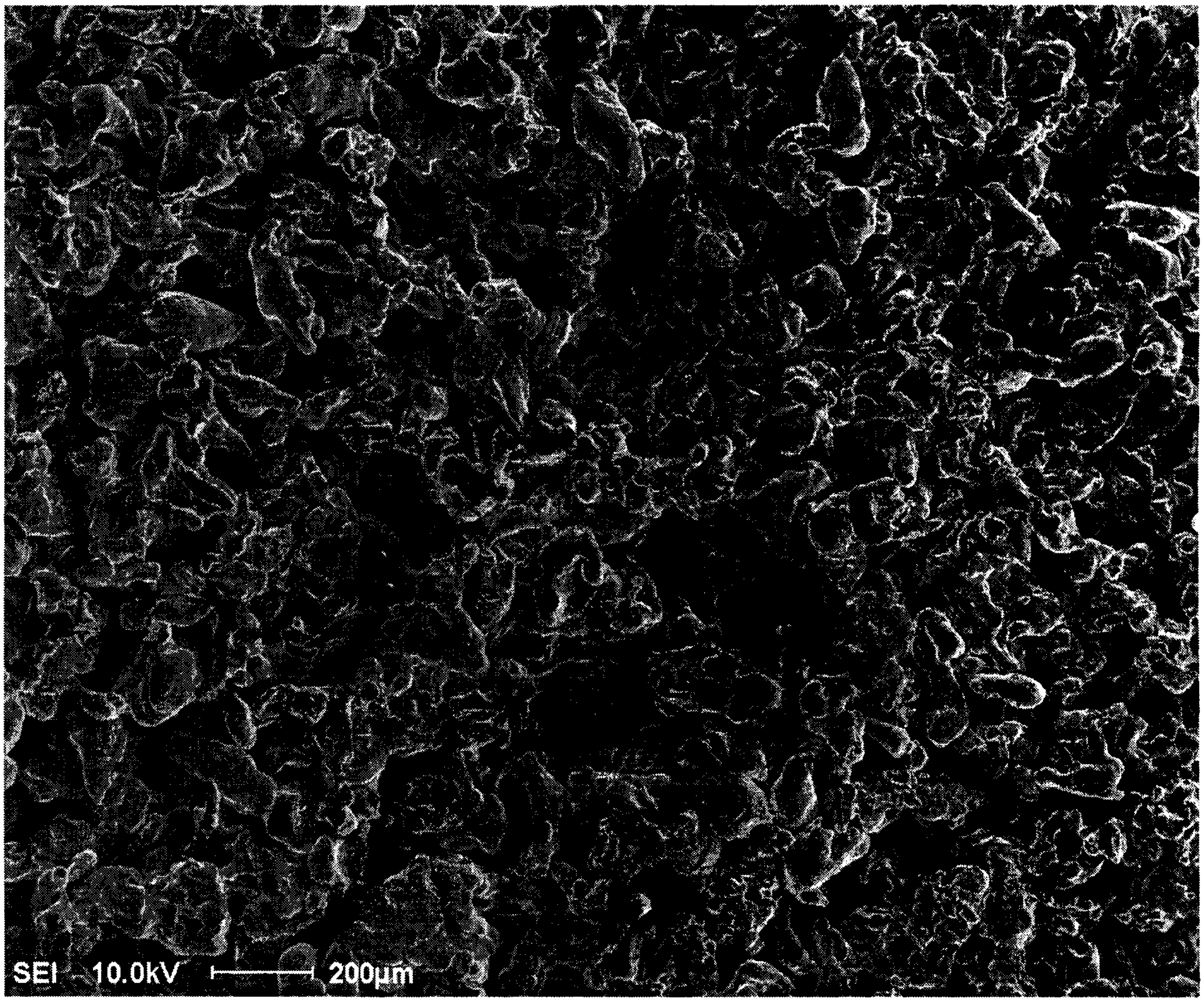

Figure 3.3: - SEM image of the surface of a stainless steel sparger (nominal pore 10µm)

3.2.2.2 Wettability effect on bubble size

Bubble formation at a rigid sparger depends on design parameters such as orifice geometry, orientation, shape, density (number per unit area) and surface properties of the material, and on operational parameters such as air flowrate, and surfactant type and concentration in the water. Generally, the larger the pore size and the higher the gas flowrate, the larger the resultant bubbles. As they are generated, bubbles tend to coalesce on the sparger surface and after as they rise. In mineral flotation, a surfactant called a frother is added to reduce coalescence. At sufficient concentration frother eliminates coalescence and the size of bubbles produced at the sparger is preserved as they rise[14].

The design parameter of interest here is material wettability. The wettability effect is controlled through the surface tension of the liquid and the contact angle at the orifice as the bubble forms. The resultant capillary force during bubble formation at the orifice of a vertical capillary is

$$F_s = \pi D \gamma_{\mathrm{lg}} \cos\theta \tag{3.1}$$

where D is the diameter of the orifice, γ_{lg} the surface tension of the liquid, θ the contact angle between the orifice surface and the liquid. From Eq. (3.1), it can be seen that if the orifice is hydrophilic, i.e. the contact angle is low, the surface tension force F_s will be large, whereas if the orifice is hydrophobic, i.e. the contact angle is high, the capillary force acting on the bubble is small.

Although contact angle is often included in bubble generation models, the wettability of an orifice surface is generally ignored, and the contact angle assumed to be zero[15,16,17].

However, a recent study[18]suggested that the contact angle should be considered, showing an increase in bubble size with contact angle on a smooth orifice surface.

Models introducing the wettability effect have been devised based on various assumptions and conditions. For a single orifice at low air flowrate, it was assumed that the bubbles were at all times spherical while they formed, and, in the case of liquids with low viscosity, were subject only to the surface tension and buoyancy. The bubbles would detach as soon as these forces were balanced[15]. For large air flowrate, inertia should be included. For a liquid of low viscosity, the bubble volume (V) was given[19] by

$$V = 1.378\frac{Q^{6/5}}{g^{3/5}} \tag{3.2}$$

where Q is air flowrate, and g the gravity acceleration. Further study[20] showed that in a high viscosity liquid, the inertial and surface tension forces could be neglected compared to the viscous force. Under these conditions, the volume of the bubble is

$$V = \left(\frac{4\pi}{3}\right)^{1/4}\left(\frac{15\mu Q}{2g}\right)^{3/4} \tag{3.3}$$

Different values of the numerical coefficient in Eq. (3.2) have been reported (e.g. 1.138[21,22], 1.72[23]). Subsequently, a large discrepancy was found between experimental and predicted data[24]. This was explained by a delay in detachment of the bubbles from the orifice, and a two stage bubble formation mechanism was proposed. In the first stage (expansion), the bubble develops at the tip. In the second stage (detachment), when buoyancy overcomes the downward acting forces, the bubble accelerates upward while still connecting to the orifice then detaches. It was shown that with this model the bubble volume could be predicted within ±5%. More general models were developed for a single orifice under constant flowrate conditions[25,26] by considering surface tension, drag, inertia and buoyancy. It was found that, by neglecting some terms, a similar equation to Eq. (3.2) could be deduced with a numerical coefficient 0.976 and an error of 30%. A modification of these models with consideration of gas momentum was studied for rigid and flexible spargers[27].

Other models for constant pressure[20,26,28], elevated pressure[29], moving liquids[30] with and without consideration of wettability, have also been developed.

From a practical point of view, the bubble formation models for a single orifice must be extended to multiple orifices. One attempt was based on extending the analysis of bubble formation from a single orifice to predict the average size of bubbles formed from a porous disc[31]. It was assumed that the orifices in the disc produced bubbles independently (still in the two stages), and the bubbles produced were arranged in hexagonal close packing. Good agreement was found between the predicted and experimental bubble size by the model using two discs with orifice diameter 110μm and 45μm over a range of air flowrates and liquid viscosities. It was concluded that the liquid surface tension affected bubble size at low air flowrate, and this effect decreased as the flowrate increased. A similar but more rigorous model was proposed by Kumar and Kuloor[26]. This model was recently used to predict the bubble size generated at a cylindrical SS sparger of the type to be used here[32]. The model was tested against experimental data assuming zero contact angle.

The orientation of an orifice is also found to have an effect on the bubble size. The bubbles generated at vertical orifices (i.e., the capillaries are vertical) appeared to be larger than those at horizontal orifices[15], although a later report showed the bubble size did not decrease continuously with increasing angle of orientation[26]. This was recently explained with the assumption of expanding bubble contact base[33].

The literature review revealed no study on the effect of sparger wettability on bubble size.

3.2.3 Kumar and Kuloor models

3.2.3.1 Single orifice

The Kumar and Kuloor model for a single orifice assumes that a bubble develops in two stages, illustrated in Figure 3.4. During the first stage, the bubble expands and ends as soon as the upward forces overcome the downward forces. In the second stage, the bubble ascends and expands but remains connecting to the orifice by a cylindrical neck. The second stage ends as soon as the vertical distance that the bubble base has moved reaches r_{fb}, the bubble radius at the end of the first stage. The final volume is then

$$V_F = V_{fb} + Qt_F \tag{3.4}$$

where V_{fb} is the volume of the bubble at the end of the first stage, t_F the time of bubble development in the second stage, and Q the gas flowrate.

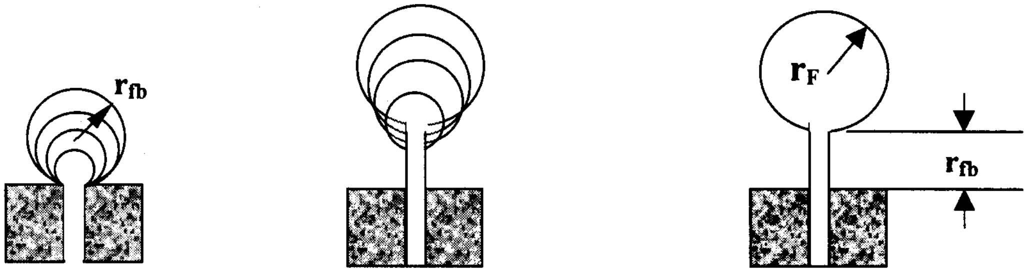

Figure 3.4: - Idealized sequence of bubble formation: Two-stage

When gas is fed through the orifice, a bubble forms and expands at a definite rate thereby increasing the inertial force and viscous drag force. In addition, it is also subject to the buoyancy and surface tension forces. From the force balance at the end of the first stage, the bubble volume is (details in Appendix A)

$$V_{fb}^{5/3} - \frac{\pi D\gamma\cos\theta}{g\rho_l} V_{fb}^{2/3} - \frac{3\mu Q}{2\cdot\left(\frac{3}{4\pi}\right)^{1/3}\cdot g\rho_l} V_{fb}^{1/3} - \frac{11Q^2}{192\pi\left(\frac{3}{4\pi}\right)^{2/3}\cdot g} = 0 \tag{3.5}$$

The second stage begins at the moment the upward forces are larger than the downward forces. According to Newton's second law of motion, the bubble movement can be expressed as

$$\frac{d}{dt}\left(Mv'\right) = (V_{fb} + Qt)\rho_l g - 6\pi r\mu v' - \pi D\gamma\cos\theta \tag{3.6}$$

where v' is the bubble velocity at its center. Solving Eq. (3.6) and rearranging the terms, the final bubble volume is

$$\begin{gathered} \frac{B}{2Q(A+1)} V_F^{6/3} - \frac{E}{AQ} V_F^{3/3} - \frac{3C}{2Q\left(A-1/3\right)} V_F^{2/3} + \\ \left(-\frac{B}{2Q(A+1)} V_{fb}^2 + \frac{E}{AQ} V_{fb} + \frac{3C}{2Q\left(A-1/3\right)} V_{fb}^{2/3} - \left(\frac{3}{4\pi} V_{fb}\right)^{1/3} \right) = 0 \end{gathered} \tag{3.7}$$

3.2.3.2 Multiple orifices

This model is an extension of the previous one on bubble formation at a single orifice. It estimates an average size of bubbles generated by a multiple orifice sparger based on the following assumptions[26]:

- The sparger has a large number of "potential sites", but only some of them are "active sites" producing bubbles.
- The gas flow through the active pore sites is constant during bubble formation.
- The number of active pore sites decreases with an increase in gas flowrate.

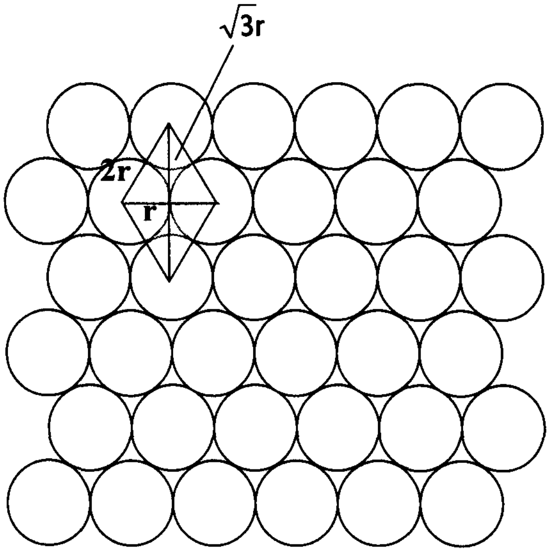

Figure 3.5: - Close packing of bubbles

The bubbles generated are assumed to be packed in such a way that they contact each other (Figure 3.5). The active pore sites per unit area, *n* is

$$n = \frac{(\frac{3}{4\pi}V_{F|Q})^{-2/3}}{2\sqrt{3}} = \frac{1}{2\sqrt{3}\cdot(\frac{3}{4\pi}V_{F|Q})^{2/3}} \tag{3.8}$$

where $V_{F|Q}$ is the calculated final bubble volume. Letting A_s be the external surface area of the porous media, then for each orifice, the gas flowrate is

$$Q = \frac{q}{nA_S} \tag{3.9}$$

where q is the total gas flowrate, and Q the gas flowrate through a single orifice.

The combination of Eqs. (3.5), (3.7), (3.8) and (3.9) can be used to estimate V_F or the average bubble diameter D_b. First, a value of *n* is assumed and the corresponding value of Q is calculated by Eq. (3.9), then V_{fb} and V_F can be solved by Eqs. (3.5) and (3.7), respectively. In turn, *n* is calculated by Eq. (3.8). This *n* is compared to the previous *n*, and the value of *n* is adjusted. This process continues until the two *n* are equal.

3.2.4 Modification and characterization of spargers

Compared to polymers, metals such as stainless steel are usually classified as high surface energy solids[34]. As a consequence, stainless steel is easily contaminated through adsorption of moisture or organics, as reflected in its reported surface energy which ranges from 34 to 278mJ/m^2. [35] In some cases, a surface oxide layer, or at least chemisorbed oxygen, alters its wettability.

The spargers used here are porous stainless steel cylinders, from Mott Industrial, Division of Mott Corporation[13]. They are made of sintered powder of 316L stainless steel. It was found that there was some organic substance contaminating the surface as a result of either the way the spargers were processed or packaged, which made the surface hydrophobic. Several techniques were considered to removed the organics, ranging from mechanical polishing, chemical, thermal, and oxygen or argon plasma treatment[36,37]. Heating proved effective to eliminate the organics and was the method used in this project to alter the wettability of the sparger.

The wettability was characterized by the contact angle. The Washburn method was used for the spargers with a water contact angle less than 90° whereas a modified Washburn method was used for those with water contact angles larger than 90°. The integrity of the pore structure as a result of the heat treatment was checked by measuring the permeability. It is essential that the permeability be the same before and after the surface treatment designated to modify only the wetting characteristics. As a measure of permeability the pressure drop of water flowing between points inside and outside the sparger as a function of water flowrate was monitored.

3.2.5 Bubble size measurement

The measurement of bubble size has attracted considerable effort. The methods developed range from simple bubble counting, to sophisticated acoustic sensors.

The counting method determines the average bubble size by determining the bubble frequency and the total volume. This technique is limited to a single orifice with low air flowrates[38]. The burette[26] and UCT[*,39,40,41] methods determine the bubble size by measuring bubble frequency and total volume. But the burette method can only be applied to situations with low bubbling frequency, and the UCT method often experiences error when measuring wide size distributions (very small and very large bubbles are missed). Bubble size can be measured by the resistance change of an electrolyte[42]. Drift flux analysis methods[43,44,45,46] calculate the mean bubble size from the gas holdup and air flowrate. Photographic techniques with image processing algorithms[47] estimate size from the bubble profiles.

The photographic method is considered the most reliable. Images (by camera[48] or camcorder[49]) can be analyzed on or off-line by increasingly sophisticated software. With

---

[*] University of Cape Town

most systems described in the literature, bubble overlap can be an issue and the systems need to be transparent. A promising technique employing a so-called bubble viewer overcomes these restrictions. Originally developed by Jameson and Allum[50] (details in Chapter 4), it is used to determine the bubble size in this work.

3.3 Removal of residual water in the froth treatment process for oil recovery from oil sands

The oil sand deposits in northern Alberta contain large reserves of bitumen that can be upgraded to petroleum products. Today, the total production of oil from oil sands amounts to 20% of Canadian oil consumption.

In the process used by Syncrude, the bitumen is recovered as a froth product that contains 60% bitumen, 30% water and 10% solids. This is followed by the froth treatment process designed to eliminate the water and fine solids. However, the product still has ca. 3% water. The water and dissolved salts are detrimental to the subsequent upgrading facilities. The residual water droplets appear to be stabilized by the fine solids, hence the stability of the water-in-oil droplets should be affected by a change in wettability of the solids. The wettability of these solids is assumed to be affected by the property of the diluent (see 3.3.3) used. To improve the quality of bitumen product, the effect of wettability of fine solids on the stability of water-in-oil droplets needs to be understood.

3.3.1 Oil sand extraction

The bitumen coexists with water and sand in deposits called oil sands (Figure 3.6)[51]. In the Athabasca area of northern Alberta/Saskatchewan, the bitumen was laid down about 110 million years ago[52]. It consists of viscous organic matter embedded in sediments of the Cretaceous McMurray and Clearwater formations. This material is a heterogeneous

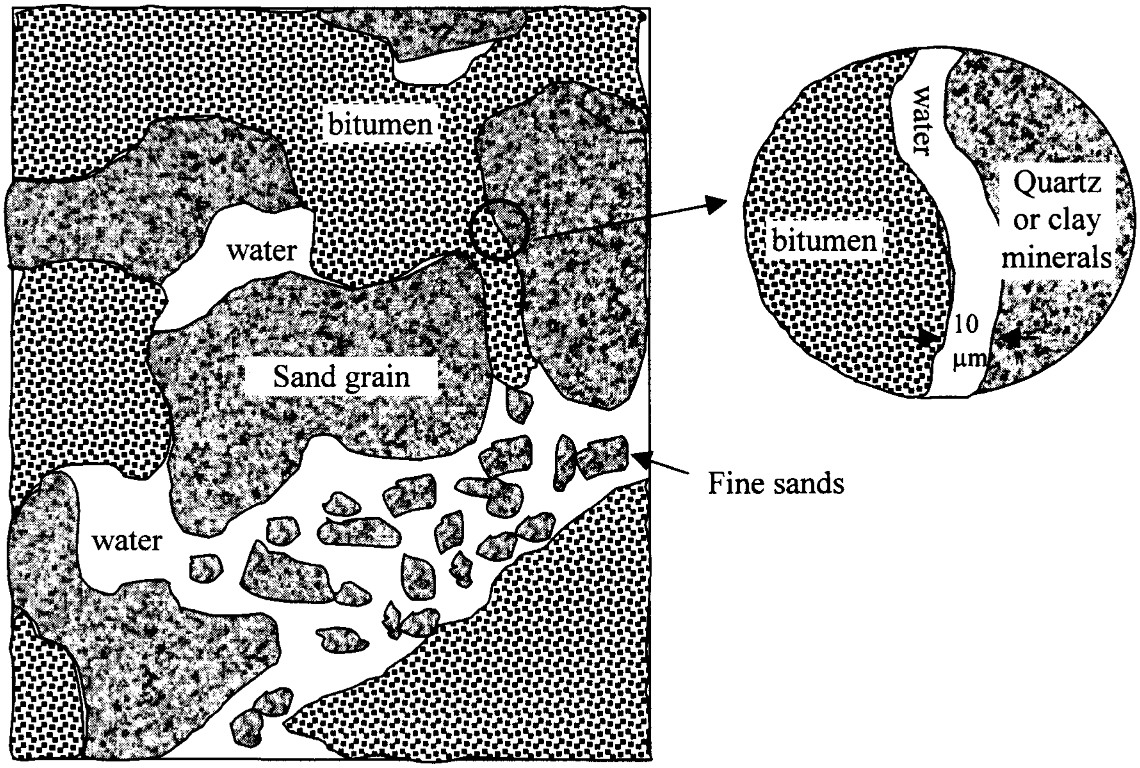

Figure 3.6: - Schematic of the arrangement of bitumen, water, sand, and fine minerals in a typical sample of Alberta oil sand

mixture of bitumen (with myriad chemical and structural forms), water, sands, clay minerals and a number of other minerals[53] (some of which may have potential economic value). The water film separates the bitumen from sands and clays. The mineral composition of sands is over 90% quartz with minor amounts of feldspar, chert and muscovite[54]. Clay minerals, dominantly kaolinite, illite and small amounts of montmorillonite, are concentrated in the fines fraction, which is normally defined as particles finer than 44μm[52].

The Clark's Hot Water Extraction Process (HWEP), and its modifications, have been used to separate bitumen from oil sands for over 60 years. In this process, the mined oil sands are tumbled and mixed with hot water, steam is injected to raise the temperature to about 85°C, and sodium hydroxide is added. The slurry is fed into large gravity separation vessels, where bitumen is recovered as a froth product in a process similar to flotation[51,55] (Figure 3.7). The froth produced typically contains ca. 60% bitumen, 30% water and 10% solids.

The froth treatment process is designed to eliminate the water and solids from this froth product in an attempt to produce solid- and water-free bitumen. In this process, the froth is treated by adding an organic liquid mixture, such as naphtha, to provide a density difference between the water and hydrocarbon phases and to reduce the viscosity of the froth (Figure 3.8). The organic liquid mixture is referred to as a "diluent". The diluted bitumen is then fed through a two-stage centrifuge to remove coarse particles in the first stage, and the remaining fine solids and dispersed water droplets in the second stage. Collectively called froth treatment, the process produces a product still containing ~3% water and 0.5% fine solids.

3.3.2 Problem of water-in-oil emulsion

The water remaining in the froth treatment product contains dissolved salts, mainly sodium chloride, which are then transferred to the downstream refinery. The chloride introduces a serious corrosion risk to the following upgrading facilities. The presence of salt also lowers the activity of the catalysts and salt deposits obstruct flow through the reactors. As a result, there is a strong incentive to reduce the amount of water in the froth treatment product before it is sent to the upgrading operations. It has been found that by changing the diluent characteristics from aromatic to paraffinic, the derived bitumen product is drier (contains less than 0.5% moisture) and is practically solids-free, but this is achieved at the cost of lower bitumen recovery (85% instead of 95% when naphtha is used as diluent)[56]. To improve the performance of froth treatment, it is necessary to understand the mechanism of water retention. The outcome should be an optimum diluent composition.

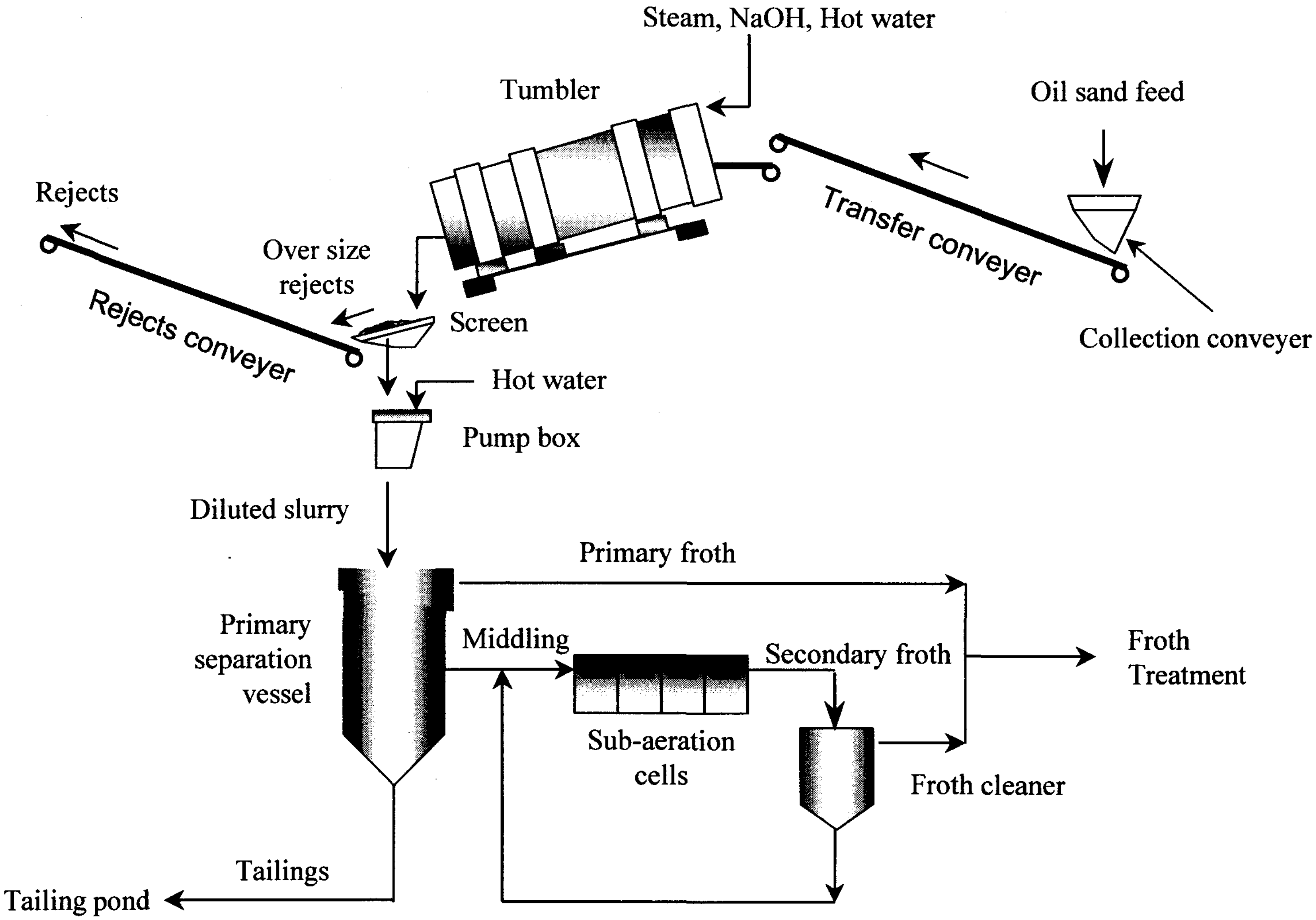

Figure 3.7: - Hot Water Extraction Process (1992, in Syncrude)

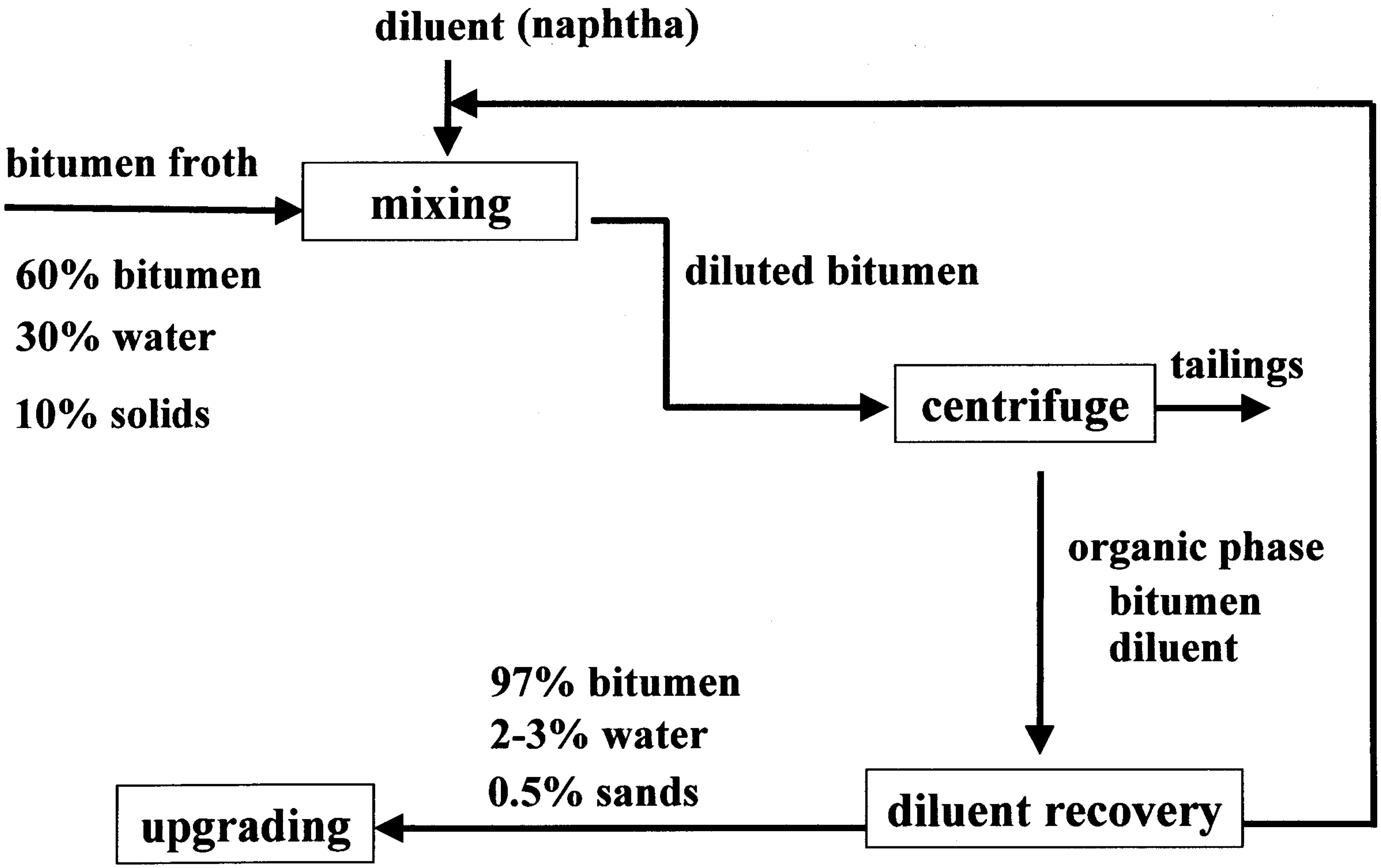

Figure 3.8: - Schematic of froth treatment process

3.3.3 Diluent system

Bitumen is a mixture of hydrocarbons[57] including asphaltenes as well as a small amount of metals. The exact chemical structure of the asphaltenes is unknown.

At Syncrude, the diluent used is naphtha that consists mainly of toluene with a small amount of aliphatic compounds. This diluent is a good solvent for bitumen, but is also a good media for retaining the fine solids because of the organic matter adsorbed on the surface which makes the particles hydrophobic.

Much research has been devoted to find alternative diluents to eliminate the residual water. Heptane has been found effective, producing bitumen with less solids and water[56]. The rejected water, fine solids and a small amount of bitumen form a so-called rag layer between the aqueous and organic phase (Figure 3.9). The formation of this rag layer is not well understood. It is postulated that the properties of the diluent will affect the wettability of fine solids, and in turn the stability of the water-in-oil droplets.

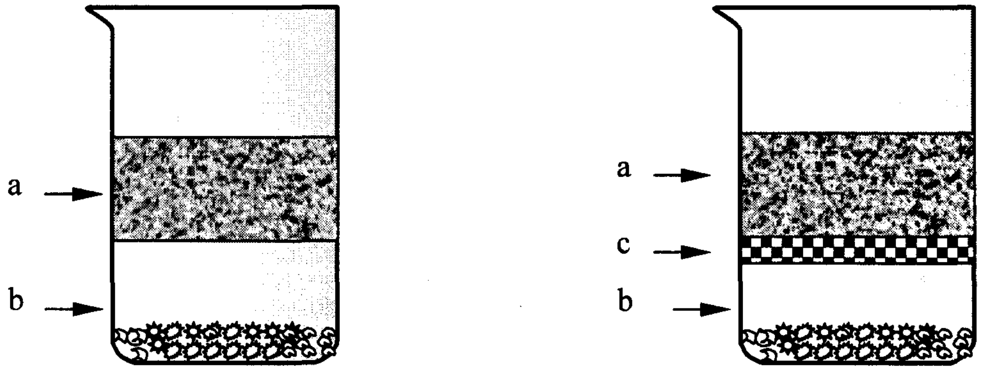

Toluene as diluent
Organic phase a: bitumen + diluent +
residual water, fine solids
Aqueous phase b: water + coarse sands

Heptane as diluent
Organic phase a: bitumen + diluent
Aqueous phase b: water + coarse sands
Rag layer c: fine solids, water + bitumen

Figure 3.9: - Froth treatment with different diluents

3.3.4 Adsorbed organics and wettability of fine solids

The fine clay solids carry adsorbed organics of various types. The organic substances, while the composition is not well defined, are thought to be mainly surfactants produced during the bitumen deposit formation and/or generated during the recovery of bitumen from the sands by HWEP.

Efforts have been made to understand the mechanism of the adsorption of organics on clay surfaces and the resultant effect on wettability of these clays. Sanford and co-workers[58,59] discovered that the role of sodium hydroxide in the HWEP process is primarily to produce surfactants from acids occurring naturally in bitumen. According to Bowman and co-workers[60,61,62], these surfactants are predominantly water-soluble salts of naphthenic acids with carboxylate-functional groups (Figure 3.10). Smaller amounts of sulfonate and related compounds were also identified. It was suggested[63,64] that oxygenated sulphur compounds, carboxylic, sulphonic and phenolic acids might also occur. Sulphoxides, sulphonic acids and carboxylic acids have been detected in the aqueous phase[65]. A tentative mechanism for their formation from organic sulphides was suggested (Figure 3.11)[66]. It was later found that the carboxylic-type compounds complexed with Fe(III) bound to the surface of the hydrophilic clays (mainly kaolinite and illite)[67]. Further evidence showed that the addition of NaOH aided in the formation of surfactants from the bitumen[58].

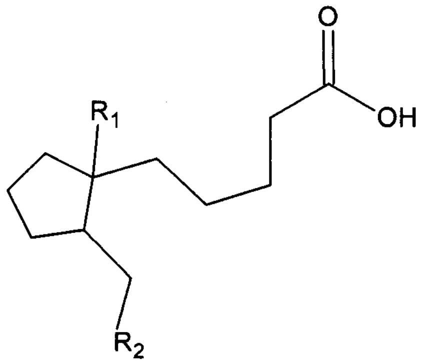

Figure 3.10: - Simplified representation of the structure of the acids from which surface-active salts are generated in HWEP. R_1 and R_2 are organic groups.

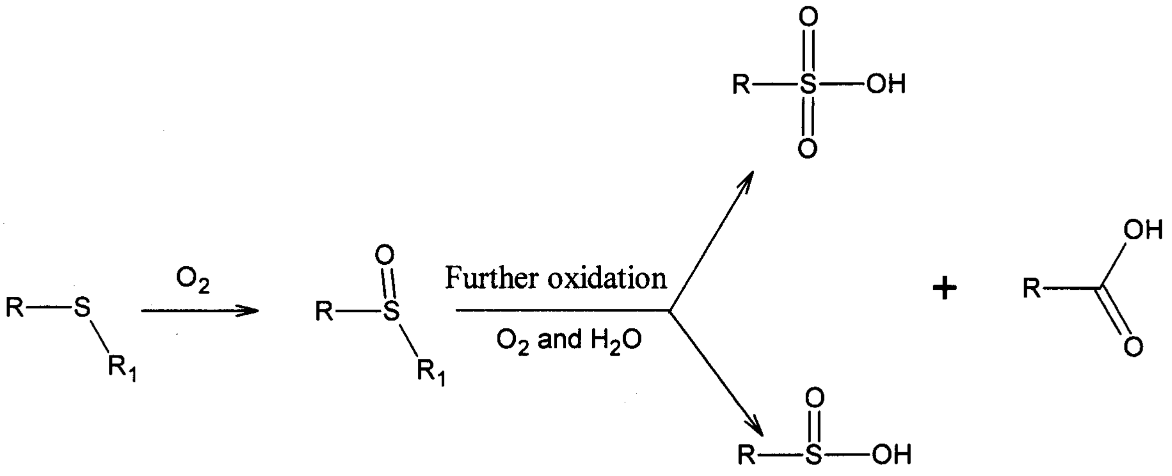

Figure 3.11: - A tentative mechanism for the surfactant formation

Infrared spectra suggested the formation of organic-clay complexes[68], probably through metal oxide/hydrous oxide sites[69]. In addtion, α, β unsaturated ketones and/or conjugated chelated diketones may also exist[70]. Majid et al. [71,72] suggested that this organic matter consisted of paraffinic and condensed aromatic rings with significant oxygenated function groups. The evidence from ^{13}C NMR (Nuclear Magnetic Resonance) suggested organic matter similar to asphaltene. Metals such as Ni, V, Cu, Cr, Fe, Ti and Zr were found by ICP-AES (inductive-coupled plasma atomic emission spectroscopy) method[73]. The NMR and IR measurements indicated that the organic matter associated with the solids in the HWEP tailing sludge was made up mostly of multicyclic aromatic compounds with a large number of oxygen and nitrogen functional groups[74,75].

The clay in bitumen was found to be concentrated in the asphaltene fraction by precipitating asphaltene from bitumen using pentane. The difficulty in removal of these clays suggested that the clay had a high affinity for certain bitumen components. These components bonded with clays were insoluble in toluene (defined as toluene insoluble organic matter, TIOM)[76], and were found to be the key to the poor dewaterability of the settled clay sludge because they formed a network structure among water/residual bitumen/fine solids[77]. A recent study showed that these TIOM were mainly humic matter. This humic matter has both hydrophobic and hydrophilic character with a strong affinity for bitumen components. Stabilization of oil droplets by biwettable solids in the extraction stage has been discussed by Levine and Sandford[78], who indicated the fine solids became partially hydrophobic by adsorption of bitumen components such as asphaltenes. Asphaltene[79,80,81]adsorption on mineral solids has been studied recently. Menon and Wasan have shown that adsorption of asphaltenes and surfactants on clay changes the oil-water-solids contact angle[79,81]. Tyerman suggested that the water-in-oil dispersions formed in froth treatment were stabilized by biwettable solids, and found that a demulsifier decreased asphaltene adsorption and reduced the water content in oil[82]. Eley et al.[83] reported an increase in quantity of water that could be dispersed in a mixture of n-heptane and m-xylene containing asphaltenes, when the volume fraction of m-xylene was decreased below about 25%. They suggested that the dispersed droplets were stabilized when the asphaltenes were on the verge of precipitation. Under these conditions, the asphaltene film at the oil/water interface might become inelastic, which would hinder coalescence. Kaolinite clay particles treated with asphaltene were used to study the partitioning of the clay particles between an oil-in-water emulsion and an aqueous phase. It was found[84] that the interaction energy of the adsorbed particles and the equilibrium ratio of the clay concentration at the oil droplet surface to that in the bulk water were a strong function of the clay contact angle when $\theta > 65^\circ$.

The quartz sands and most of the clay particles in the froth are hydrophilic and go to tailing stream during the froth treatment process. However, there is a small portion of the clay that remains after froth treatment. This portion is hydrophobic or biwettable because of the adsorption of organic substances. Some of the organic substance can be removed by toluene, but others chemically bonded to the solid surface are toluene insoluble (TIOM). The fine solids coated with strongly bound TIOM have "asphaltene-like characteristics" and tend to collect at the oil/water interface. They are considered to be the key component responsible for the presence of residual water in the bitumen froth[85].

3.3.4 Stability of water-in-oil droplets

It is well known that fine solids can stabilize a water/oil emulsion. Pickering originally noted that fine particles that were wetted more by water than by oil could stabilize oil-in-water droplets[86], but the stabilization mechanism is still not elucidated fully.

Generally, solids with a contact angle slightly less than 90° stabilize oil-in-water emulsions, while solids with a contact angle slightly larger than 90° stabilize water-in-oil emulsions[87]. Many have studied solid-stabilized emulsions experimentally and theoretically. Briggs[88] studied the role of fine solids on the stability of water/benzene emulsions, and indicated it was necessary for the solids to form a barrier at the interface. A complex structure at the interface of a water-in-oil emulsion stabilized by solids was suggested[89]. Tadros and Vincent[90] concluded that particles tend to remain at an oil-water interface when the contact angle is 90^o. For droplet coalescence to occur, particles must submerge into one of the phases. Levine and Sanford[78] studied the thermodynamics of an oil-in-water emulsion stabilized by fine solids, and indicated that almost all the fine solids tend to collect at the oil/water interface.

From this brief review, what emerges is that adsorption of particles at the water droplet surface forms a protective layer which contributes to the stabilization of water-in-oil emulsion. Stabilization of the water droplet dispersion in oil due to fine solids is illustrated in Figure 3.12. If the particles is strongly hydrophilic (water contact angle $<30^o$), it tends to immerse in the aqueous phase. If it is very hydrophobic (contact angle $>150^o$), it tends to stay in the organic phase. For angles in between, the particles accumulate at the water/oil interface tending to stabilize the water-oil emulsion.

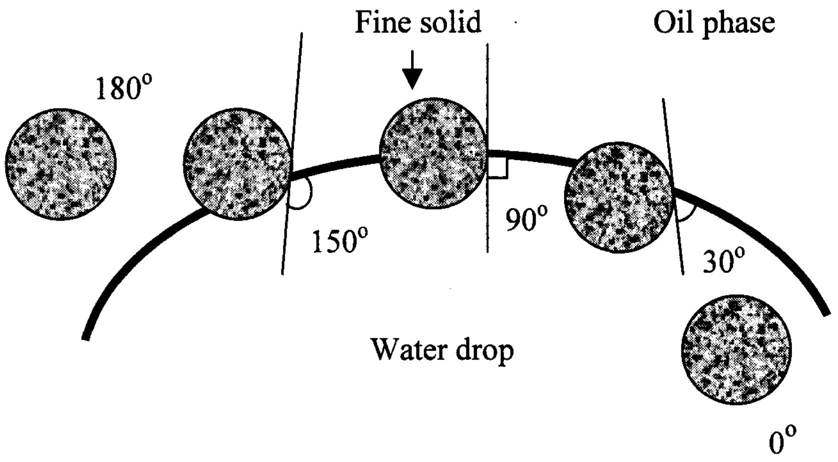

Figure 3.12: - Schematic of water droplet stabilized by fine solids

3.3.6 Characteristics of toluene and heptane

Toluene is an aromatic compound of chemical formula $C_6H_5CH_3$, and structure

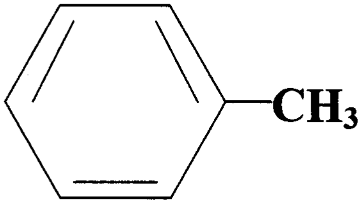

The aromatic ring has delocalized electrons that tend to interact with the electrons in other aromatic rings or with other organics which accept electrons[91]. This gives it an affinity for aromatic compounds such as those that make up bitumen and the surfactants presented in the bitumen froth and adsorbed on fine solids. The $-CH_3$ group in the molecule makes toluene polar, improving affinity with water and surfactant molecules.

Heptane is a paraffinic compound of chemical formula C_7H_{16}, and structure

$$CH_3(CH_2)_5CH_3$$

It is apolar because of its symmetric molecular structure, i.e. the dipole moment is zero. Compared to toluene, heptane has a weaker affinity for aromatic compounds. It is also expected that large aromatic molecules will be less soluble in heptane than in toluene.

The mixture of heptane and toluene is expected to have properties ranging from aromatic to paraffinic, which will vary the wettability of the fine solids in the froth.

3.3.7 *Characterization techniques for fine solids from froth treatment*

Techniques employed to characterize the fine solids from the bitumen recovery process include: elemental analysis for carbon, hydrogen and nitrogen content; IR and solid state ^{13}C NMR for functional group identification; and, X-Ray Photo-Electron Spectroscopy

(XPS) to obtain elemental and valence state of surface elements. Other techniques are Transmission Electron Microscopy (TEM)[57,67], emission spectroscopy, and X-ray diffraction (XRD)[92].

Infrared spectroscopy has been widely used to identify organic functional groups on solid surfaces[69]. A carbonyl group conjugated with a carbon-carbon double bond, hydrogen bonded, or associated with a carboxylate anion or a diketonic structure was found by IR analysis on clay sludge[67,70]. Quinone species were suggested to be present from interpretation of IR signals[73].

Partition has generally been used to illustrate the biwettable behavior of fine solids in the froth treatment process. Recently, it was used to study a solids-stabilized oil-in-water emulsion[84]. An oil-in-water emulsion stabilized by asphaltene-coated kaolinite can be demulsified by addition of fresh oil[93].

Contact angle is a direct method to characterize the wettability of solids. Many techniques have been developed. The Wilhelmy method needs the sample to be in a well-defined shape such as a plate, rod or cylinder with a known wetting perimeter. The Washburn method needs capillaries for the imbibition of test liquid by capillary force. Unfortunately, these methods are not applicable to the fine solid samples in this project. The conventional sessile drop method is appropriate and convenient for measuring the contact angle of fine solids involved in this work.

References

---

[1] Sanford, E.C. and Seyer, F. A., *CIM Bulletin*, 72, 164-169(1979).

[2] Leichtle, G.F., *Analysis of Bubble Generating Devices in a Deinking Column*, M.Eng. Thesis, McGill University, 1998.

[3] Hardie, C.A., *In-Plant Comparison of Internal and External Spargers for Flotation Column Deinking*, M.Eng. Thesis, 1998.

[4] Yoon, R. H. and Luttrell,G.H., *Coal Preparation*, 2, 179-192(1986).

[5] Maksimov, I.I., Borkin, A.D. Yemelyanov, M.F. and Koltunova,T.Y., in *Flotation* Volume II, Ed: Castro, S. and Alvarez, J., Chile, Andros Ltd., pp. 161-167, 1994.

[6] Kim, J. Y., Lajoie, S. and Godbehere, P., in *Proceeding of the International Symposium: Waste Processing and Recycling in Mineral and Metallurgical Industry II.*, Ed: Rao, S.R., Amaratunga, L.M. Richards, G.G. and Kondos, P.D., The Mettallurgical society of the Canadian Institute of Mining, Metallurgy and Petroleum, pp. 221-234, 1995.

[7] Finch, J.A. and Dobby, G.S., *Column Flotation*, Camborne School of Mines, Cornwall, England. 1989.

[8] Glembotskii, V. A., *Flotation*, New York, Primary Sources, 1963.

[9] Pryor, E.J. *Mineral Processing*, Amsterdam, Elsevier, 3rd ed., 1965.

[10] Ahmed, N. and Jameson, G.S. *International Journal of Mineral Processing*, 14, 195(1985).

[11] Finch, J.A. and Dobby, G.S., *Column Flotation*, 1st edition, Pergamon Press, Oxford, England, pp. 48-55, 1990.

[12] Finch, J. A., Gomez, C.O., Hardie, C., Leichtle,G., Filippone, R. and Leroux, D., *in "Proceedings-31st Annaul Meeting of the Canadian Mineral Processors*, Ottawa, Ontario, pp. 199-210, 1999.

[13] Mott Industrial, *Mott Porous metal Media Design & Specification Guide*, Mott Industrial, Division of Mott Corporation, Formington, CT, USA.

[14] Finch, J.A. and Dobby, G.S., *Column Flotation*, 1st edition, Pergamon Press, Oxford, England, p. 21, 1990.

---

[15] Datta, R.L., Napier, D.H. and Newitt,,D.M., in *Conference on Formation and Properties of Gas Bubbles*, Burlington House, London, Fabruary, pp. 14-26, 1950.

[16] Coppock, P.D. and Meiklehohn, G.T., *Trans. Instn. Chem. Engrs.*, 29, 75(1951).

[17] Benzing, R.J. and Myers, J.E., *Industrial and Engineering Chemistry*, 47(10), 2087(1955).

[18] Lin, J.N., Banerji, S.K. and Yasuda, H., *Langmuir*, 10, 936-942(1994).

[19] Davidson, J.F. and Schüler, B.O.G, *Trans. Inst. Chem. Eng.*, 28, 335-342(1960).

[20] Davidson, J.F., Mech, A.M.I. and Schüler., B.O.G., *Trans. Instn. Chem. Engrs.*, 38, 144-154(1960).

[21] Walters, J.K. and Davidson, J.F., *J. Fluid Mech.,* 12, 408-416(1962).

[22] Davidson, J.F. and Harrison, D., *Fluidised Particles,* London, Cambridge University Press, pp. 50-62, 1963.

[23] VanKrevelen, D.W. and Hoftijzer, P.J., *Chem. Eng. Prog*. 46, 29-35(1950).

[24] Krishnamurthi, S, Kumar, R. and Kuloor, N.R., *I&EC Fundamentals*, 7(4), 549-554(1968).

[25] Ramakrishnan, S., Kumar, R., and Kuloor, N.R., *Chemical Engineering Science*, 24, 731-747(1969).

[26] Kumar., R. and Kuloor, N.R., *Advanced in Chemical Engineering*, Ed: Drew, T.B., Cokelet, G.R., Hoopes, J.W. nad Vermeulen, T., Volume 8, New York, Academic Press, pp. 255-368, 1970.

[27] Geary, N.W. and Rice, R.G., *AIChE Journal*, 37(2), 161-168(1991)

[28] Satyanarayan, A., Kumar, R., and Kuloor, N.R., *Chemical Engineering Science*, 24, 749-761(1969).

[29] LaNauze, R.D. and Harris, I.J., *Transactions Institution of Chemical Engineers,* 52, 337-348(1974).

[30] Sullivan, S.L., Hardy, B.W. and Holland, C.D., *AIChE. Journal*, 10(6), 848-854(1964).

[31] Bowonder, B. and Kumar, R., *Chemical Engineering Science*, 25, 25-32(1970).

[32] Escudero, R.E., Ph.D. Thesis, *Characterization of Rigid Spargers and Their Selection for Flotation Columns*, Montreal, McGill University, 1998.

[33] Lin, J. N., Banerji, S. K. and Yasuda, H., *Langmuir*, 10, 943-948(1994).

[34] Kinloch, A.J., in *Adhesion and Adhesives*, Capman and Hall, New York, pp.32-34, 1990.

[35] Boulanger-Petermann., L., Baroux, B., and Bellon-Fontain, M.N., *J. Adhes. Sci. Technol*, 3, 221(1993).

---

[36] Mantel, M., Rabinvovich, Y.I., Wightman, P. and Yoon, R.H., *Journal of Colloid and Interface Science,* 170, 203-214(1995).

[37] Mantel, M. and Wightman, J.P., *Surface and Interface Analysis*, 21, 595-605(1994).

[38] Maier, C. G., *U.S. Bureau of Mines, Bulletin*, 260, 62-120(1927).

[39] Randall, E.W., Goodall, C.M., Fairlamb, P.M., Dold, P.L., and O'Connor, C.T., *J. Phys. E. Sci. Instrum*. 22, 827(1989).

[40] O'Connor, C.T., Randall, E.W., and Goodall, C.M., *International Journal of Mineral Processing*, 28, 139-149(1990).

[41] Tucker, J.P., Deglon, D.A., Franzidis, J.P., Harris, M.C. and O'Connor, C.T., *Minerals Engineering*, 7, 667(1994).

[42] Lewis, D. A., Nicole, R. S. and Thomepson, J. W., *Chem. Eng. Research and Design*, 62, 334(1984).

[43] Banisi, S. and Finch, J.A., *Minerals Engineering*, 7(12), 1555(1994).

[44] Dobby, G.S., Yianatos, J. B. and Finch, J.A., *Canadian metallurgical Quarterly*, 27(2), 85-90(1988).

[45] Xu, M. and Finch, J.A., *Journal of Colloid and Interface Science*, 140(1), 298-299(1990).

[46] Yianatos, J.B., Finch, J. A., Dobby, G. S. and Xu, M., *Journal of Colloid and Interface science*, 126(1), 37-44(1988).

[47] Sadr-Kasemi, N. and Cilliers, J.J., *Minerals Engineering*, 10(10), 1075(1997).

[48] Walsh, A.L. and Mulhearn, P.J., *Journal of Geophysical Research*, 92(c13), 553(1987).

[49] Pamperin, O. and Rath, H.J., *Chemical Engineering Science*, 50(19), 3009(1995).

[50] Jameson, G.J. and Allum, P., A Survey of Bubble Sizes in Industrial Flotation Cells, A report submitted to Aust. Min Ind. Res. Assoc. 1984.

[51] Helper, L.G. and Smith, R.G., *AOSTRA Technical Publication*, Series #14, AOSTRA, 1994.

[52] Takamura, K., *The Canadian Journal of Chemical Engineering,* 60, 538-545(1982).

[53] Bichard, J.A., *AOSTRA Technical Publication.*, Series #4, AOSTRA, Edmonton, 1987.

[54] Carrigy, M.A. and Kramers, J.W., "*Guide to the Athabasca Oil Sands Area*", Alberta Research Council, 1973.

---

[55] Mikula, R.J., Axelson, D.E. and Sheeran, D., *Fuel Science and Technology Int'L.*, 11(12), 1695-1729(1993).

[56] Shelfantook, W.E. and Tipman, R.N., Research Paper Presented at the Syncrude R&D Seminar on Alternative Diluents, Edmonton, November, 1995.

[57] Kotlyar, L.S., Sparks, B.D., Woods, J.R., Raymand, S., Page, Y.L. and Shelfantook, W., *Petroleum Science and Technology*, 16(1&2), 1-19(1998).

[58] Sandford, E.C. and Seyer, F.A., *CIM Bulletin*., 72, 164-169(1979).

[59] Levine, S. and Sandford, E.C., *Pro. 30th Can. Chem. Eng. Conf.*, 4, 1112(1980).

[60] Bowman, C.W., *Pro. 7th World Petrol. Congr*., 3, 583(1967).

[61] Baptista, M.V. and Bowman, C.W., *19th Can. Chem. Eng. Conf.,* Edmonton, Alberta, 1969.

[62] Leja, J. and Bowman, C.W., *Canadian Journal of Chemical Engineering*, 46, 479(1968).

[63] Moschopedis, S.F., Fryer, J.F. and Speight, J.G., *Fuel*, 56, 109(1977).

[64] Schramm, L.L. and Smith, R.G., *The Canadian Journal of Chemical Engineering*, 65, 799-214(1987).

[65] Latif H. Ali, *Fuel*, 57(6), 357-360(1978).

[66] Ali, L.H., *Fuel*, 57, 357-360(1978).

[67] Kessick, M.A., *Calys and Clay Minerals*, 27(4), 301-302(1979).

[68] Teresa M. Ignasiak, Luba Kotlyar, Frederick J. Longstaffe, Otto P. Strausz and D. S. Montgomery, *Fuel*, 62(3), 353-362(1983).

[69] Kotlyar, L. S., Sparks, B. D. and Kodama, H., *AOSTRA Journal of Research*, 1(1), 99-106(1984).

[70] Ignasiak, T. M., Zhang, Q., Kratochvil, B., Maitra, C., Montgomery, D. S., and Strausz, O. P., *AOSTRA Journal of Research*, 2, 21-35(1985).

[71] Majid, A. and Ripmeester, in *ACS Symposium*, Series 344; Met. Complexs Dossil Fuels, Ed: Filby, R.H. and Branthaver, J.F. Ed: Amer. Chem. Soc., Washington, D.C. p.290, 1987.

[72] Majid, A.,and Ripmeester,J.A., *Fuel*, 69, 1527(1990).

[73] Kotlyar, L. S. and Sparks, B. D., *AOSTRA Journal of Research*, 7(2), 111-117(1991).

---

[74] Majik, A., Ripmeester, J.A. and Davidson, D.W, National Research Council of Canada Report, Report No. C1095-82S (1982).

[75] Majik, A., Ripmeester, J.A., *Fuel*, 65, 1714(1986).

[76] F. Bensebaa, L.S. Kotlyar, B.D. Sparks and K.H. Chung, *The Canadian Journal of Chemical Engineering*, 78, 610-616(2000).

[77] Kessick, M.A., *J. Can. Petrol. Technol.*, 18, 49-52(1979).

[78] Levine, S. and Sandford, E., *The Canadian Journal of Chemical Engineering*, 62, 258-268(1985).

[79] Menon, V.B. and Wasan, D.T., *Colloids and Surfaces*, 19, 89-107(1986).

[80] Marlow, B.J., Sresty, G.C., Hughs, and Mahajan, O.P., *Colloids and Surfaces*, 24, 283(1987).

[81] Menon, V.B. and Wasan, D.T., *Colloids and Surfaces*, 25, 387(1987).

[82] Drelich, J., Lelinski, D., and Miller, J.D., *Colloids and Surfaces* A: Physicochemical and Engineering Aspects, 116, 211-213(1996).

[83] Eeley, D.D., Hey.M.J. and Symonds, J.D., *Colloids and Surfaces*, 32, 87(1988).

[84] Yan, N. and Masliyah, J.H, *Colloids and Surfaces* A: Physicochemical and Engineering Aspects 96, 229-242(1995).

[85] Kotlyar, L. S., Sparks, B. D., Woods, J. R., Raymond, S., Page, Y. Le and Shelfantook, W., *Petroleum Science and Technology*, 16(1), 1-19(1998).

[86] Pickering, S.U., *J. Chem. Soc.*, 91, 2001(1907).

[87] Schulman, J.H. and Leja, J., *Trans. Faladay Soc.*, 50, 598(1954).

[88] Briggs, T.R., *Ind. Eng. Chem.*, 13, 1008(1921).

[89] Meson, V.B. and Wasan, D.T., *Sep. Sci. Technol.*, 23, 2131(1998).

[90] Tadros, T.F. and Vincent, B., in *Encyclopedia of Emulsion Technology*, Vol. 1, Ed: Becher, P., New York, Dekker, p.272, 1983.

[91] Davis, M.M, in *The Chemistry of nonaqueous Solvents*, Vol. 3, Ed: Lagowski, J.J., New York, Academic Press, pp. 21-22, 1970.

[92] Kotlyar, L. S. and Sparks, B. D., *AOSTRA Journal of Research*, 4(4), 277-285(1988).

---

[93] Yan, N., Kurbis, C. and Masliyah, J. H., *Ind. Eng. Chem. Res.*, 36, 2634-2640(1997).

Chapter 4

Characterization Techniques

Contents

4.1 Introduction

The characterization techniques used in this work can be classified into wettability (contact angle, surface tension and partition), infrared spectroscopy, pore structure (pressure drop) and bubble size (bubble viewer methods). Each technique is described.

4.2 Contact angle

4.2.1 Washburn method

When a liquid contacts a capillary with a contact angle less than 90°, the liquid will rise into the capillary (by capillary force). The Washburn method[1], also called capillary rise method, is based on the Washburn equation for liquid penetration into a packed powder column or porous media. Washburn method monitors the weight change of liquid as liquid rises[2,3]. If the sample is powder, this approach needs minimal sample preparation and the powder can be kept in its original form after being packed into a sample cell. If the sample is a porous material it can be used directly (with certain shape restrictions).

Figure 4.1 shows a typical experimental setup for a powder sample. The sample is packed into a tube connected to an electronic balance. The bottom of the tube is a piece of fritted glass. When the tube is brought to touch the surface of the probing liquid, the liquid penetrates through the glass frit and rises into the powder bed under capillary attraction. An electronic balance records the weight change with time. The experimental data are analyzed using the Washburn equation[4]

$$w^2 = \frac{C\rho^2\gamma\cos\theta}{\mu} \bullet t \qquad (4.1)$$

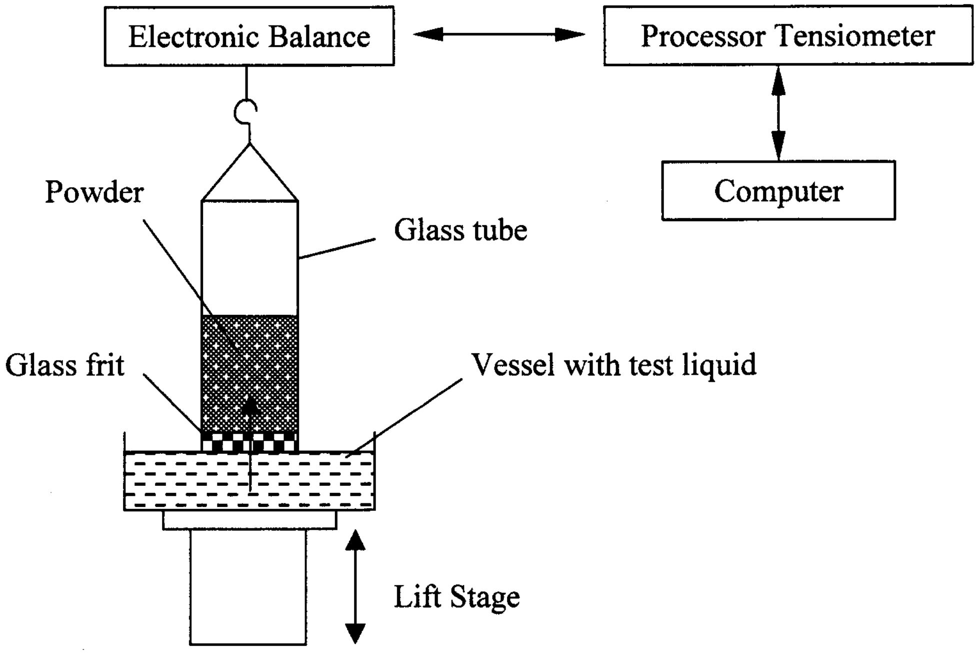

Figure 4.1: - Schematic of Washburn (capillary rise) method

where w is the weight of the liquid that has penetrated into the powder bed after time t; ρ, μ and γ are the density, viscosity and surface tension of the liquid, respectively. The constant C is determined collectively by particle size, shape and packing density (or the pore size and number in case of the sparger), and is determined using a reference liquid which completely wets the powder sample, i.e., a zero contact angle

$$C = \frac{w_r^2}{t_r} \bullet \frac{\mu_r}{\rho_r^2 \gamma_r} \tag{4.2}$$

where subscript *r* refers to reference liquid. From Eqs. (4.1) and (4.2), the contact angle of the test liquid can be calculated by

$$\cos\theta = \frac{w_p^2}{t_p} \bullet \frac{\mu_p}{C\rho_p^2\gamma_p} \tag{4.3}$$

where subscript *p* refers to the test liquid. A typical "wetting" curve is in Figure 4.2,

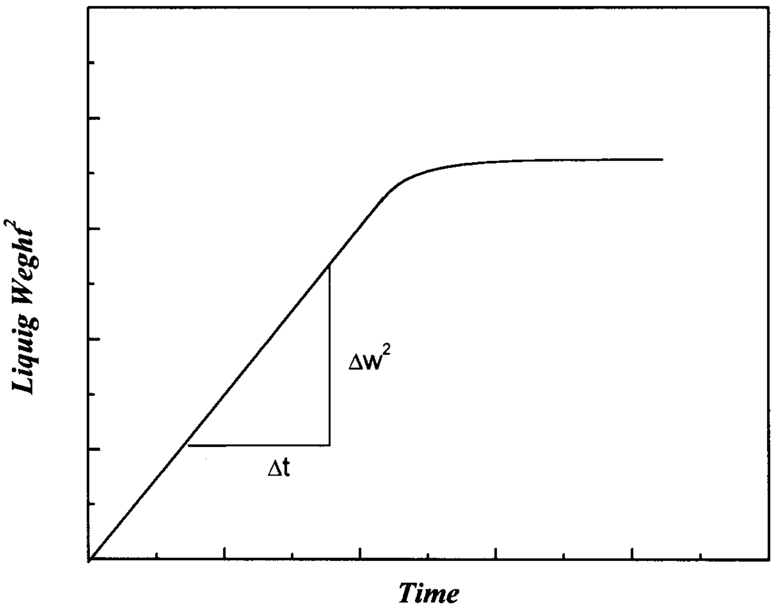

Figure 4.2: - Typical wetting curve using Washburn method

which shows that w^2 varies linearly with t at the early stage of penetration. The slope, $\Delta w^2/\Delta t$, over this period can be obtained and the contact angle calculated from Eq. (4.3).

The sample must have a contact angle less than 90° with the test liquid, otherwise there will be no liquid imbibition. In the case where θ larger than 90°, a modified Washburn or Wilhelmy method may be used.

4.2.2 Modified Washburn method

The modified Washburn method uses a two-liquid mixture as the test liquid[5]. As water cannot wet a highly hydrophobic surface, a lower surface tension liquid, e.g. ethanol (γ=22.4 mN/m)[6], is mixed with water to lower the surface tension. At a given ethanol content, the mixture will be raised into the sample by capillary force. A series of ethanol-water mixtures are used as test liquids, and the same procedure as in the Washburn method is applied. The resulting contact angle vs. ethanol content is plotted and extrapolated to zero ethanol content to yield the water contact angle.

4.2.3 Sessile drop method

Among the many methods of contact angle determination, the sessile drop technique[7,8,9,10] is one of the simplest. Here, a test liquid drop is placed on a solid surface, as shown in Figure 2.1. The contact angle θ is determined directly by a protractor eyepiece on a goniometer or by photographing the drop and measuring the angle on the image. Recently, image digitization combined with curve fitting has improved the reliability of the method[11].

The sessile drop method is restricted to contact angle measurements on well-defined (i.e. smooth, homogeneous and non-deformable) surfaces, such as polymer films. In the case of sufficiently small particles, such as the fine particles of interest here, a smooth deposit on a flat substrate might be achieved and then this technique could be used. The sessile drop method does allow contact angle measurement of one liquid in the presence of another[12]. This is potentially attractive in the present context where the fine solids of the rag layer retains both water and diluent liquids.

4.3 Surface tension

Many methods have been developed to measure the surface tension of a liquid, including du Nouy Ring, Axisymmetric drop shape analysis (ADSA) and Wilhelmy plate methods. The Ring method measures the force on a metal or plastic ring immersed in the test liquid[13,14,15]. Axisymmetric drop shape analysis determines the interfacial tension from the analysis of the meniscus shape of sessile or pendent drops[16,17,18].

The Wilhelmy plate method exploits the theory of capillary force. In this method, a plate is connected to an electronic balance (Figure 4.3), and the test liquid contained in a vessel is raised by a motor-driven platform. While the sample is immersing in the liquid, the electronic balance records the force applied. The force F measured is a summation of the gravity force on the plate (mg), the buoyancy imposed by the liquid ($lda\rho$) and the capillary force ($2(l+a)\gamma\cos\theta$), i.e.

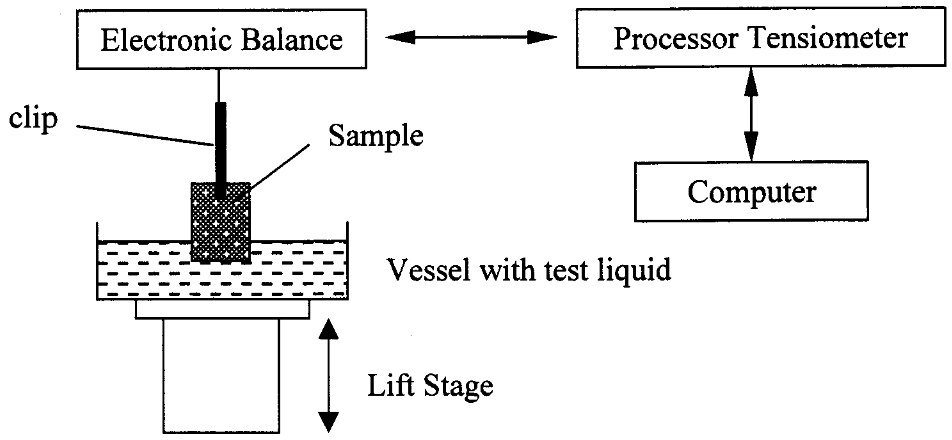

Figure 4.3: - Schematic of Wilhelmy plate method

$$F = mg - ld a\rho + 2(l + a)\gamma \cos\theta \qquad (4.4)$$

where m is the mass of the sample, g the acceleration of gravity, l the width of the plate, a the thickness of the plate, d the immersion depth, ρ the density of the liquid, γ the surface tension of the liquid, and θ the contact angle. Generally, the electronic balance tares the reading to zero before the plate contacts the liquid to eliminate the gravity force mg, and the plate is roughened to ensure the contact angle is zero. Then the capillary force F can be obtained by reducing Eq. (4.4) to

$$F = 2(l + a)\gamma - ld a\rho \qquad (4.5)$$

from which the surface tension γ is calculated by measuring F. This method has proved highly reproducible[19,20]. It was used to measure the surface tension of the liquids in this work.

4.4 Partition

The partition technique is used to characterize the hydrophobicity of solids by determining fractions in an organic and aqueous phase, respectively. The fine solids are placed in an organic-aqueous mixture, shaken rigorously and conditioned for a given period of time. The hydrophobic components collect in the organic phase while the

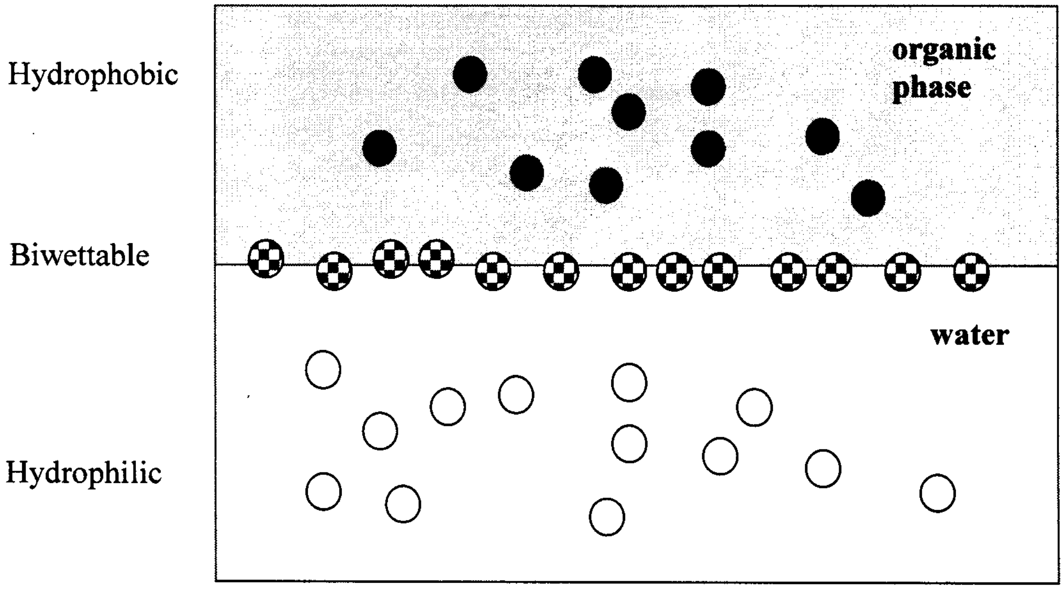

Figure 4.4: - Schematic of partition method

hydrophilic ones collect in the aqueous phase (Figure 4.4). Some particles tend to accumulate in the interphase region and are referred to as "biwettable" particles. The amount of the solids in each phase is evaluated.

4.5 Infrared Spectroscopy

4.5.1 Infrared spectroscopy

To understand the nature of wetting, it would be useful to know the surface chemical characteristics. For this purpose, infrared spectroscopy provides some answers. Infrared Spectroscopy (IR) refers broadly to the part of the electromagnetic spectrum between the visible and microwave regions. Infrared radiation in the range from about 10,000-100cm^{-1} is absorbed and converted by molecules into energy of molecular vibrations, resulting in an infrared spectrum.

Not all molecular vibrations can be detected. To be infrared active, a vibration must produce a net change in the dipole moment of the molecule, which means that symmetrical vibrations are weak or invisible in IR[21].

One of the vibrations between two atoms connected by a chemical bond (e.g. as in the molecule CO) is due to stretching, the bond length alternately increases and shortens. In this case, the frequency (ω) of the vibration can be related to the mass (μ_m) of the atoms and the strength of the bond (defined by the force constant, k_m) by the following relation:

$$\omega = \frac{1}{2\pi}\sqrt{\frac{k_m}{\mu_m}} \tag{4.7}$$

It is clear in Eq. (4.7) that as the strength of the bond increases, the frequency of the vibration increases, and as the mass of the atoms increases the frequency decreases. The frequency of the vibration, therefore, is sensitive to k_m and μ_m[22,23].

Bending is another type of molecular vibration, consisting of a change in bond angle between atoms in one group or a movement of one group of atoms with respect to the remainder of the molecule. For example, twisting, rocking, and torsional vibrations involve a change in bond angles (with reference to a set of coordinates arbitrarily established within the molecule).

4.5.2 Diffuse reflectance infrared Fourier-Transform spectroscopy (DRIFTS)

DRIFTS allows for a rapid analysis of powder samples, paper, cloth, or simple chunks[24]. Dilution of the sample by a non-adsorbing matrix is usually required to reduce spectral distortions caused by the mixing of reflectance components of the measured radiation. In addition, multiple scans and the use of a sensitive detector such as mercury cadmium telluride (MCT) are employed to increase signal-to-noise ratio in a highly adsorbing sample.

Three types of reflectance occur when a beam of infrared radiation is focused onto the surface of a sample consisting of discrete particles (Figure 4.5). True specular reflectance occurs when the incident ray angle is equivalent to the reflected angle. Diffuse specular reflectance is characteristic of a ray which has undergone multiple "mirror like" reflections within the sample, which may ultimately emerge at any angle relative to the incident radiation. Both true specular and diffuse specular rays are not absorbed by the sample (Figure 4.5). The ray labeled as absorption/reflection has, as the name indicates, been reflected within the sample and was adsorbed by the sample. Only this ray contains information about the absorptivity (α) of the sample. This absorption/reflection radiation is eventually diffused and scattered from the sample where it is collected and focused onto a detector.

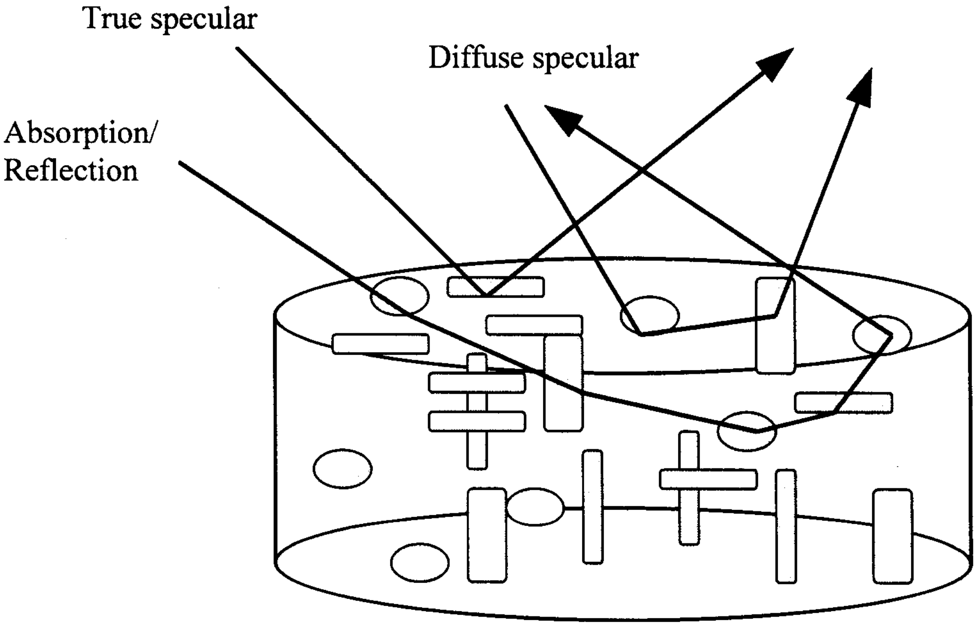

Figure 4.5: - Three types of reflection from a powder surface in DRIFTS

A general theory for diffuse reflectance from powder samples was developed by Kubelka and Munk[25]. This theory relates sample concentration and scattered radiation intensity. For an infinitely thick layer, the Kubelka Munk (KM) equation is

$$f(R_\infty) = \frac{(1-R_\infty)^2}{2R_\infty} = \frac{k}{s} = \frac{c}{k'} \tag{4.8}$$

where R_∞ is the absolute reflectance of the layer, s a scattering coefficient, k the molar absorption coefficient, c the concentration of the sample, and $k' = s/2.030e$.

4.6 Pore structure

A rigid porous sparger contains many interconnected pores. The pore structure (i.e. pore size and density) can be characterized by permeability, which measures the capacity of a porous medium to transport fluids (or the reciprocal of the resistance of the porous medium to fluid flow). For the rigid porous cylindrical sparger used here with an incompressible fluid, the permeability (P_k) is given by[26]

$$P_k = \frac{q_m^n \mu}{2\pi L_s (P_i - P_o)} \ln \frac{r_o}{r_i} \tag{4.9}$$

where q_m is the flowrate of the fluid used, L_s the sparger length, P_i and P_o the pressure inside and outside the sparger, respectively, and r_i and r_o the inner and outer radius of the sparger, respectively.

The pore structure will be reflected in the magnitude of $(P_i\text{-}P_o)$, other factors remaining the same. If $(P_i\text{-}P_o)$ at the same fluid flowrate does not change before and after surface

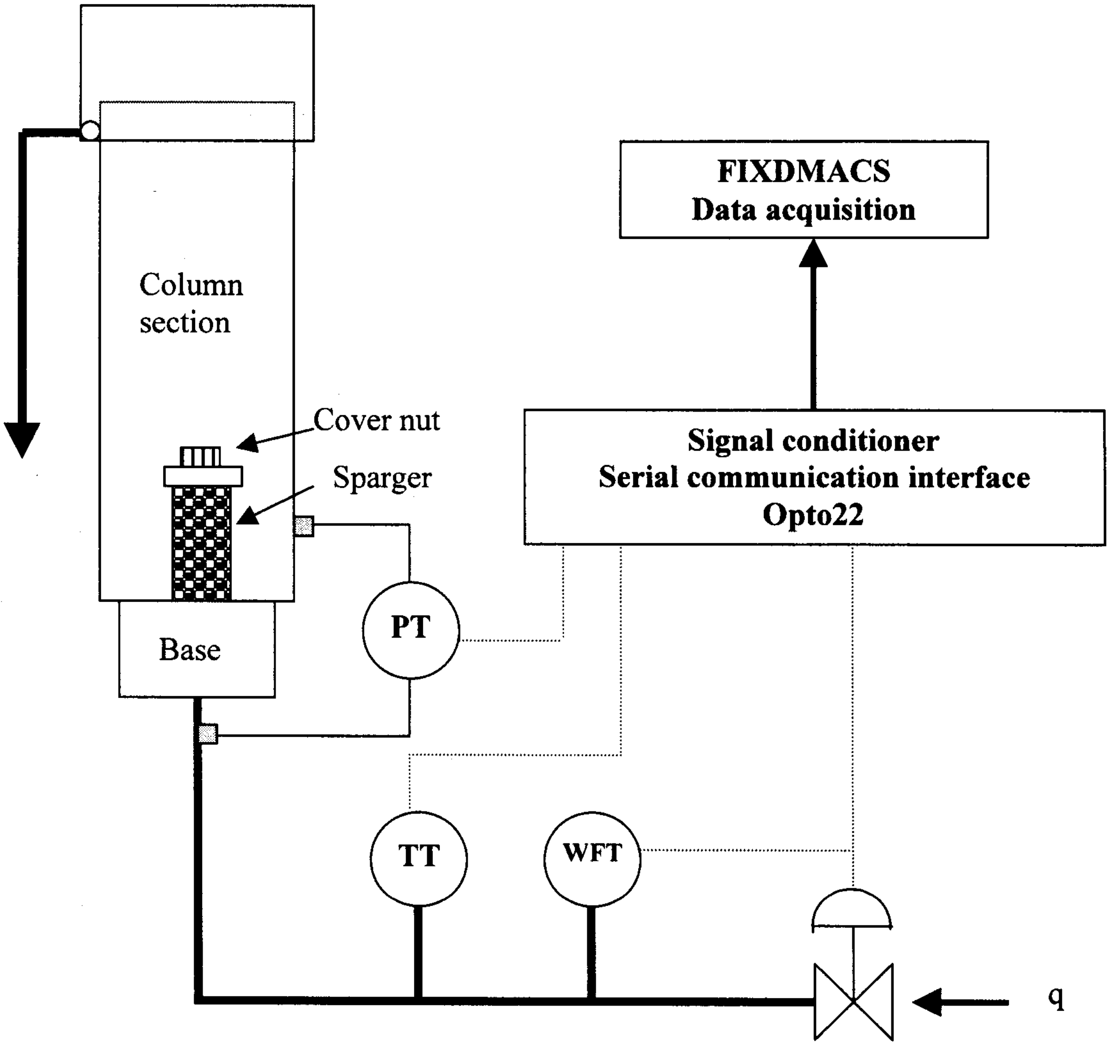

Figure 4.6: - Experimental setup for pore structure test

modification designed to alter wettability (as will be attempted in this thesis), it can be claimed that pore structure is the same before and after modification. Figure 4.6 is the schematic of the setup for the (P_i-P_o) measurement.

4.7 Bubble size measurement

The bubble size measurement used in this work was the bubble viewer method[27]. The bubble viewer (Figure 4.7) used here consists of a viewing chamber made of Plexiglas, and a buffer cylinder, tube and cap made of PVC. The chamber is 16.5cm wide, 20cm

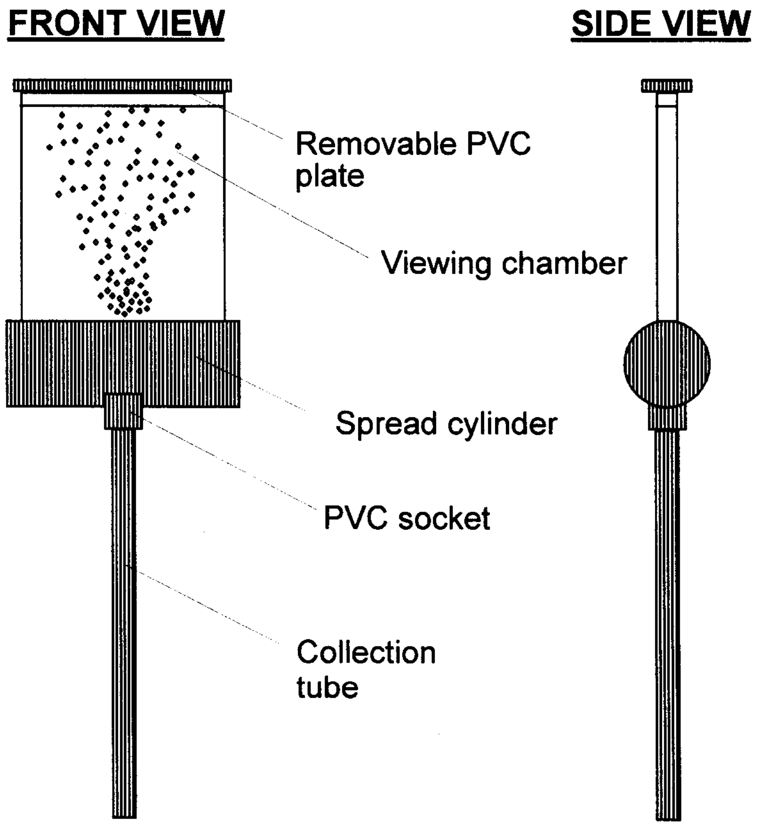

Figure 4.7: - Bubble viewer

high and 1cm think, while the tube is 80cm long and has an inner diameter of 1.27cm. The chamber and the tube are connected by the buffer cylinder (5cm in diameter). The cylinder helped to spread the bubbles across the chamber to reduce overlap.

Prior to sampling, frother solution was placed in the bubble viewer (it was inverted and filled via the tube). It was tapped to remove bubbles adhering to the walls. The camcorder was adjusted to the sampling plane by focusing on a 1mm diameter copper wire. A plug was placed on the tube end and the viewer was placed vertically in a bubble column. The plug was removed and bubbles were sampled into the viewing chamber. The bubbles in the viewer were imaged by a camcorder at a shutter speed 1/500-600. As the bubbles burst and air accumulated, the liquid level was pushed down. The air was allowed to accumulate at the top of the chamber as there was no discernable effect on the bubble size.

The bubble image was analyzed by Scion Image analysis software (USA). The diameter of the bubble was measured and compared to that of the reference wire to yield bubble diameter using

$$Bubble\ diameter = \frac{Diameter\ of\ reference\ wire \times Diameter\ of\ bubble\ image}{Diameter\ of\ reference\ wire\ image} \tag{4.10}$$

References

---

1 Washburn, E.W., _Physical Review_, 17(3), 273-283(1921).

2 Alain Siebold ect., _Journal of Colloid and Interface Science_, 186, 60-70(1997).

3 Ayala,E., Casassa, E. Z. and Parfitt,G. D. _Powder Technology_, 51, 3-14(1987).

4 Siebold, A., Walliser, A., Nardin, M., Oppliger, M. and Sshultz, J. _Journal of Colloid and Interface Science_, 186, 60-70(1997).

5 Hansford, D.T, Grant, D.J.W. and Newton, J.M., _J.C.S. Faraday I_, 76, 2417-2431(1980).

6 Jasper, J.J., _J. Phys. Chem. Ref. Data_, 1, 841(1972).

[7] Kossen, W. K. and Heertjes, P. M., _Chem. Eng. Sci._, 20, 593(1965).

[8] Heertjes, M., and Kossen, N. W. K., _Powder Technol._, 1, 33(1967).

[9] Matijevic, E., _Surface and colloid Sci._, Volume 2, New York, John Wiley & Sons, Inc., p. 115, 1969.

[10] Cordeiro, N., Autenty, P., Belgacem, M. N., Gandina, A. and Neto, C. P., _Journal of Colloid and Interface Science_, 187, 498(1997).

[11] Lahooti S., Del., R. O. I. Neumann, A. W. and Cheng, P., Axisymmetric Drop Shape Analysis(ADSA), in _Applied surface thermodynamics_, Surfactant Science Series, Volume 63, Ed: Neumann, A. W. and Spelt, J. K, New York, Marcel Dekker, Inc., pp. 441-508, 1996.

[12] Johnson Jr. Rulon E. and Dettre R. H., Wetting of Low-Energy Surfaces, in _Wettability_, Surfactant Science Series, Volume 49, Ed: J. C. Berg, , New York, Marcel Dekker Inc., pp. 1-73, 1993.

[13] P. Lecomte du Nouy, _J. Gen, Physiol._, 1, 521(1919).

[14] Harkins, W.D. and Jordan, H. F., _J. Am. Chem. Soc._, 52, 1751(1930).

[15] Huh, C. and Mason, S. G. _Colloid Polym. Sci._, 253, 566(1975).

[16] Kwok, D.Y., Hui, W. and Neumann, A.W., _Langmuir_, 11, 2669(1995).

[17] Rotenberg, Y., Boruvka, L. and Neumann, _Journal of Colloid and Interface Science_, 93, 169(1983).

[18] Cheng, P., Li, D., Boruvka, L., Rotenberg, Y. and Neumann, A.W., _Colloids and Surfaces_, 43, 151(1990).

---

[19] Martin David A. and Vogler Erwin A., *Langmuir*, 7, 422-429(1991).

[20] Vogler E. A., Spencer, K. B. and Montgomery, D. B., *Langmuir*, 9, 2470(1993).

[21] Jones, M., *Organic Chemistry*, New York, W.W.Norton & Company, Inc., p. 699, 1997.

[22] Skoog, D.A., West, D.M., in *Principles of Instrumental Analysis*, 2nd edition, Saunders College, USA, 1980.

[23] Loudon, G.M., in *Organic Chemistry*, 2nd edition, Benjamin/Cummings, USA, 1988.

[24] Fuller, M.P., Griffiths, P.R., *American Laboratory*, 69-80, (October, 1978).

[25] Fuller, M.P., Griffiths, P.R., *Analytical Chemistry*, 50(30), 1906(1978).

[26] Escudero, R., Ph.D. Thesis, *Characterization of Rigid Spargers and Their Selection for Flotation Columns*, Montreal, McGill University, 1998.

[27] Chen, F., Finch, J.A. and Gomez, C.O., Technical Note: Bubble Size Measurement with Bubble Viewer, *Minerals Engineering*, 14(4), 427-432(2001).

Chapter 5

Role of Solid Wettability on Bubble Generation from Porous Media

Contents

Abstract

The role of solid wettability on bubble formation was examined using three rigid spargers with water contact angles 0, 64 and >90°. The contact angles, varied by heating the sparger material, were determined by the Washburn and modified Washburn methods. It was confirmed by permeability measurement that the heating had no effect on pore structure. The results showed no effect of sparger wettability on the size of bubble produced. The bubble size can be calculated assuming the contact angle is zero in the Kumar and Kuloor model using the concept of equivalent pore diameter.

5.1 Introduction

In some adsorptive bubble reactors, bubbles are generated by rigid porous spargers. They are extensively used in laboratory flotation columns, for instance, and periodically, in industrial flotation columns, most notably in de-inking and de-oiling applications. The sparger material can be ceramic or metal, including stainless steel.

Bubble formation at a rigid sparger depends on design parameters including pore geometry, orientation, shape, density (number per unit area) and surface properties, and on operational parameters such as air flowrate and the surfactant type and concentration. The wettability effect is controlled through the surface tension of the liquid and the contact angle at the orifice as the bubble forms. The resultant capillary force varies with the contact angle, i.e., the wettability of the orifice. The capillary force in bubble formation at a vertical orifice (i.e., the capillary is vertical) is

$$F_s = \pi D \gamma_{\mathrm{lg}} \cos\theta \tag{5.1}$$

where D is the diameter of the orifice, γ_{lg} the surface tension of the liquid, and θ the contact angle measured through the liquid phase at the three-phase contact point.

Although a possible wettability effect on bubble formation has long been recognized, it is generally ignored and the contact angle assumed to be zero[1,2,3]. But it has been shown[4] that the bubble size can vary with contact angle on a smooth orifice surface, and thus the contact angle should be considered.

Bubble size prediction models considering a wettability effect have been devised based on various assumptions and conditions. For a single orifice, at low air flowrate, it was assumed that the bubbles were at all times spherical while they formed, and were subjected only to the surface tension force and buoyancy in the case of low viscosity liquids. The bubbles would detach as soon as these forces were balanced[1]. It was shown[5] that in a low viscosity liquid at large flowrate, the surface tension force can be neglected, and the inertia force should be considered. In this case, the bubble volume was

$$V = 1.378 \frac{Q^{6/5}}{g^{3/5}} \tag{5.2}$$

where Q is air flowrate, and g the gravity acceleration. Different values of the numerical coefficient in Eq. (5.2) have been reported[6,7,8]. More general models were developed for a single orifice under constant flowrate conditions[9,10], considering surface tension, drag, inertia and buoyancy. In these models, it is assumed that the bubble formation experiences two stages: an expansion stage and detachment stage. It was found[10] that a similar equation to Eq. (5.2) can be deduced from one of these models with numerical coefficient 0.976 by neglecting small terms, with an error of ca. 30%. It was also observed that the surface tension force had an effect on bubble size, but the effect vanished at high gas flowrate. Other models for constant pressure[11], elevated pressure[12], flowing liquid[13], and high density gas[14] conditions with/without consideration of wettability have also been developed.

From a practical point of view, bubble formation models for a single orifice must be extended to multiple orifices. One attempt[15] for a porous disk was based on the assumption that the orifices produced bubbles independently in the two stages, and the bubbles produced were in hexagonal close packing. Good agreement was found between the experimental and model predicted data using a disc with orifice diameter 110μm and 45μm over a range of air flowrate and liquid viscosity. It was concluded that the surface tension of liquid affected bubble size at low air flowrate, and this effect decreased as the flowrate increased.

A similar but more rigorous model was proposed by Kumar and Kuloor[10]. This model was recently used to predict the size of bubble produced by a cylindrical rigid porous SS sparger of the type used here by combining the Kumar and Kuloor model with drift flux analysis[16]. This approach was tested against experimental data assuming zero contact angle in the model.

The orientation of an orifice was also found to have an effect on the bubble size. The bubbles generated at vertical orifices appeared to be larger than those at horizontal orifices[1], but a later report showed that the bubble size did not decrease continuously with increasing angle of orientation[10]. This observation was recently explained by the assumption of expanding bubble contact base[17]. In our laboratory, no effect of orientation was found for the sparger to be used in this thesis.

The literature review showed there has been no work on the effect of wettability on the size of bubble produced at a rigid porous sparger. This deficiency is now addressed.

5.2 Kumar and Kuloor models

Among the models, those of Kumar and Kuloor were found to be suitable to describe the process of bubble formation at orifices in a rigid sparger[16]. The models assume a two stage bubble formation process at each orifice. During the first stage, the bubble expands at a definite rate thereby increasing the inertial force and viscous drag force. This stage ends as soon as the upward forces overcome the downward forces. From the force balance, at the end of the first stage, *V*=V_{fb}, yields the bubble volume (first introduced in Chapter 3, and details in Appendix A)

$$V_{fb}^{5/3} - \frac{\pi D\gamma\cos\theta}{g\rho_l}V_{fb}^{2/3} - \frac{3\mu Q}{2\cdot\left(\frac{3}{4\pi}\right)^{1/3}\cdot g\rho_l}V_{fb}^{1/3} - \frac{11Q^2}{192\pi\left(\frac{3}{4\pi}\right)^{2/3}\cdot g} = 0 \qquad (5.3)$$

The second stage begins at the moment when the upward forces are larger than the downward forces. The bubble moves away from the orifice with a cylindrical neck connecting to the orifice while it expands. It is assumed to detach when the vertical displacement is r_{fb}, the radius from the first stage. The bubble size at the end of the second stage is

$$\begin{aligned}&\frac{B}{2Q(A+1)}V_F^{6/3} - \frac{E}{AQ}V_F^{3/3} - \frac{3C}{2Q(A-1/3)}V_F^{2/3} + \\ &\left(-\frac{B}{2Q(A+1)}V_{fb}^2 + \frac{E}{AQ}V_{fb} + \frac{3C}{2Q(A-1/3)}V_{fb}^{2/3} - \left(\frac{3}{4\pi}V_{fb}\right)^{1/3}\right) = 0\end{aligned} \qquad (5.4)$$

with

$$A = 1 + \frac{1.25\cdot 6\pi\cdot\left(\frac{3}{4\pi}\right)^{1/3}V_{fb}^{1/3}\mu}{Q\cdot\left[\rho_g + \frac{11\rho_l}{16}\right]} \approx 1 + \frac{1.25\cdot 96\cdot\pi\cdot r_{fb}\mu}{11\rho_l\cdot Q} \qquad (5.5)$$

$$B = \frac{(\rho_l - \rho_g) \cdot g}{Q \cdot \left[\rho_g + \frac{11\rho_l}{16} \right]} \approx \frac{16 \cdot g}{11 \cdot Q} \tag{5.6}$$

$$C = \frac{3\mu}{2 \cdot \left(\frac{3}{4 \cdot \pi} \right)^{1/3} \left[\rho_g + \frac{11\rho_l}{16} \right]} \tag{5.7}$$

$$E = \frac{\pi D \gamma \cos\theta}{Q \cdot \left[\rho_g + \frac{11\rho_l}{16} \right]} \approx \frac{16\pi D \gamma \cos\theta}{11 Q \rho_l} \tag{5.8}$$

For a sintered disk with a large number of orifices, only some are active in producing bubbles. The bubbles forming at the orifice are in contact with each other, which imposes space restriction; bubbles produced are assumed to be closely packed into hexagonal arrays. As a consequence, as bubble size increases with increasing gas rate, the number of active sites decreases. The number of active sites per unit area *n* is

$$n = \frac{(\frac{3}{4\pi} V_{F|Q})^{-2/3}}{2\sqrt{3}} = \frac{1}{2\sqrt{3} \cdot (\frac{3}{4\pi} V_{F|Q})^{2/3}} \tag{5.9}$$

where $V_{F|Q}$ bubble volume. Letting A_s be the surface area of the porous media, then for each orifice, the gas flowrate is

$$Q = \frac{q}{nA_S} \qquad (5.10)$$

where q is the total gas flowrate, and Q the gas flowrate through a single orifice. The combination of Eqs. (5.3), (5.4), (5.9) and (5.10) can be used to estimate V_F or the bubble diameter D_b.

It is difficult to measure the pore diameter exactly because of irregular shape of the orifices in the sparger surface. Methods to determine an equivalent pore diameter of a sparger D_e were proposed by Escudero[16] and Gomez et al.[18] In one approach, measured bubble size (from image analysis) is compared with that predicted by the Kumar and Kuloor model for a given D_e which is searched till the predicted matches the measured bubble size; the D_e when the match is struck is the sparger equivalent pore diameter. The equivalent pore diameter was used to predict bubble size or gas holdup by a combination of Kumar and Kuloor model and drift flux analysis. One outcome was a set of sparger selection criteria for use in flotation columns[16].

5.3 Experimental setup

5.3.1 Modification of sparger wettability

The spargers tubes used were from Mott Co. They were 2.54cm outer-diameter and 1.90cm inner-diameter, and were cut into 6.0cm long sections. The nominal pore size, as quoted by the manufacturer, was 10μm.

The modification of sparger wettability was by heating. The spargers were placed in a ceramic bowl, and heated in a furnace at a set temperature (105, 200 and 300°C) for a desired period of time. They were cooled to room temperature in air prior to use. The furnace was from Linberg, General Signal Co. (Watertown, Wisconsin, USA).

5.3.2 Characterization

5.3.2.1 Contact angle

The contact angle of the sparger material was determined by the Washburn and modified Washburn methods. The two test liquids were solutions of 30ppm DOW 250C frother in tap water (surface tension 62.0 mN/m), and Milli-Q water (surface tension 72.3mN/m, from Department of Chemistry, McGill University). The reference liquid was hexane (95+% with water less than 0.02%, from Aldrich Inc, surface tension 18.2mN/m). A K12 tensiometer from Kruss Co., USA, was the instrument used.

After many trials to obtain reproducible results, the following procedure was adopted. The sparger was cleaned by toluene for 3 minutes in an ultrasonic bath, then was placed on a cleaned culture disk, and put into the oven and dried at 105°C for 20 minutes, followed by cooling to room temperature. It was then cleaned 2 times in the ultrasonic bath with Milli-Q water, put into the oven and dried at 105°C for 60 minutes, then cooled to room temperature. Between each experiment, it was cleaned in the ultrasonic bath for 3 minutes in Milli-Q water and dried at 105°C for 60 minutes. The sparger was then cleaned in methanol (99.93%, HPLC grade, from Aldrich) in the ultrasonic bath for 1 minute to discharge any static charge and dried at 105°C for 15 minutes. Finally, it was cleaned in toluene for 3 minutes in the ultrasonic bath, and dried at 105°C for 15 minutes.

In the contact angle measurement, hexane was placed in the vessel held on the movable platform of the tensiometer. The sparger was attached to the electronic balance and the measurement started (Figure 4.3). After this, the hexane was changed for water, ethanol-water, or frother solution and the same procedure applied. The contact angle was calculated. At least three measurements were performed for each liquid with each sparger.

5.3.2.2 Pore structure

The integrity of the pore structure was checked by determining the pressure drop across a sample of sparger as a function of water flowrate. Figure 4.6 is the schematic of the setup used for the measurements. The PT is a differential pressure transducer (Bailey, Model PTSDDD1221B2100). The temperature is monitored by an ICTD temperature transducer (TT, from Transduction Ltd., model ICTDP/N1662). The water flowrate was recorded by a magnetic flowmeter (WFT, Bailey, model 10D1475PNO7PL29AY11C1112C1C81). The base that supports the sparger was mounted in an acrylic tube. The sparger was fixed and sealed at the top using a cover nut. After the pressure transducer was tared to zero, pressure was recorded (by PT) as a function of increasing water flowrate (recorded by WFT). The temperature was recorded by TT.

All the instruments were connected to an interface and signal conditioner (Transduction Ltd., model Opto22). The signal output from Opto22 was monitored and sampled over an interval of 2 seconds with an interface board and FIX32 (Intellution, MMI version 6.15) installed in a PC. Five readings were taken for each flowrate. Each experiment was performed three times to test reproducibility. The mean and 95% confidence are reported.

5.3.3 Bubble generation

The sparger was placed in a column, 10.15cm (4inch) inner diameter and total height 4m (Figure 5.1). The variables monitored were air flowrate q (L/min), temperature inside the system T (°C), and pressure near the sparger p (cmH_2O). The pressure was measured by a differential pressure transducer PT (Bailey, Model PTSDDD); the temperature was monitored by an ICTD temperature detector (Transduction Ltd.); and air flowrate was recorded (and controlled) by a mass flowmeter transducer/controller MFT (MKS Instruments, model 1562). The 30ppm DOW 250C frother solution was used as the liquid phase.

All the instruments were connected to an interface and signal conditioner (Transduction Ltd., model Opto22). The signal output from Opto22 was monitored and sampled over an interval of 2 seconds via an interface board and FIX32 (Intellution, MMI version 6.15) installed in a PC.

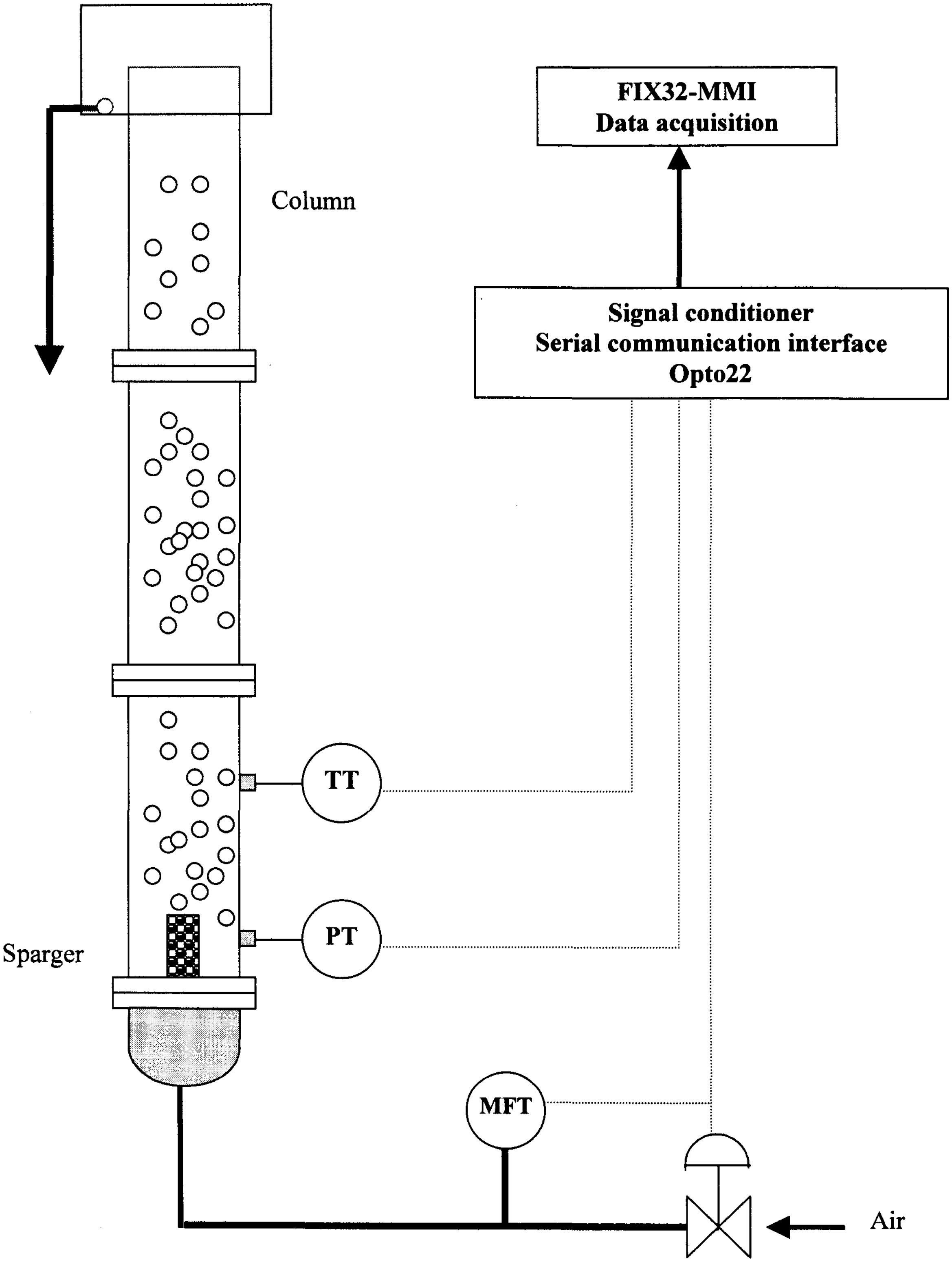

Figure 5.1: - Experimental setup for bubble generation

Air was introduced through the sparger placed vertically at the bottom of the column. When the system was stable, 5 readings were taken for each condition. Each experiment was performed three times to test reproducibility. The mean and 95% confidence interval are reported.

5.3.4 Bubble size measurement

Bubble size measurement was accomplished by a bubble viewer (Figure 4.7). The images on the videotape were sampled and transmitted to a PC as Windows bitmap format and were analyzed by Scion Image software, Version Beta 3b, Scion Co., USA. Bubbles overlapping by more than a quarter were ignored. The diameter of the bubbles was calculated by Eq. (4.10).

5.4 Results and discussion

5.4.1 Contact angle of spargers

5.4.1.1 Water contact angle before modification

Generally, the contact angle of a porous sample of regular shape is determined by the Washburn method. The test liquid rises into the capillaries in the porous material by surface tension force. The liquid weight in the sample as a function of time is recorded, and the contact angle is obtained by Eq. (4.3). If the contact angle is larger than 90°, the capillary force does not lift the liquid into the sample. Figure 5.2 is a typical water wetting curve of a stainless steel sparger. The water does not penetrate into the sparger indicating that the sparger is hydrophobic. In this case, the contact angle was determined by the modified Washburn method.

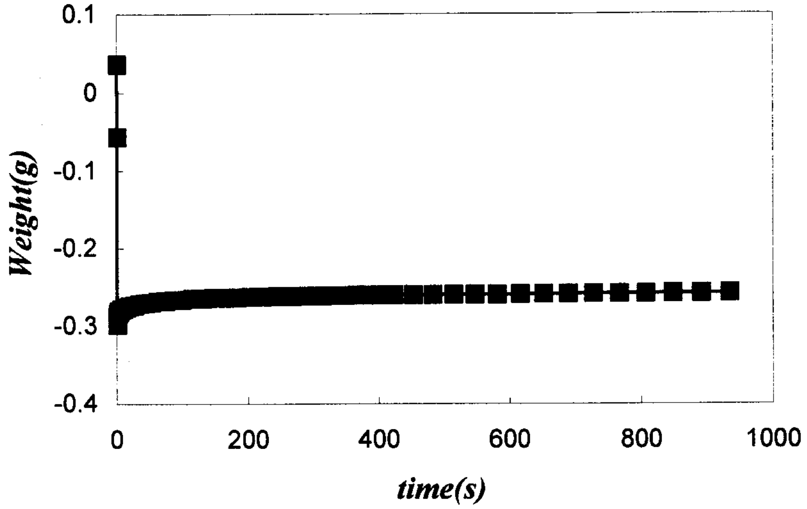

Figure 5.2: - Water wetting curve (Washburn method) of stainless steel sparger prior to modification

In the modified Washburn method, a two-liquid mixture (water-ethanol) was used. The constant C in Eq. (4.2) was obtained using hexane as reference liquid. The low surface tension of the ethanol-water mixture allowed liquid to rise into the sample capillaries. With solutions of varying ethanol content, a series of contact angle values were obtained. Figure 5.3 shows the surface tension of the solution as a function of ethanol content. The contact angle values measured with ethanol solution are shown in Figure 5.4. To obtain the water contact angle, the procedure is to extrapolate to zero ethanol content. The water contact angle is clearly >90°, but the value is difficult to estimate by extrapolation.

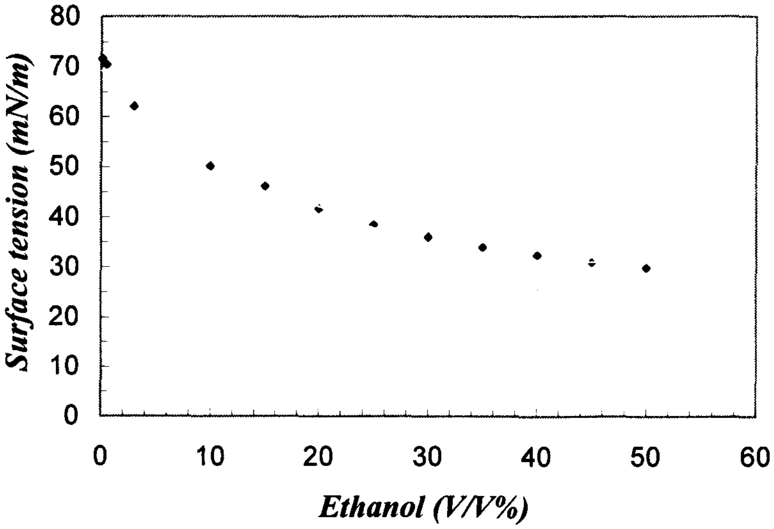

Figure 5.3: - The surface tension of ethanol-water solutions

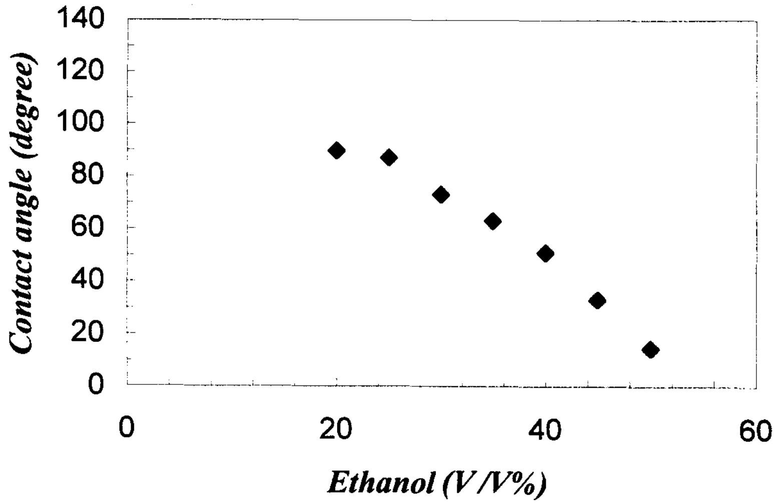

Figure 5.4: - The contact angle of stainless steel sparger measured using modified Washburn method with ethanol-water solutions

5.4.1.2 Water contact angle after modification

The decrease in contact angle depended on the temperature and time of heating. To help establish the heating range, the water contact angle measurement was performed on 316L stainless sheet (Wilhelmy plate method), and the results are shown in Figure 5.5. The contact angle decreased as the temperature increased, then rose above 450°. The experiments also indicated that temperature did not affect the wettability when the heating temperature was below 105°C. Based on these observations, the temperature range 105 - 300°C was chosen.

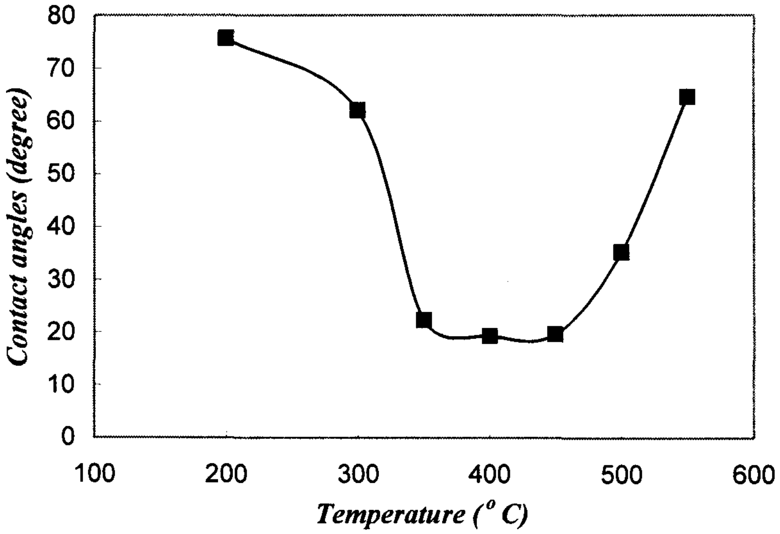

Figure 5.5: - Change of contact angle of stainless steel sheet with temperature

Table 5.1 lists the water contact angles of the sparger after heating. The sparger remained strongly hydrophobic up to 105°C (Figure 5.6, test using ethanol-water by modified Washburn method), and became hydrophilic (zero contact angle) after heating at 300°C.

Table 5.1 The water contact angles of stainless steel sparger as a function of heating temperature

Temperature($^{\circ}C$)	105	200	300
Time (min)	30	50	20
Contact angle (^{0})	>90	64	0

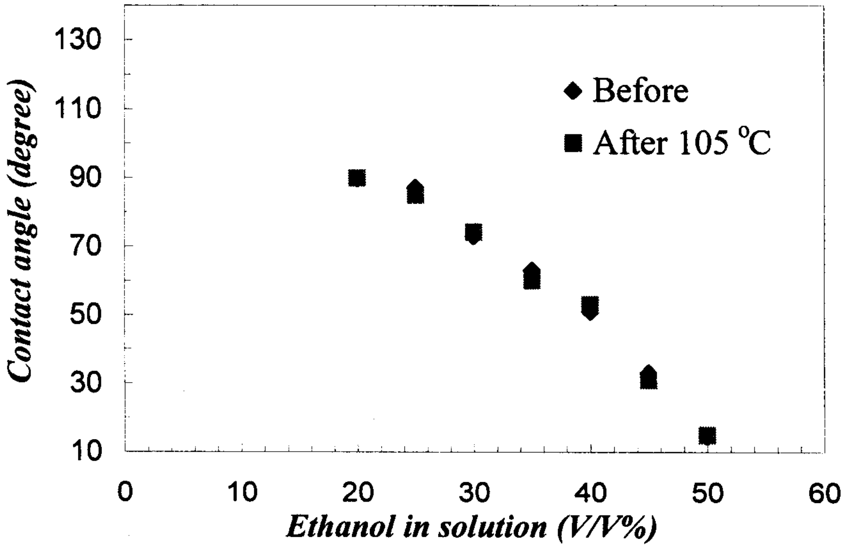

Figure 5.6: - Wettability of sparger before and after heating at 105°C.
Test liquid: ethanol-water mixture

5.4.1.3 Water contact angle after gas injection

Measurement of water contact angle was used to test any wettability change after the sparger was used for bubble generation. Table 5.2 shows the contact angle before and after 6 hours of bubbling in 30ppm 250C DOW frother solution. The constant contact angle established that use of the sparger did not affect the wetting properties.

Table 5.2 The contact angles of stainless steel sparger
before and after bubbling

Bubbling	Modification temperature (°C)		
	105	200	300
	Contact angle (°)		
Before	>90	64	0
After	>90	62	0

5.4.1.4 Solution contact angle

Since the spargers were operated in 30ppm frother solution, contact angles were measured in this solution and the values (Washburn method) are listed in Table 5.3. The magnitude is lower in these solutions than in water, and is referred to as "solution contact angle" to distinguish from the "water contact angle".

Table 5.3 The Contact angle of sparger in frother solution compared to water

Liquid	Modification temperature (°C)		
	105	200	300
	Contact angle (°)		
Water	>90	64	0
Frother solution	66	41	0

5.4.2 Pore structure before and after modification

The pore structure should not be affected by heating in order to attribute any effects to wettability. The relative pressure drop across a sparger when a fluid is passed can be used to check for any change in the pore structure. Water was used as test fluid.

Figure 5.7 shows that the pressure drop vs. flowrate is the same for the three spargers before heat treatment. Figure 5.8 further shows that the variation of pressure drop and flowrate did not change after heat treatment. These observations indicate that the heat treatment did not change the pore structure. Further proof of this was obtained using the Washburn procedure. In Eq. (4.2), C is the capillary factor that includes the pore size and number of capillaries in a sparger (i.e., pore structure). Consequently, C should remain constant if pore structure is unaffected by the heat treatment. Hexane was used as a test liquid. The fact that the wetting kinetics remained the same before and after modification indicates that this capillary factor did not change (Figure 5.9).

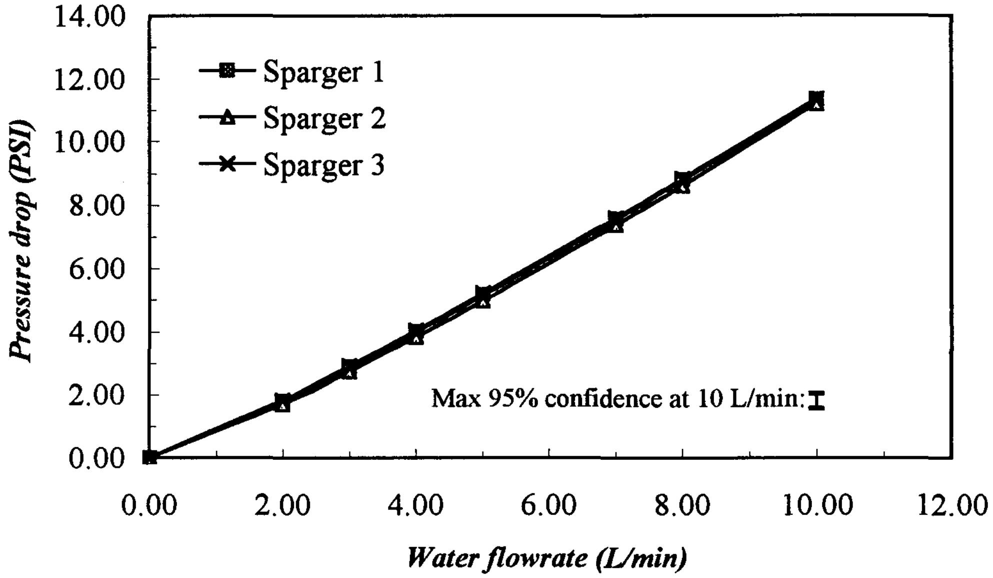

Figure 5.7: - Pore structure integrity test: pressure drop as a function of flowrate for three spargers before heat treatment

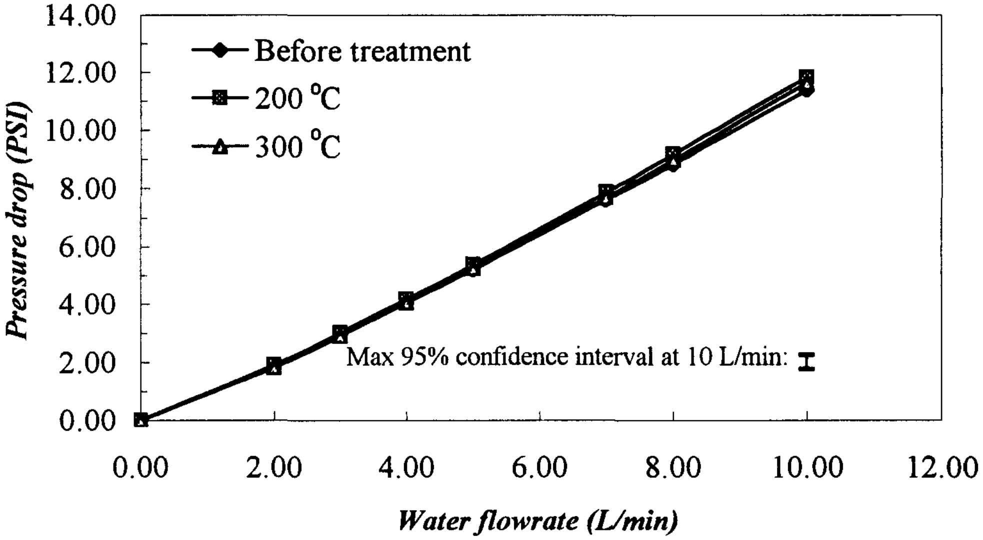

Figure 5.8: - Pore structure integrity test: pressure drop across the spargers as a function of water flowrate before and after modification

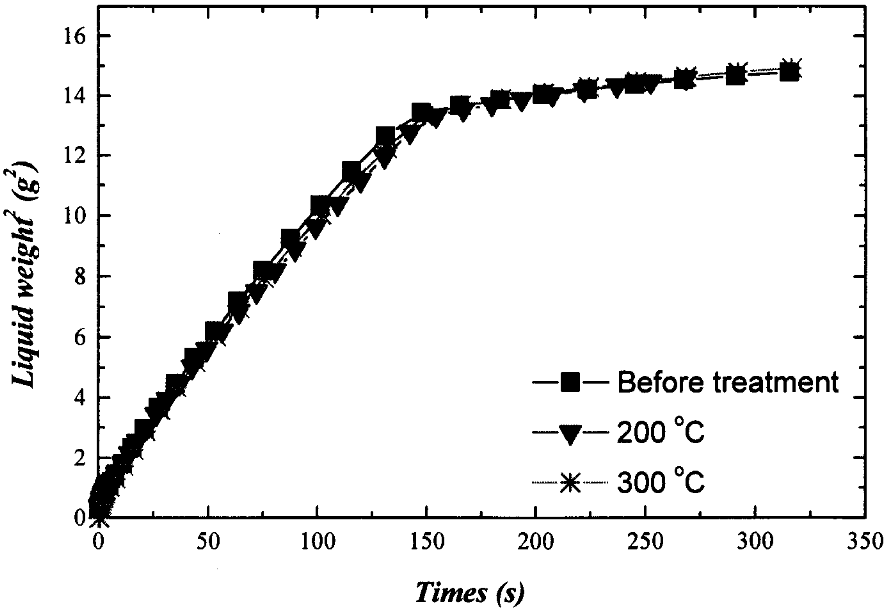

Figure 5.9: - Wetting curve (hexane) before and after modification

5.4.3 Bubble size

5.4.3.1 Air flowrate range

The choice of air flowrate here respected the typical range in column flotation, up to a superficial gas velocity, J_g, of ca. 2cm/s, where J_g is given by

$$J_g = \frac{q}{A_c} \tag{5.11}$$

and, q is air flowrate (cm^3/s), and A_c the cross section area of column (cm^2). Accordingly, as the column used here is 10.16cm (4inch) in diameter, the q (L/min) and the corresponding J_g are given in Table 5.4. Also included is air flowrate per unit area of sparger, J_a.

Table 5.4 Air flowrates q and corresponding J_g, J_a
(Sparger surface area: 47.9cm^2)

Air flowrate q (L/min)	0.776	2.383	4.034	7.637
J_g (cm/s)	0.160	0.490	0.829	1.570
J_a (cm/s)	0.270	0.829	1.404	2.657

5.4.3.2 Frother concentration

It is known that the frother concentration affects bubble size. By a combination of surface tension reduction (Figure 5.10) and retardation of coalescence, frother permits small bubbles to be generated and preserved[19]. Bubble sizes decrease with an increase in frother concentration up to a certain value (ca. 20ppm in case of DOW 250C, Figure 5.11)[20,21]. A 30ppm frother-water solution was used, minor changes in concentration (it tends to decrease) during the bubbling should have negligible impact on bubble size.

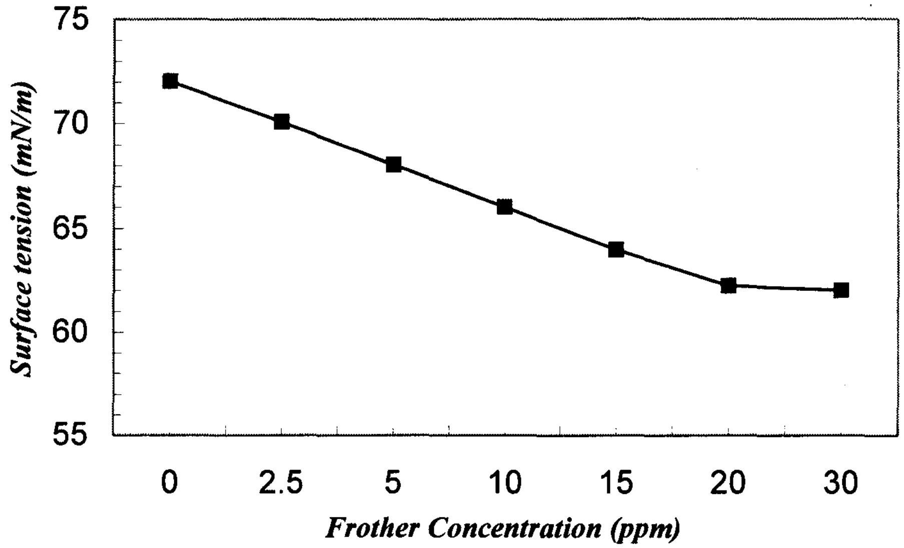

Figure 5.10: - Surface tension as a function of frother (DOW 250C) concentration

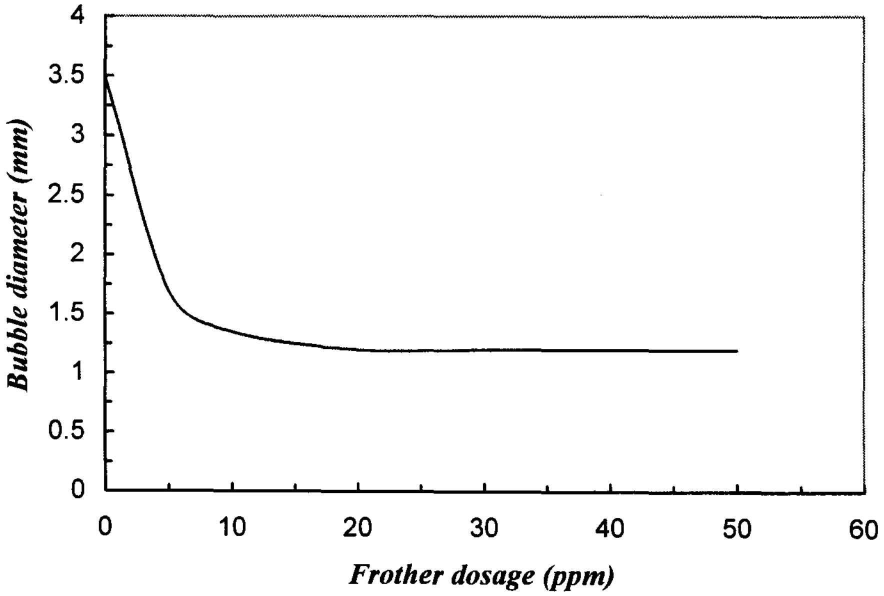

Figure 5.11: - Illustration of the effect of frother (DOW 250C) on size of bubble generated at a glass frit[20]

5.4.3.3 Size distribution

Figure 5.12 is a an image of bubbles generated at J_g=0.490cm/s in 30ppm DOW 250C solution using a sparger with a solution contact angle 66°. The bubbles were sampled by the bubble viewer from near the top of the column. Clearly, there is a distribution of bubble sizes, as evidenced in the histogram shown in Figure 5.13.

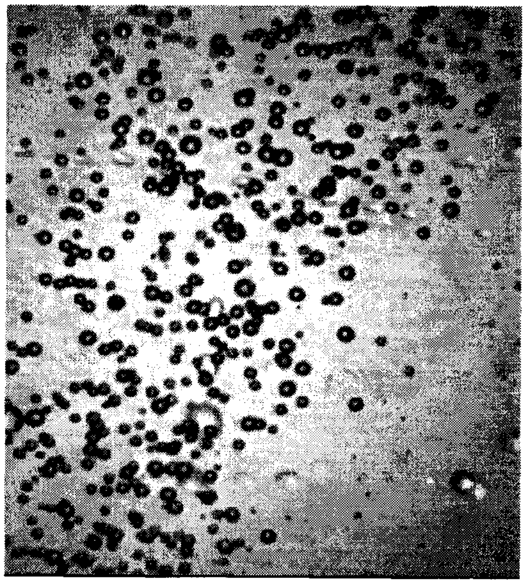

Figure 5.12: - Bubble image at the bubble viewer

Two mean sizes of a distribution are frequently computed, the number mean[22,23] and the Sauter mean[24]. The number mean is D_{10} calculated from

$$D_{10} = \sum \frac{n_i d_i}{n_i} \tag{5.12}$$

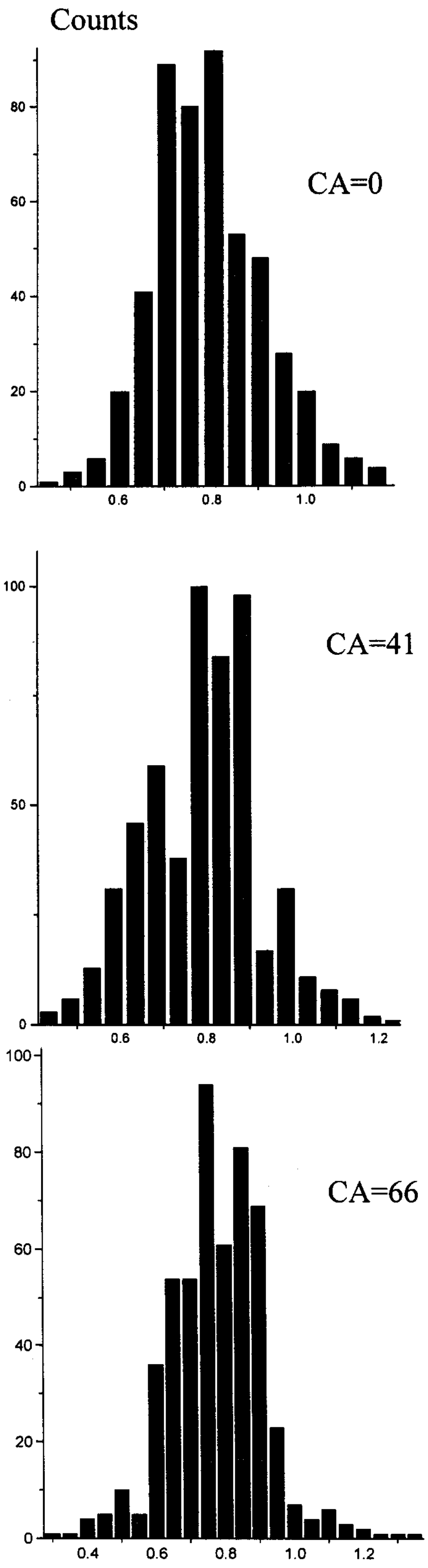

Figure 5.13: - Histogram of bubble sizes at the top of the column, generated at J_g=0.490cm/s in 30ppm DOW 250C frother solution.

where n_i is the number of bubbles in the i-th size class and d_i is the mid-point diameter of i-th size class. Table 5.5 and Figure 5.14 give the number mean bubble size. (All the bubble sizes hereafter are the bubble sizes at the surface of the sparger, if not specified otherwise.) The bubble sizes are in the range of 0.6~1.2mm, and show no difference in size between bubbles generated by the three spargers with different wettability.

Table 5.5 Number mean bubble size generated by spargers with different contact angles in 30ppm DOW 250C frother (along with 95% confidence)

Air flowrate	Contact angle (Degree)		
J_a	0	41	66
cm/s	Bubble diameter (cm)		
0.270	0.065±0.001	0.063±0.001	0.063±0.001
0.829	0.073±0.001	0.072±0.001	0.072±0.001
1.404	0.087±0.002	0.084±0.001	0.084±0.002
2.657	0.105±0.003	0.106±0.003	0.105±0.003

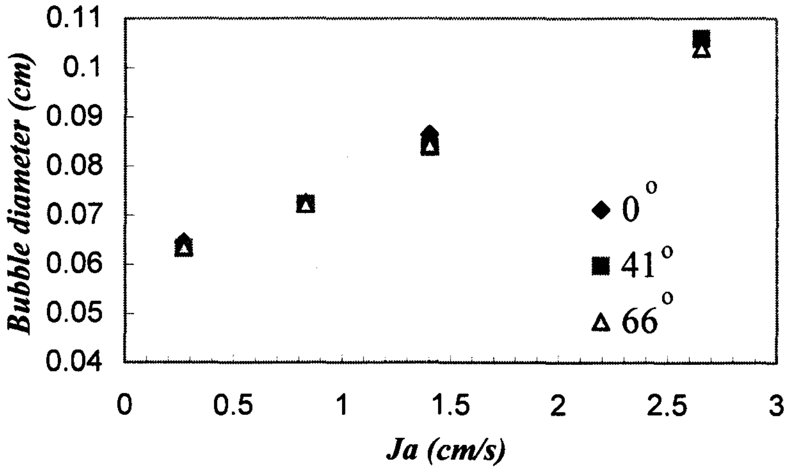

Figure 5.14: - Number mean bubble size as a function of *Ja* and sparger contact angle (95% confidence interval is omitted for clarity)

The Sauter mean bubble diameter D_{32} is usually quoted because it relates directly to the bubble surface area flux[25,26]. The definition of D_{32} is

$$D_{32} = \sum \frac{d_i^3}{d_i^2} \tag{5.13}$$

The Sauter mean diameter of bubbles generated by the spargers as a function of contact angle and air flowrate is given in Table 5.6. Again, the bubble sizes are in the range 0.6-1.5mm and are not affected by the wettability of the sparger.

Table 5.6 Bubble size (Sauter mean) generated by spargers with different contact angles in 30ppm DOW250C frother

Air flowrate	Contact angle (Degree)		
J_a	0	41	66
cm/s	Bubble diameter (cm)		
0.270	0.069±0.003	0.068±0.003	0.069±0.003
0.829	0.076±0.003	0.076±0.003	0.077±0.003
1.404	0.096±0.003	0.091±0.003	0.095±0.003
2.657	0.124±0.003	0.132±0.002	0.131±0.002

5.4.4 Wettability

The effect of capillary (surface tension) force on bubble size is well recognized when bubble formation occurs at circular orifices with flat cross-section and well-defined perimeter[1,3]. The bubble size can be calculated unambiguously when the bubble base adheres to the edge of the orifice during formation[27]. However, if the bubble base shifts due to wetting effects[4,17], or the shape of the orifice is not circular, the contact perimeter may not be the same as that of the orifice. In this case, the perimeter of the contact base is not well-defined, and it is difficult to estimate the capillary force. A systematic approach to solve this problem has been made by Krishnamurhsi and Kumar[28,29]. They compared the bubble volume obtained by using, alternatively, a standard circular orifice of arbitrary diameter and sets of orifices of other geometries such as triangular, square, etc., chosen to have perimeters or areas equal to that of the standard. Their work indicated that the bubble volumes obtained from the circular orifice did not correspond exactly to those from the noncircular orifices whether compared on an equal-perimeter or equal-area basis. For the porous rigid sparger used here, non-circular orifices are clearly present. The orifices on the sparger surface are actually slices through interconnected capillaries, There is neither a flat, smooth surface, nor a well-defined perimeter (Figure 3.3). These factors may reduce the impact of wettability on bubble size as seen here. It is evident that the wettability of the orifice may play a role in bubble formation at a single orifice with a well-defined perimeter and flat surface, but not in bubble formation at a rigid porous sparger.

5.4.5 Demonstration of bubble size calculation at a rigid porous sparger

Several models have been proposed to predict size of bubbles generated at an orifice. For bubble formation from multiorifices in a sparger, the models of Kumar and Kuloor have been proven to be the most appropriate.[10,16] Because of the structure of a rigid porous sparger, it is difficult to apply the concepts of capillary force and wettability during bubble formation due to the irregular nature of the orifice perimeter. To overcome this, a common practice is to assume the contact angle is zero, i.e., perfect wetting. In addition, the pore diameter can be modeled as an equivalent circular (i.e., equivalent diameter D_e)[16,18]. The number of active pores (i.e., those producing bubbles) can be estimated by Eq. (5.9). By fitting experimental bubble sizes to the calculated ones by a trial-and-error, the equivalent pore diameter can be obtained at the point corresponding to minimum sums of squares of the difference between predicted and measured bubble sizes.

Using the Kumar and Kuloor model (Eqs. (5.3)-(5.10)) and the trial-and-error routine with zero contact angle, the equivalent diameter was found to be 7μm. Table 5.7 lists the active pore number n (calculated from Eq. (5.9) within 5% error) and the calculated bubble size compared to the experimental. A good agreement between the two bubble sizes is evident (see also Figure 5.15). An extension of this approach is in the prediction of gas holdup and in establishing criteria for sparger selection[16].

Table 5.7 Bubble sizes predicted (D_e=7μm) and measured for vertical orifices at a sparger

Ja	n	Experimental D_b	Predicted D_b
cm/s		cm	cm
0.270	247	0.065±0.001	0.070
0.829	191	0.073±0.001	0.080
1.404	149	0.087±0.002	0.086
2.657	110	0.105±0.003	0.100

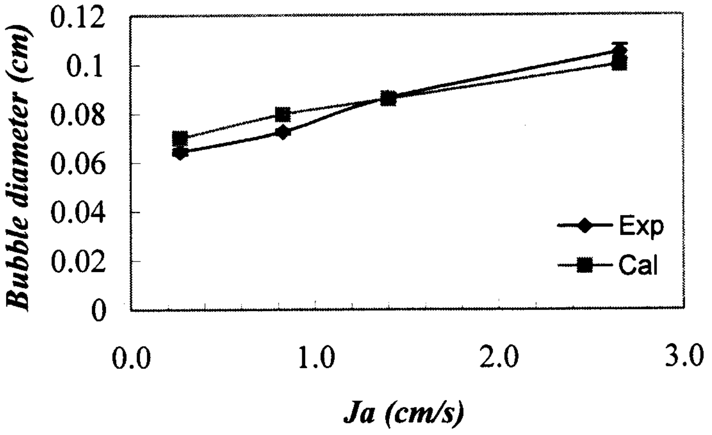

Figure 5.15: - Experimental and calculated bubble size

To include the effect of orifice orientation on bubble generation, a similar model to the above can be constructed by considering the capillary force component at any operating angle ϕ (see Appendix A for details). The D_e and calculated bubble size from this model (Eqs. (A23), (A24), and (A27)) are summarized in Table 5.8. The result shows that the ability to predict bubble size is almost the same as in vertical orientation (Table 5.7) although D_e is different. Thus orifice orientation affects D_e but this is not significant in terms of bubble size prediction. Despite the success of the model, bubble formation at a rigid sparger is more complex than the model assumes. Factors such as gas momentum, and liquid motion between bubbles on the sparger surface are neglected. However, from an engineering point of view the demonstrated ability to predict bubble size is sufficient to justify the present approach.

Table 5.8 Bubble sizes predicted (D_e=15μm) and measured with consideration of orifice orientation

Ja	*n*	Experimental D_b	Predicted D_b	Predicted D_b by vertical orifice model
cm/s		cm	cm	cm
0.270	243	0.065±0.001	0.071	0.070
0.829	194	0.073±0.001	0.079	0.080
1.404	155	0.087±0.002	0.084	0.086
2.657	122	0.105±0.003	0.095	0.100

5.5 Conclusions

The size of bubbles generated at a rigid sparger is not affected by the wettability of the sparger material. This may be attributed to the irregular pore shape and surface.

Assuming zero contact angle the model of Kumar and Kuloor can be used to estimate an equivalent pore diameter, following the approach of Escudero[16]. The ability to accurately predict bubble size using the model was demonstrated.

References

---

[1] Datta, R.L., Napier, D.H. and Newitt,,D.M., *Trans. Instn. Chem. Engrs.*, 28, 14-26(1950).

[2] Coppock, P.D. and Meiklehohn, G.T., *Trans. Instn. Chem. Engrs.*, 29, 75-86(1951).

[3] Benzing, R.J. and Myers, J.E., *Industrial and Engineering Chemistry*, 47(10), 2087-2090(1955).

[4] Lin, J.N., Banerji, S.K. and Yasuda, H., *Langmuir*, 10, 936-942(1994).

[5] Davidson, J.F. and SchÜler, B.O.G, *Trans. Inst. Chem. Eng.*, 28, 335-342(1960).

[6] Walters, J.K. and Davidson, J.F., *J. Fluid Mech.*, 12, 408-416(1962).

[7] Davidson, J.F. and Harrison, D., *Fluidised Particles*, London, Cambridge University Press, pp. 50-62, 1963.

[8] VanKrevelen, D.W. and Hoftijzer, P.J., *Chem. Eng. Prog*. 46, 29-35(1950).

[9] Ramakrishnan, S., Kumar, R., and Kuloor, N.R., *Chemical Engineering Science*, 24, 731-747(1969).

[10] Kumar., R. and Kuloor, N.R., *Advanced in Chemical Engineering*, Ed: Drew, T.B., Cokelet, G.R., Hoopes, J.W. nad Vermeulen, T., Volume 8, New York, Academic Press, pp. 255-368, 1970.

[11] Satyanarayan, A., Kumar, R., and Kuloor, N.R., *Chemical Engineering Science*, 24, 749-761(1969).

[12] LaNauze, R.D. and Harris, I.J., *Transactions Institution of Chemical Engineers,* 52, 337-348(1974).

[13] Sullivan, S.L., Hardy, B.W. and Holland, C.D., *AIChE Journal*, 10(6), 848-854(1964).

[14] Geary, N.W. and Rice, R.G., *AIChE Journal*, 37(2), 161-168(1991).

[15] Bowonder, B. and Kumar, R., *Chemical Engineering Science*, 25, 25-32(1970).

[16] Escudero, R.G., Ph.D. Thesis, *Characterization of Rigid Spargers and Their Selection for Flotation Columns*, Montreal, McGill University, 1998.

[17] Lin, J. N., Banerji, S. K. and Yasuda, H., *Langmuir*, 10, 943-948(1994).

[18] Gomez, C.O., *Canadian Journal of Minerals and Minerals Engineering*, 78(4), 785-792(2001).

[19] Leja, J., *Surface Chemistry of Froth Flotation*, New York, Plenum Press, pp. 269-284, 559-571, 1982.

[20] Flint, I.M., MacPhail, P. and Dobby. G.S., *CIM. Bulletin*, 81(913), 81-84(1988).

[21] Finch, J.A. and Dobby, G.S., *Column Flotation*, Oxford, Pergamon Press, pp. 9-36, 1990,

---

[22] Asche, H.E., Edinger, C., Kömpel, H. and Hofmann, H., <u>Chem. Eng. Technol.,</u> 13, 341(1990).

[23] Yao, B.P., Zheng, C., Gasche, H.E. and Hofmann, H., <u>Chem. Eng. Process.</u>, 29, 65(1991).

[24] Solanski, M.K.S., Mukherjee, A.K. and Das, T.R., *The Chemical Engineering Journal*, 49, 65-71(1992).

[25] Svendsen, H.F., Luo, H.A., Hjarbo, K.W. and Jakobsen, H.A., *Chinese Journal of Chemical Engineering*, 6(1), 29-41(1998).

[26] Parthasarathy, R. and Ahmed, N., *Journal of Chemical Engineering of Japan*, 29(6), 1030-1034(1996).

[27] Pamperin, O. and Rath, H.J., *Chemical Engineering Science*, 50(19), 3009-3024(1995).

[28] Krishnamurthi, S., Kumar, R. and Dutta, R.L., *Indian J. Tech.*, 2, 3-6(1964).

[29] Krishnamurthi, S., Kumar, R. and Dutta, R.L., *Trans. Indian, Inst, Chem, Engrs.*, 14, 78-85(1961-62).

Chapter 6

Role of Solid Wettability on the Froth Treatment in Processing Oil Sands

Contents

Abstract

Production of oil from oil sand deposits in northern Alberta involves open pit mining, mixing the mined ore with water, extraction of bitumen by aeration into a froth (Hot Water Extraction Process), removal of water and solids from the froth (froth treatment process), and upgrading the bitumen to liquid hydrocarbons. The success of the froth treatment stage depends on control of wettability of the fine solids by the aqueous phase. A mixture of heptane and toluene of varying ratio (called "diluent") was used to study the wettability of the fine solids isolated from the bitumen froth. Partition of the solids among the aqueous, organic and interphase regions was measured, and the wettability was evaluated from contact angle measurements. The effect of diluent composition, sample drying, and surface washing were examined. The partition of fine particles correlated well with their contact angle, and the results helped interpret observations from froth treatment practice.

6.1 Introduction

The oil sand deposits in northern Alberta contain large reserves of bitumen (a composite of hydrocarbons) which can be upgraded to petroleum products. The solids in oil sands are composed of quartz, clay and a number of other minerals[1]. The clay minerals are predominantly kaolinite and illite finer than 44μm[2].

Clark's Hot Water Extraction Process (HWEP), and its modifications, have been used to extract bitumen from oil sands. The HWEP produces bitumen as a froth product[3] (Figure 3.7) containing ca. 60% bitumen, 30% water, and 10% solids. The objective of the froth treatment process is to eliminate the water and solids from the froth. This is accomplished by adding naphtha (referred to as a "diluent") to dissolve the bitumen providing a density difference between the water and hydrocarbon phases and reducing the viscosity of the froth (Figure 3.8). The diluted froth is centrifuged to remove solids and water, producing a product containing ~3% water and 0.5% solids.

The water remaining in the froth treatment product contains dissolved salts, mainly sodium chloride, which are detrimental to the downstream upgrading operations. Efforts have been made to reduce the amount of water in the froth treatment product before it is sent to upgrading. It has been found that by changing the diluent characteristics from aromatic to paraffinic, the derived bitumen product is drier (contains less that 0.5% moisture) and is practically solids-free, but this is achieved at the cost of low bitumen recovery (85% instead of 95% obtained with naphtha as diluent).

When using heptane as diluent instead of naphtha, a "rag layer" is produced between the organic and aqueous phases. The rag layer is composed of fine solids, water and bitumen. The fine solids in the rag layer were found to be hydrophobic and biwettable (i.e., partially wettable by both water and organic phase). This may be attributed to adsorbed organics on the surface[4]. These organics are mainly surfactants produced during the

HWEP or/and asphaltene-like substances derived from bitumen. Some of these organics can be removed by toluene, the remaining being referred to as toluene insoluble organic matter (TIOM)[4,5]. The adsorption of these organic substances renders the fine solids hydrophobic or biwettable. Biwettable fine solids have a tendency to accumulate at the water/oil interface, and it is speculated, to stabilize the water droplets in the oil phase, i.e., stabilize a water-in-oil emulsion.

The mechanism of adsorption of TIOM on the clay surface and stabilization of the water-in-oil emulsion have been the subject of several studies. Naphthenic, carboxylic, sulphonic and phenolic acids have been found in the aqueous phase[6,7,8,9,10]. In addtion, α, β unsaturated ketones and/or conjugated chelated diketones may also exist[11]. Some of these surfactants may form organic-clay complexes on the clay surface through bonds with metal oxides and hydroxides[12,13]. Majid et al.[14,15] suggested the TIOM consisted of condensed aromatic rings with a significant number of oxygenated functional groups. The TIOM was found to be similar to asphaltene, and contained transition metals[5]. Other reports showed that TIOM was made up mostly of multicyclic aromatic compounds with a large number of oxygen and nitrogen functional groups[16,17]. A recent study showed that the TIOM were mainly humic matter which could have hydrophobic and hydrophilic sites and exhibit strong affinity for bitumen components.

Clays with adsorbed TIOM were found to be the key to poor dewatering of clay sludge tailings because of the formation of a network structure among water, residual bitumen and fine solids[18]. Stabilization of oil droplets by biwettable solids in the extraction stage has been discussed by Levine and Sandford[19], who indicated the fine solids become partially hydrophobic by adsorption of bitumen components such as asphaltenes. Asphaltene[20,21,22] adsorption on mineral solids has been studied. Menon and Wasan[20,22] showed that adsorption of asphaltenes and surfactants on clay changes the oil-water-solids contact angle. Tyerman suggested that the water-in-oil dispersions in froth treatment were stabilized by biwettable solids, and he found that a demulsifier can decrease the asphaltene adsorption on the solid surface and affect emulsion stability and water content in the oil[23]. Eley et al.[24] suggested that the dispersed droplets were stabilized when the asphaltenes were on the verge of precipitation. Under these conditions, the asphaltene film at the oil/water interface might become inelastic, which would hinder coalescence. Kaolinite clay particles treated with asphaltene were used to study the partitioning of the clay particles between an oil-in-water emulsion and an aqueous phase. It was found[25] that kaolinite will stabilize the oil-in-water emulsion if the clay contact angle is greater than 65°.

These fine clays coated with strongly bound TIOM have "asphaltene characteristics" and show a strong tendency to collect at the oil/water interface. They are considered by some researchers to be the key component responsible for the presence of residual water in the bitumen froth[4]. To improve the performance of the froth treatment, it is necessary to understand the mechanism of water retention, and the role of the diluent in controlling the wettability.

6.2 Experimental setup

6.2.1 Preparation of fine solids from rag layer

The heptane and toluene, spectrophotometric grade, were from Aldrich. A sample of bitumen froth, taken from a commercial primary separation vessel and stored in CANMET's facility in Devon (Edmonton), was transferred to a 1L glass bottle and kept in a refrigerator until needed. During the preparation, the sample was heated to ca. 85°C to thaw the bitumen, followed by the addition of heptane in a ca. 2:1 heptane-to-froth weight ratio while mechanically stirring. The mixture was then transferred to a large separation funnel in which phase separation occurred and three distinct phases formed within ca. 2h. (Figure 6.1). On the top was a nonaqueous phase and at the bottom was an aqueous phase hosting most of the sands entrained in the froth. The middle layer was most likely a bi-continuous phase (or rag layer) containing fine solids, water, and bitumen. After separating the coarse solids and water from the bottom, the rag layer was collected into a glass bottle for further washing with heptane. For each washing, the sample was centrifuged at 3000 rpm for 20 minutes to separate the washing liquid from the solids (the centrifuge is an Oil Centrifuge Tube, Model JP1-33, From Wheaton, N.J., USA). A heptane wash was used because it does not dissolve asphaltene, and therefore it is expected to cause minimal change in surface properties of fine solids. The treated solids were dried in a vacuum oven at 40°C for four hours to remove excess water. Sample preparation up to this point was performed at Syncrude Canada Ltd. (Research Center, Edmonton). The solid thus prepared contained varying amounts of liquid (not measured) and were stored in sealed glass bottles for future use. Further washing of the sample with heptane or toluene (to examine their ability to remove surface coatings) was conducted in 50ml centrifuge tubes in a Superspeed Centrifuge RC-5, from Du Pont Instrument, USA. The sample dried in an oven at 60°C for 72 hours is referred to as dried sample.

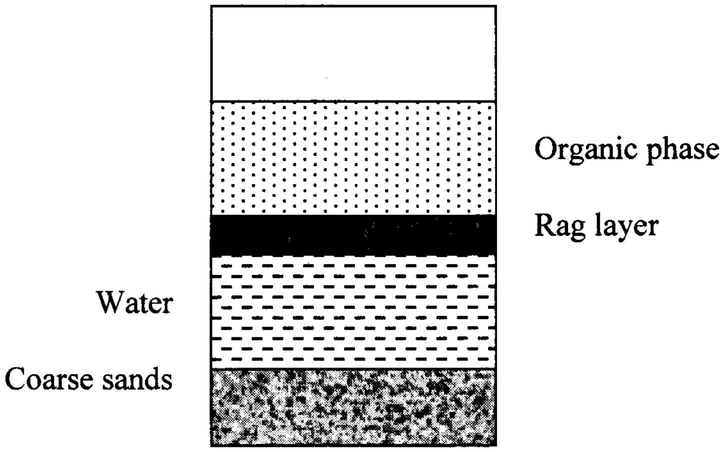

Figure 6.1: - Preparation of fine solid from froth by heptane

6.2.2 *Surface tension of heptane-toluene mixture*

The surface tension of the liquid plays a role in determining solid wettability. The surface tension of heptane-toluene mixtures at different ratios (simulating diluent of different chemical composition) and interfacial tensions of the mixtures against water were determined by the Wilhelmy plate method using a K12 automatic tensiometer (Kruss Ltd, USA). The measurements were conducted at 24±5°C. Each datum reported was an average of 10 readings. A Milli-Q water with surface tension of 72.3mN/m was used in this project.

6.2.3 Contact Angle

The contact angles were determined by the sessile drop method. Because it was difficult to make a pellet of wet fine solids by means of hydraulic press, a special device was designed to make pellets (Figure 6.2). An aluminum cylinder with a bottom threaded cap was used to hold the sample. First inserted into the bottom cap is a piece of mica with a piece of Teflon on the top, to ensure a smooth surface. The bottom cap was then screwed to the cylinder with an inner metal ring. The samples (mixed with small amount of wash liquid to make it paste-like) were added into the cylinder. A centrifugal force of ca. 5000g was applied to the samples in the cylinder. A compact pellet formed in the ring and was pushed out through the bottom by a piston mounted on the top of the cylinder. The smooth bottom surface of the pellet was used to measure the contact angle. It is important to note that wash liquid (toluene or heptane) evaporates rapidly even at ambient temperatures so that the effect of residual wash liquid on the measured contact angle can be considered negligible. For a dried sample, it was pressed into a pellet of 1.3cm diameter and about 3mm thickness by a hydraulic press (Specac Ltd., UK) at ca. 6000kg.

For contact angle measurements, a glass cuvette 3×3×4cm^3 was used to hold the heptane-toluene mixture. A water drop of ca.10-20μl was placed by a micro-syringe on the pellet in the heptane toluene mixture. The image (photo) of the water drop was taken by a Sony Video 8 professional video recorder with a close-up function for macro shooting, or by a Canon AE-1 camera with macro focus length. The angle was measured in the water phase, i.e. a large contact angle represents a more hydrophobic or oil wettable surface. The centrifuge method developed in this study to prepare the pellets proved adequate, giving an average variation of ±3° in contact angle measurements.

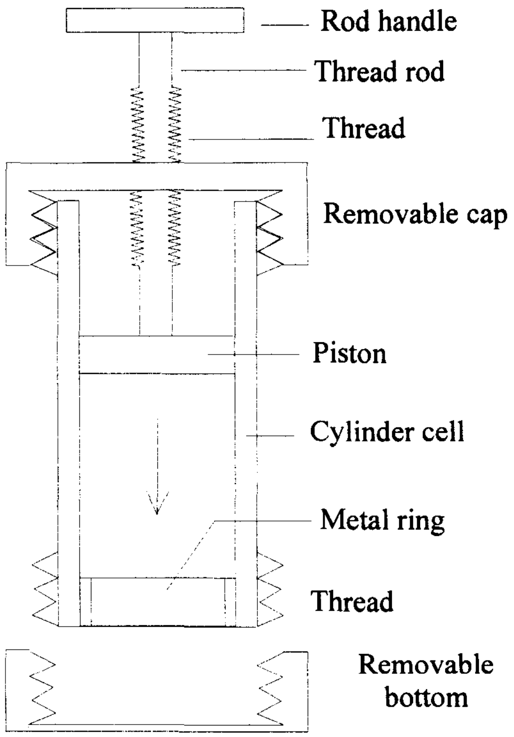

Figure 6.2: - Cell used to prepare the sample

6.2.4 Partition

A 50ml plastic tube was used to hold the test liquid, diluent and water. A hole was made in the wall of the tube just below the interface, and blocked by a plug (Figure 6.3). A 0.3g wet or 0.1g dry sample of fine solids from the rag layer was placed in the liquid and hand-shaken vigorously to mix the three phases. The mixture was then left still, and phase separation occurred immediately. The solids partitioned to the organic phase, aqueous phase or organic-aqueous interphase, depending on the solid wettability. The mixture

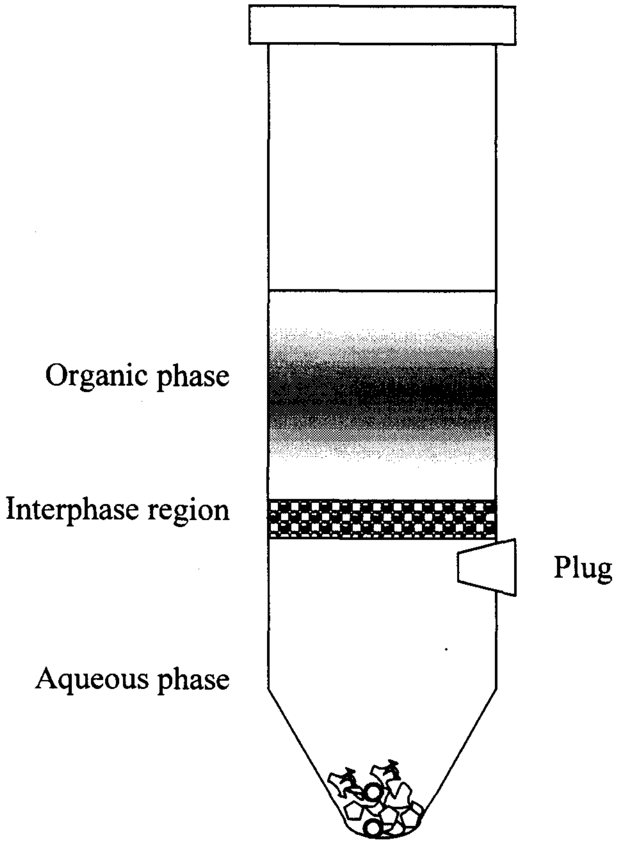

Figure 6.3: - Schematic diagram of two-phase partition

was left for 6 hours to ensure complete separation. The organic phase was removed carefully with a pipette, and the plug was removed to isolate the solids remaining in the interphase region from aqueous phase. The solids that sank in the aqueous phase and those that remained in the organic and interphase regions were collected separately and weighed after being dried in an oven at 60°C for 72 hours. The weight fraction of solids partitioned to each phase was calculated. A 0.5g wet sample was dried under the same conditions to correct for the initial water content (details are in Appendix C).

6.2.5 Infrared spectroscopy

A Bruker IFS 66 Fourier transform IR spectrometer was used. Potassium bromide (KBr IR grade) from Aldrich was used to dilute the sample. The DRIFTS technique was used to obtain the IR spectra. A 3M IR card, from 3M Co. was used to obtain the transmission IR spectra of species washed off by the solvent. A drop of the washed supernatant was placed and dried under ambient conditions. The spectra were recorded at the mid-IR region (about 5000-500cm^{-1}) with 100 scans and presented with background correction. For quantitative analysis, the characteristic IR band intensity was determined using the built-in fitting procedure in a commercial OPUS system supplied with the IFS-66 FT spectrometer.

6.3 Results and Discussion

6.3.1 Surface tension of diluent

The surface tension of heptane and toluene and the interfacial tension against water are shown in Table 6.1. These values are in excellent agreement with those reported in the literature[26,27].

Table 6.1 Comparison of measured surface and interfacial tensions with those reported in literature

Liquid	Surface tension (mN/m)		Interfacial tension (mN/m)	
	Measured	Reported	Measured	Reported
Heptane	20.0	20.1	50.9	50.2
Toluene	28.2	28.5	36.0	36.1

Figure 6.4 shows that the surface tension of the heptane-toluene mixture (diluent) decreases with increasing heptane concentration, whereas the interfacial tension against water increases. The decrease in the aromatic component in the diluent as the heptane concentration increase is considered to weaken interactions between the diluent and water molecules across the interface, thus causing the interfacial tension to increase. (Toluene has a stronger affinity for water molecules than does heptane, as shown by a lower interfacial tension of toluene/water (36.0mN/m) than heptane/water (51.0 mN/m)). This

change of interfacial tension with aromatic content in diluent plays an important role in froth treatment, as illustrated later. A change of diluent composition is likely to change both γ_{sd} and γ_{wd}. From Young's equation applied to the system (Figure 6.5 and Eq. (2.3))[28], i.e. $\cos\theta=(\gamma_{sd}-\gamma_{sw})/\gamma_{wd}$, if the contact angle >90°, an increase in interfacial tension of water/diluent (γ_{wd}) will increase $\cos\theta$, and hence decrease the contact angle. If the contact angle <90°, an increase in interfacial tension of water/diluent will decrease $\cos\theta$, and hence increase the contact angle. The increase in interfacial tension of diluent/solid (γ_{sd}) will decrease the contact angle. As a consequence, an increase in γ_{wd} and γ_{sd} will decrease the contact angle for the case of contact angle>90°. An increase in γ_{wd} and γ_{sd} will have the opposite effect for the case of contact angle<90°. If the increase of γ_{sd} dominates over γ_{wd}, the contact angle will decrease. Their relations are shown is Table 6.2.

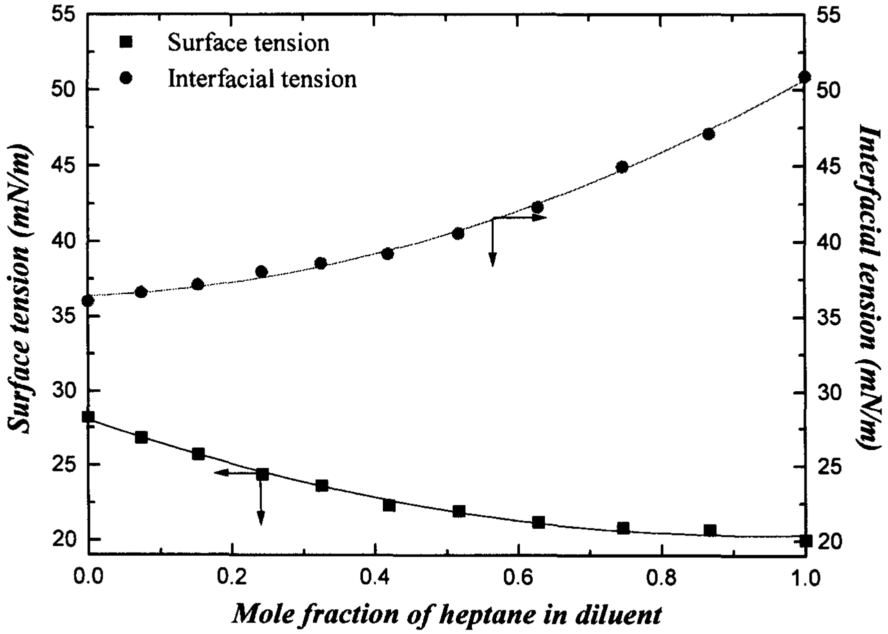

Figure 6.4: - Surface tension and interfacial tension as a function of the heptane concentration in the diluent

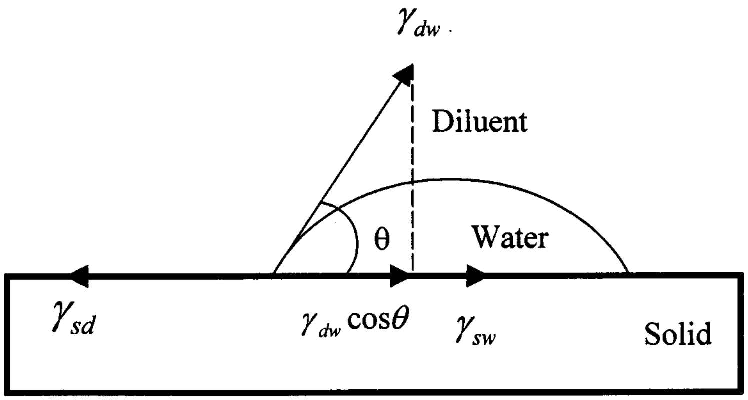

Figure 6.5: - Water contact angle on fine solid surface immersed in diluent

Table 6.2 The relations of θ, $\cos\theta$ and surface/interfacial tensions

(↑: increase; ↓: decrease)

increase	$\theta>90^\circ$		$\theta<90^\circ$	
	$\cos\theta$	θ	$\cos\theta$	θ
γ_{sd}	↑	↓	↑	↓
γ_{sw}	↓	↑	↓	↑
γ_{wd}	↑	↓	↓	↑

6.3.2 Contact angle

Typical variation of the water contact angle on pellets as a function of diluent composition is illustrated in Figure 6.6. (In this example, pellets were prepared from particles washed by toluene six times and dried.) A clear trend of decreasing contact angle with increasing heptane concentration in diluent is observed.

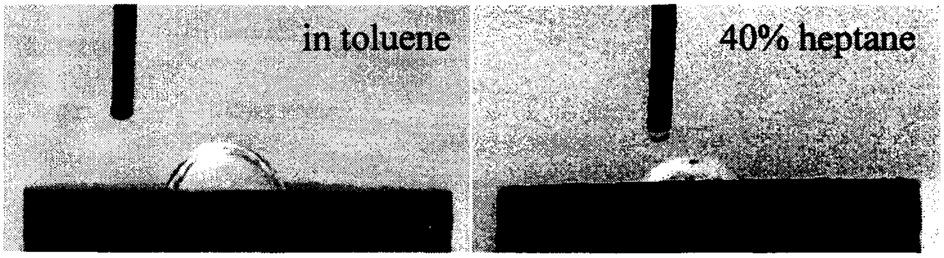

Figure 6.6: - Variation of the contact angle of water on fine solids in diluent: fine solids washed with toluene six times and dried in an oven at 60°C for 72hrs.

The contact angles measured with *"wet"* pellets are shown in Figure. 6.7 (note: *"wet"* is used qualitatively). It was observed during the measurement that moisture on the surface

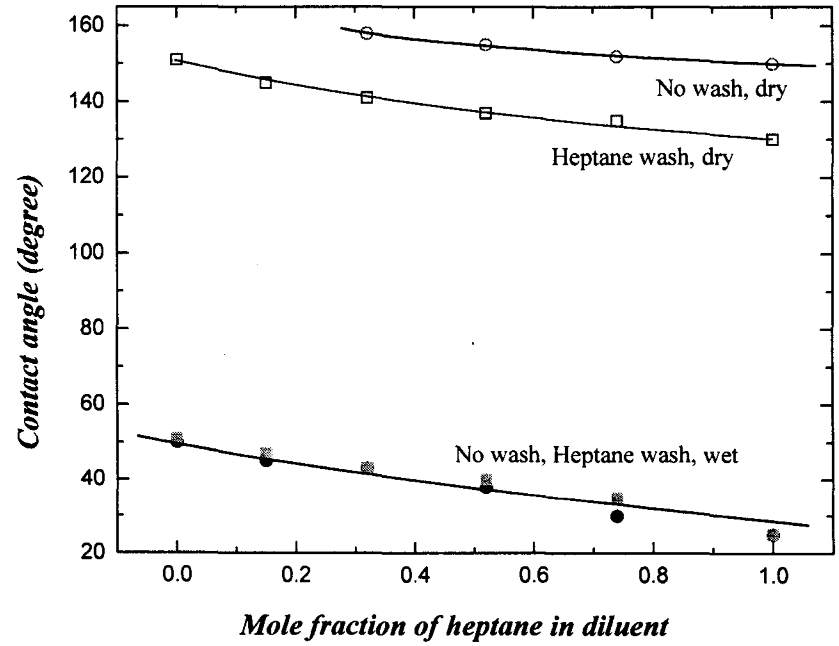

Figure 6.7: - Effect of heptane washing and sample drying on the contact angles of water on fine solids in the diluent

had a significant impact on wettability and made accurate measurement of contact angle difficult.

Nevertheless, it is evident that contact angle decreases with increasing mole fraction of heptane in diluent. In air, water wets the solids with a near zero contact angle. These observations suggest that with increasing concentration of heptane, the solids tend to leave the organic phase. This may suggest that increasing heptane content weakens the interaction of diluent with solids, which increases γ_{sd} and thus, decreases the contact angle. That the fine solids tend to leave the organic phase with an increase in heptane content is consistent with the observed decrease of solid (and hence water) content in the organic phase when the froth is treated with an alkane (paraffinic) diluent.

To examine the impact of washing on the wettability of fine solids, the extracted solids were further washed six times by either heptane or toluene, and the contact angle of water measured on the pellets. For wet pellets, the wetting characteristics were similar with and without this further heptane washing (Figure 6.7), suggesting that heptane washing does not alter the surface wetting property of the fine solids substantially. This is related to heptane's poor or dissolving power for organic substances, especially the multicyclic aromatic compounds suspected to be present on the solid surface.

When the extracted sample was washed with toluene, on the other hand, water spread readily on *wet* solids (contact angle <10°), and the effect of diluent composition could not be detected. It is clear that the strong dissolving power of the aromatic toluene removes organic substances from the solid surface, resulting in an increased wettability by water. The practical implication of this finding is that a good diluent should have a strong dissolving power for organic substance, to make fine solids hydrophilic and remain in the aqueous phase.

The decrease in contact angle with increase of heptane content in the diluent may be attributed to the reduction in the interaction between the diluent and solid surfaces. This reduction increases $\gamma_{sd,}$ and hence decreases the contact angle.

Also evident in Figure 6.7 is that the contact angle of water on dry pellets in the diluent is as high as ca. 150°, significantly greater than on wet samples (ca. 50°). In this case, the water contact angle on the solids decreased only marginally with increasing heptane concentration in the diluent. The significant increase in water contact angle upon drying the solids suggests that caution has to be exercised in sample preparation when studying the wettability of the fine solids from oil sands in relation to understanding froth treatment performance; using wet samples appears to be essential in this context. However, the observed change accompanying the sample drying process does shed light on the wetting mechanism. Whether the observed change of contact angle upon sample drying is due to the removal of water from the solid surface or originates from the alteration of surface chemistry remains to be elucidated. It appears that the evaporation of moisture and solvent during drying caused a preferential orientation of the low-energy hydrocarbon chain towards the air, forming a closely packed assembly of adsorbed surfactant molecules. As a result, an increased water contact angle is anticipated. This explanation is further supported by the irreversible nature of the drying process, i.e. the dried pellet remained dry even after being dipped in water and contact angle remained high and unchanged.

For toluene washed particles, it appears that their surfaces still retain some toluene insoluble organic matter. The drying process changed a solid from water wettable to oil wettable with a contact angle as high as 80°, decreasing with increasing heptane content in the diluent (Figures 6.6 and 6.8). Compared with heptane washing, toluene washing results in a much lower contact angle at a given diluent composition, confirming the removal of surface hydrophobic species by the toluene wash. As a result, the attraction across the water/solid interface increases, γ_{sw} decreases. Also, the contact angle showed a greater dependency on diluent composition (changed from 80° in toluene to 20° in heptane), in contrast to particles washed with heptane. It appears that a low surface coverage of organics after toluene washing is responsible for the reduced contact angle of water in diluent with increasing heptane concentration. After the toluene wash, more bare solid surfaces and TIOM are exposed. The bare surface and TIOM have more polar groups. These polar groups have stronger affinity for toluene than heptane. The increase in heptane content in the diluent will weaken this affinity, hence decreasing γ_{sd}, which may dominate over the change in γ_{wd} and thus decrease the contact angle. As a result, the fine solids showed a stronger dependency of wettability on the aromaticity of the diluent. It is clear that the study using dried fine solid samples does provide some insight into the role of diluent composition in froth treatment, although it is less relevant to practice.

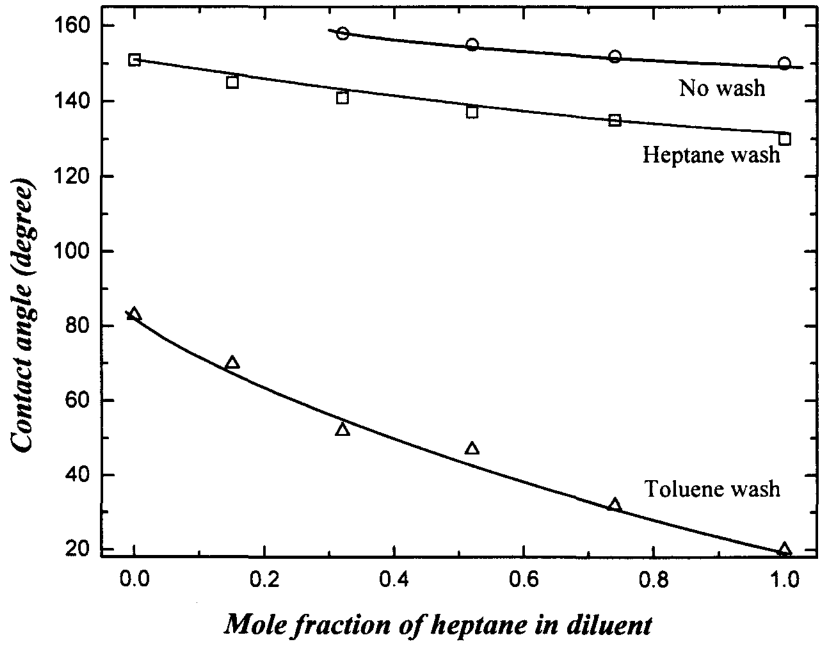

Figure 6.8: - Effect of toluene washing on the contact angles of water on fine solids in the diluent (dried sample)

Another important observation derived from the above discussion is that it is the change in surface chemistry rather than removal of moisture upon drying that appears to determine the wettability of the fine solids. This is concluded from the fact that the moisture content would be, at most, the same, if not lower, after toluene washing whereas the toluene washing resulted in a significant increase in the wettability of the fine solids was observed. The effect of moisture on the wettability should not be overlooked, however, as a significant increase in contact angle (from zero to ca. 80^{o}) was obtained by drying toluene washed fine solids (Figure. 6.8).

It is important to note that the effect of diluent composition on froth treatment is probably more complex than presented here, although the measurements do correspond to what is generally observed in froth treatment practice. For example, the important effect of diluent composition on the formation of finely dispersed water droplets in diluted bitumen needs to be considered, in addition to possible stabilization of these water droplets by biwettable fine solids.

In summary, the contact angle measurements indicate that toluene wash decreases the contact angle significantly whereas heptane wash causes little change. The toluene wash affects contact angle by the removal of organics whereas the effect of heptane content in diluent may be attributed to the change of the interaction of diluent/solid and diluent/water (i.e., change in γ_{sd} and γ_{wd}).

6.3.3 Partition

A general observation from the partition experiments is that the water phase was always clear. A stable interphase between the organic and aqueous phases, consisting of organics, water and fine clays, was observed in all the partition tests. The organic phase was clear or turbid with a color depending on the wash treatment and the diluent composition.

The results from partition tests with "wet" particle samples are shown in Figure 6.9. The fine solids were partitioned mainly between the organic phase and the interphase with a negligible amount in the aqueous phase. With a diluent of low heptane content (less than 40%), a majority of fine clays (ca. 80%) resided in the organic phase, suggesting that most particles are

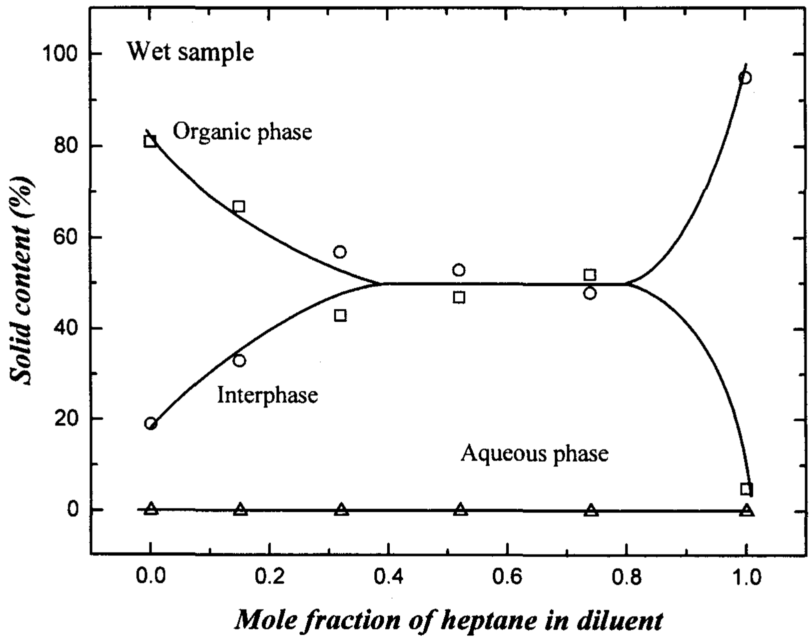

Figure 6.9: - Effect of diluent composition on fine particle partition among the various phases (wet sample)

strongly hydrophobic and hence oil wettable, with the rest being of moderate hydrophobic and biwettable. This again shows that the heptane weakens the interaction of fine solids and diluent, causing the fine solids to leave the organic phase. With a more paraffinic diluent (heptane concentration higher than 80%), the partition between organic phase and interphase is reversed. The observed increase of fine particle partition to the interphase is consistent with the decreased water contact angle on the particles with increased heptane concentration in the diluent (Figure 6.7). A wide range of surface hydrophobicity is seen in these tests.

For the dried particles, a similar variation in partition between the organic phase and interphase was observed, but to a lesser extent (Figure 6.10). This observation corresponded well to the marginal decrease in contact angle of water upon increasing heptane concentration (Figure 6.8). Compared to wet samples, the partition to the organic phase increased only slightly unless a pure paraffinic diluent was used, even though a much greater contact angle was measured with dried powders. This finding indicates that the drying process makes the solid surface less sensitive to the heptane content. This may be attributed to a reduced heptane penetration after the sample is dried. When dried, the organic substance on the solid surface tends to pack more closely, which prevents the heptane from penetrating and making contact with the inner layer molecules of the organic substances. As a consequence, only the outer layer of molecules is exposed to the diluent, hence the response is less sensitive to diluent composition. That is, the partition of dried sample did not significantly change with the change in diluent composition.

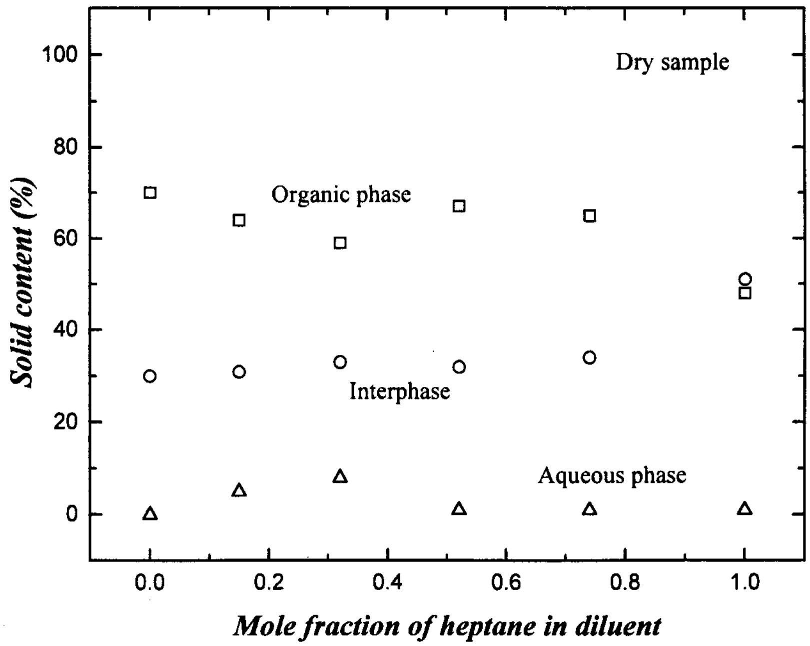

Figure 6.10: - Effect of diluent composition on fine particle partition among the various phases (dried sample)

The partition tests conducted with fine solids washed by heptane and toluene, in parallel to contact angle measurements, confirmed the effect of solvent washing on wettability. For heptane washed particles, a similar trend in partition curve to that without washing was obtained, as anticipated from the wettability measurements (Figure 6.11). However, with toluene washing majority of fine solids became hydrophilic, with a small amount being biwettable (implying the presence of some TIOM) (Figure 6.12). This observation is consistent with the observed near zero contact angle of particles in diluent, and the observed lack of diluent composition effect. It is the removal of surface hydrophobic species by dissolution in toluene that is responsible for the inversion of partition from the organic to aqueous phase. As expected, hydrophobicity is the key to controlling the partition of fine solids among various phases. The accumulation of biwettable fine solids at the water/diluent interface would stabilize the phase boundary, and hence stabilize the finely dispersed water droplets. This is an undesirable feature of the current bitumen froth treatment process. The experimental findings suggest that the key to improving the removal of fine solids and associated water from the organic phases during froth treatment is to increase the wettability of the fine solids. This can be achieved either by removal of the organic substance from the surface or by weakening the interaction between the fine solids and diluent, which may destabilize the water-in-oil emulsion by triggering coalescence, flocculation[29].

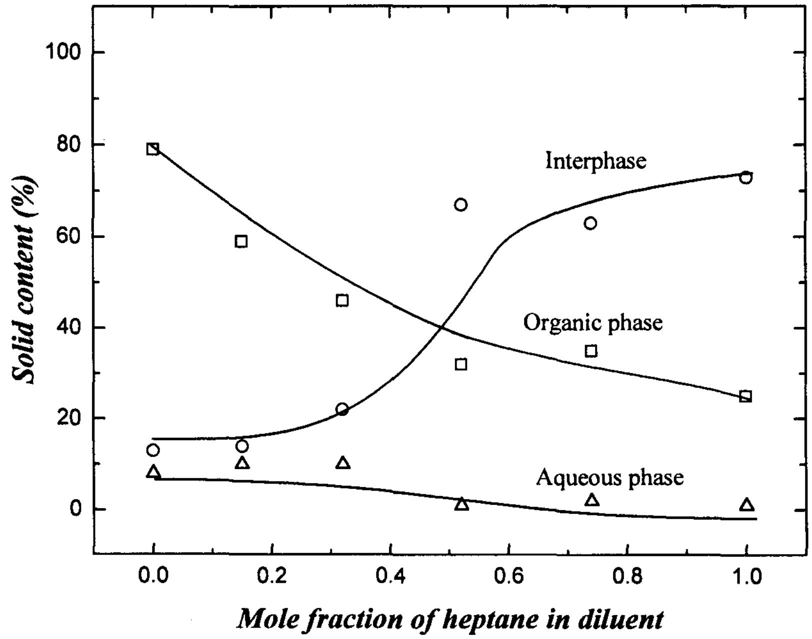

Figure 6.11: - Effect of heptane wash on fine solid partition among the various phases (wet sample)

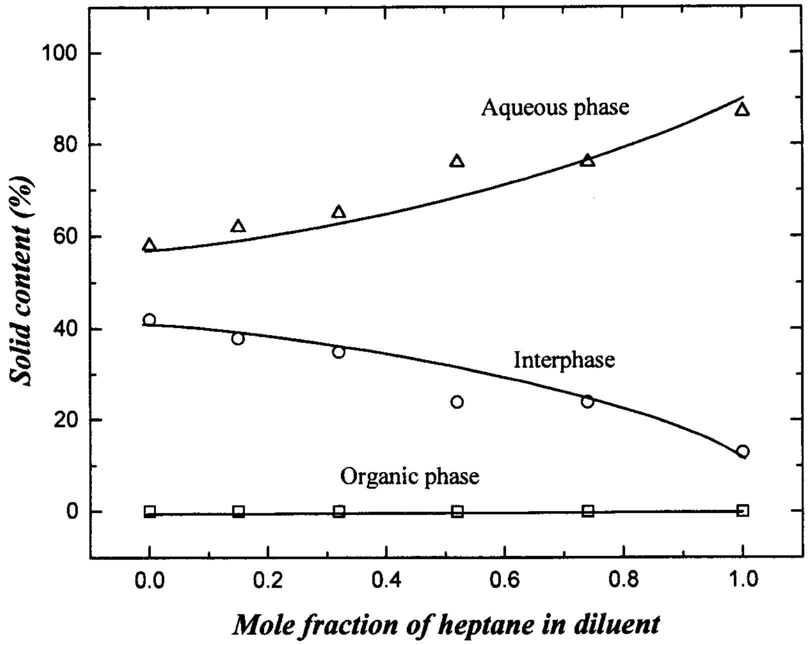

Figure 6.12: - Effect of toluene wash on fine solid partition among the various phases (wet sample)

6.3.4 Infrared Spectroscopy

The IR spectra in Figure 6.13 show the presence of organics on the surface. The strong bands around 2900cm^{-1} arise from the antisymmetric and symmetric stretch of CH_3 and CH_2 groups[13]. The presence of carboxylate/carboxylic groups is supported by bands at 1700cm^{-1}(C=O), 1600 and 1376cm^{-1}.[30] The band at 1600cm^{-1} may overlap with that assigned to C=C in the benzene ring, which is supported by the band at 1508cm^{-1}(Figure 6.14)[31]. The band at 1450cm^{-1} may indicate a carbonate (possibly metal carbonate) and/or a CH_3 group on the solid surface. The strong bands at 1005 and 1030cm^{-1} suggest the presence of sulfoxy species[11,32,33], and the bands at ca. 1110cm^{-1} may be caused by Si-OH vibrations[34]. The presence of these bands along with those assigned to carboxylic confirmed the contamination of the fine solids by natural surfactants. The strong, sharp peaks above 3600 cm^{-1} are indicative of the presence of inherent hydroxyls in clays[35,36].

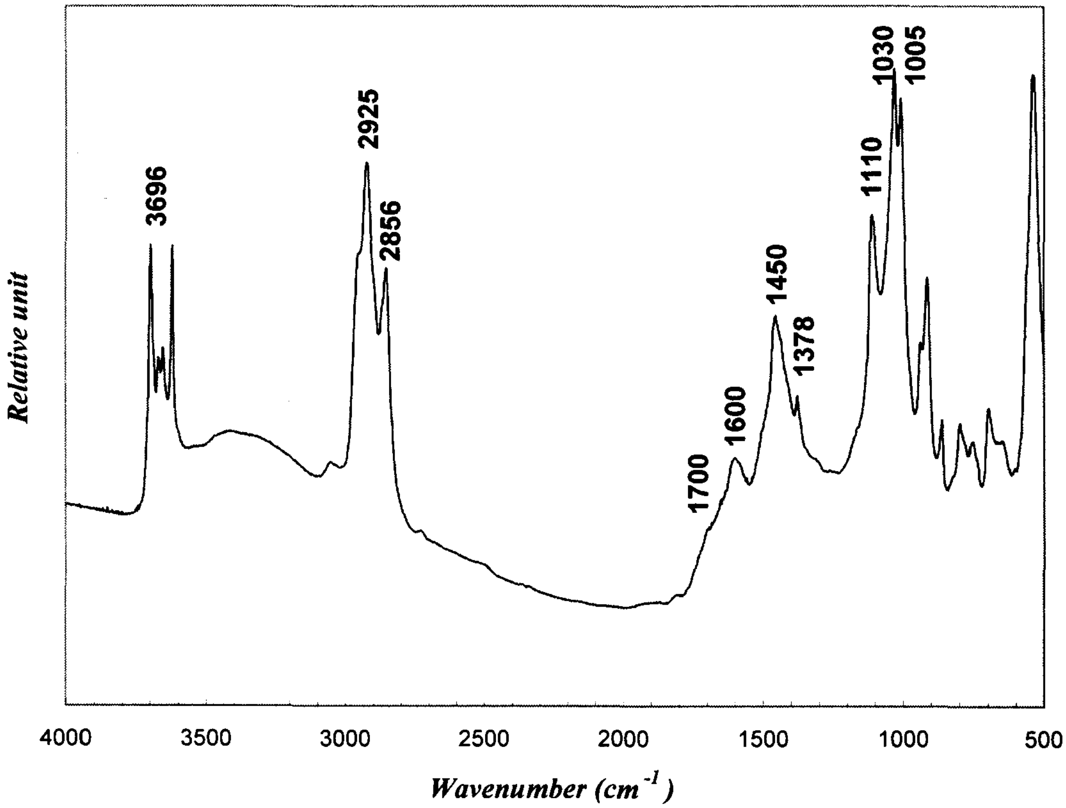

Figure 6.13: - IR spectra of fine solids extracted from bitumen froth (wet sample)

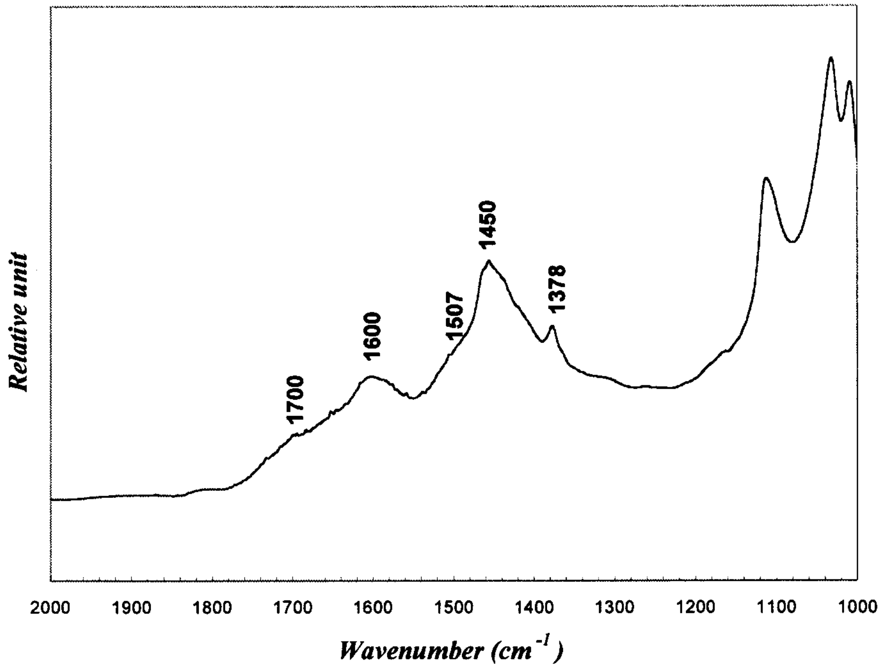

Figure 6.14: - IR spectra of fine solids extracted from bitumen froth (dried sample, region from 1000-2000cm^{-1} amplified)

The IR spectra of wet solids extracted from bitumen froth using heptane, with and without washing by heptane or toluene, are shown in Figure 6.15, and those corresponding to the dried solids, in Figure 6.16. The IR spectra in both figures show similar general features regardless of treatment, except that the broad band at 3300 cm^{-1}, corresponding to hydrogen-bonded water, diminished upon drying. Considering the high sensitivity of the IR technique to water, the amount of water removed during drying is considered marginal, yet, as described, a significant impact of drying on the wettability of the fine solids was observed. The band at 3696cm^{-1}, assigned to internal OH, was used as an internal standard for quantitative analysis.

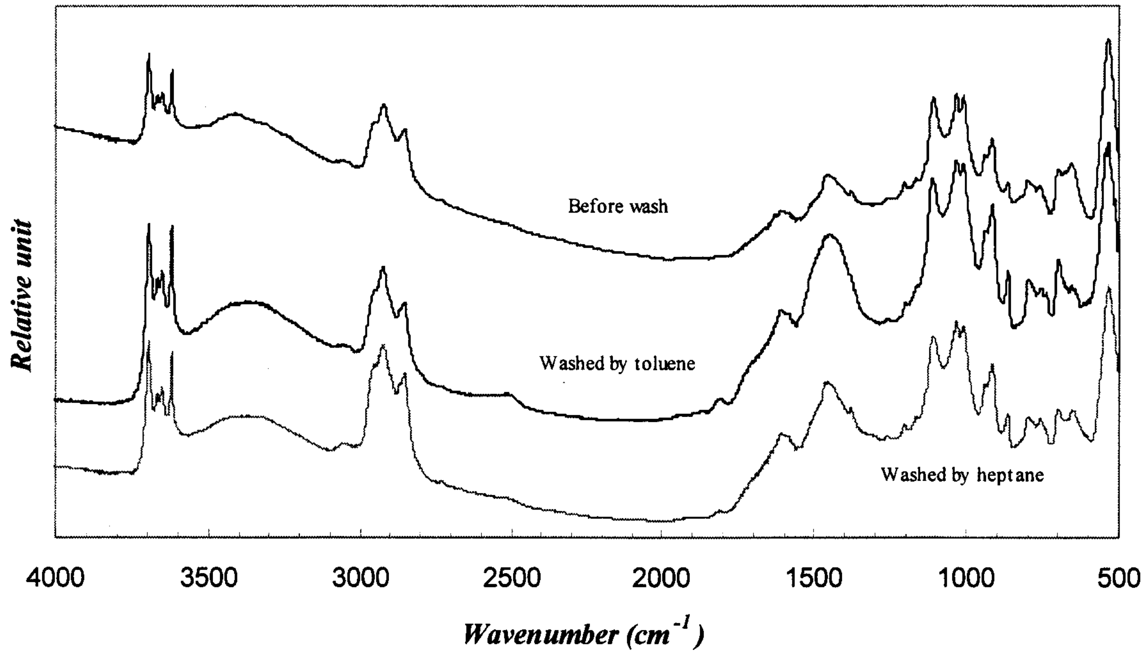

Figure 6.15: - IR spectra of fine solids extracted from bitumen froth before and after washing by heptane and toluene (wet sample)

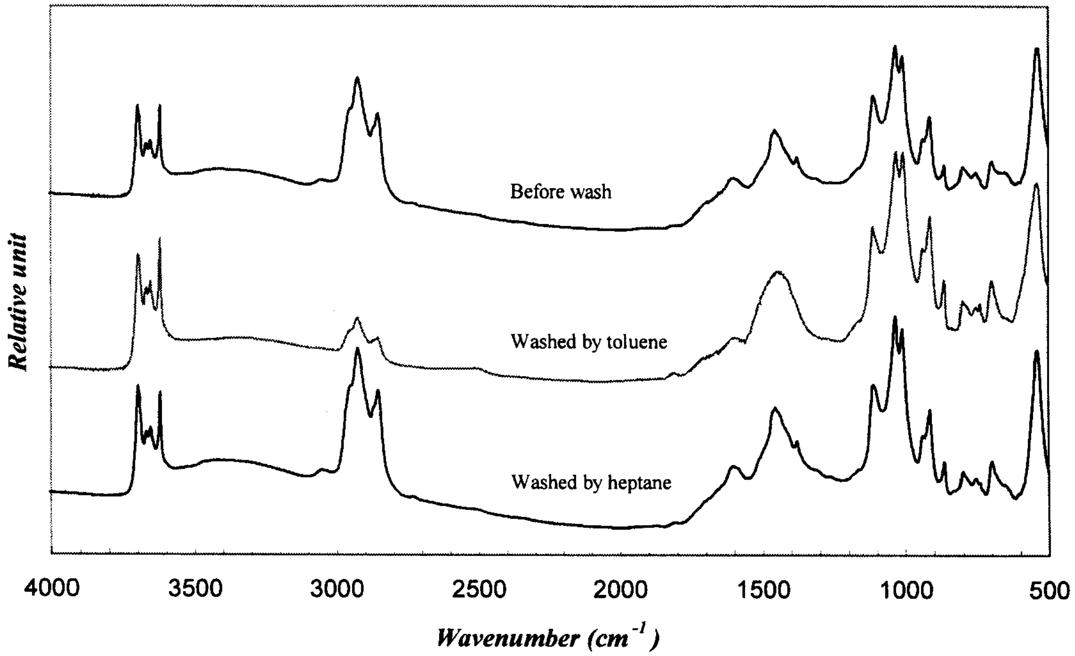

Figure 6.16: - IR spectra of fine solids extracted from bitumen froth before and after washing by heptane and toluene (dried sample)

The relative intensity of the bands assigned to CH_2 (at 2925cm^{-1}) with respect to the band for the internal OH group (at 3696cm^{-1}) was determined for each spectrum of dried sample and the results are give in Table 6.3[37,38]. It is observed in Table 6.3 that heptane washing did not change the relative band intensity substantially for hydrocarbons (from 1.14 to 1.11), while a significant reduction from 1.14 to 0.28 was observed with toluene wash. Clearly, the toluene wash removed most of the adsorbed hydrocarbon species, considered to be surfactants. The removal of hydrocarbons results in the increase in wettability as described earlier in this chapter.

Table 6.3 Relative intensity (ratio) of characteristic IR band at 2925cm^{-1} with respect to the band of internal OH group at 3696cm^{-1}

Sample treatments	Relative intensity
Before wash	1.14
Heptane wash	1.11
Toluene wash	0.28

The removal of organic species by washing with various solvents was investigated using IR spectroscopy on the supernatant. In solid-free heptane supernatants, no additional species could be detected. However, in the supernatant from the toluene wash, bands attributed to carboxylic/carboxylate and sulfoxy groups were observed, confirming the removal of organic species from the surface. The fact that the various treatments did not change the spectral features in spite of removal of organic species suggests that the contamination of the fine solids is by natural surfactants from the bitumen. These contaminated fine solids are strongly hydrophobic/biwettable. They tend to accumulate at the aqueous-diluent interface, stabilizing water-in-oil emulsions and contributing to the residual water and fine solids in the froth treatment product. The study therefore suggests that a possible, practical solution to minimize the water and fine solids in bitumen froth treatment is to control the wettability of the fine solids and hence to destabilize the water-in-oil emulsion. One of the approaches to consider is the composition of the diluent.

6.4 Conclusions

The wettability of water on fine solids in bitumen froth treatment process increased with increasing heptane (paraffinic) component in the diluent, resulting in an increased partition of the solids to the interphase region. A change in the interactions of solid/diluent and diluent/water may be responsible.

The wettability of water on fine solids changed marginally by washing the solids with heptane, but increased significantly after toluene washing. An inversion in solids partition from organic to aqueous phase was observed in the latter case. The strong dissolving power of toluene for surface organic substances made the fine solids more water wettable.

Drying caused a change in wettability. A significant decrease in wettability with a corresponding change in partition characteristics was measured with dried particles, which caused the fine solids to partition in organic phase or interface region. The partition was less sensitive to the heptane content in the diluent.

A general correlation was found between wettability of fine solids and their partition among the various phases (i.e., organic, aqueous and interphase). The key to improve the froth treatment process (i.e., to produce a bitumen product free of fine solids and water) is to control the wettability of fine solids. This can be achieved by either removing the organic substance from the solid surface, or increasing the paraffinic characteristic of the diluent. An ideal diluent should posses dissolving power for organic substances while retaining its paraffinic property (with minimum bitumen loss). This will destabilize the water–in-oil emulsion, and reduce the solids and the water content in the organic phase during froth treatment. The current study accounts for the practical observation of froth treatment: paraffinic diluent produces a dryer diluted bitumen than aromatic diluent.

References

---

[1] Bichard, J.A., *AOSTRA Technical Publication.*, Series #4, AOSTRA, Edmonton, 1987.

[2] TaKamura, K., *The Canadian Journal of Chemical Engineering*, 60, 538-545(1982).

[3] Mikula, R.J., Axelson, D.E. and Sheeran, D., *Fuel Science and Technology Int'L.*, 11(12), 1695-1729(1993).

[4] Kotlyar, L. S., Sparks, B. D., Woods, J. R., Raymond, S., Page, Y. Le and Shelfantook, W., *Petroleum Science and Technology*, 16(1), 1-19(1998).

[5] Kotlyar, L. S. and Sparks, B. D., *AOSTRA Journal of Research*, 7(2), 111-117(1991).

[6] Bowman, C.W., *Pro. 7th World Petrol. Congr.*, 3, 583(1967).

[7] Baptista, M.V. and Bowman, C.W., *19th Can. Chem. Eng. Conf.*, Edmonton, Alberta, 1969.

[8] Leja, J. and Bowman, C.W., *Canadian Journal of ChemicalEngineering*, 46, 479(1968).

[9] Moschopedis, S.F., Fryer, J.F. and Speight, J.G., *Fuel*, 56, 109(1977).

[10] Ali, L. H., *Fuel*, 57(6), 357-340(1978).

[11] Ignasiak, T. M., Zhang, Q., Kratochvil, B., Maitra, C., Montgomery, D. S. and Strausz, O. P., *AOSTRA Journal Of Research*, 2, 21-35(1985).

[12] Ignasiak, T. M., Kotlyar, L., Longstaffe, F. J., Strausz, O.P. and Montgomery, D. S., *Fuel*, 62(3), 353-362(1983).

[13] Kotlyar, L. S., Sparks, B. D. and Kodama, H., *AOSTRA Journal of Research*, 1(1), 99-106(1984).

[14] Majid, A. and Ripmeester, in *ACS Symposium*, Series 344; Met. Complexs Dossil Fuels, Ed: Filby, R.H. and Branthaver, J.F. Ed: Amer. Chem. Soc., Washington, D.C. p.290, 1987.

[15] Majid, A.,and Ripmeester,J.A., *Fuels*, 69, 1527(1990).

[16] Majik, A., Ripmeester, J.A. and Davidson, D.W, *National Research Council of Canada Report*, Report No. C1095-82S (1982).

[17] Majik, A., Ripmeester, J.A. *Fuel*, 65, 1714(1986).

[18] Kessick, M.A., *J. Can. Petrol. Technol.*, 18, 49-52(1979).

---

[19] Levine, S. and Sandford, E., *The Canadian Journal of Chemical Engineering*, 62, 258-268(1985).

[20] Menon, V.B. and Wasan, D.T., *Colloids and Surfaces*, 19, 89-107(1986).

[21] Marlow, B.J., Sresty, G.C., Hughs, and Mahajan, O.P., *Colloids and Surfaces*, 24, 283(1987).

[22] Menon, V.B. and Wasan, D.T., *Colloids and Surfaces*, 25, 387(1987).

[23] Drelich, J., Lelinski, D., and Miller, J.D., *Colloids and Surfaces*, A: Physicochemical and Engineering Aspects, 116, 211-213(1996).

[24] Eeley, D.D., Hey.M.J. and Symonds, J.D., *Colloids and Surfaces*, 32, 87(1988).

[25] Yan, N. and Masliyah, J.H, *Colloids and Surfaces*, A: Physicochemical and Engineering Aspects 96, 229-242(1995).

[26] van Oss, C. J., *Interfacial Forces In Aqueous Media*, p.171, Marcel Dekker, Inc., New York, 1994.

[27] Donhue, J. and Bertell, F. E., *J. Phys. Chem.*, 56, 480(1952).

[28] Berg, J. C., *Wettability*, Surfactant Science Series, Volume. 49 , New York, Marcel Dekker, Inc., p. 57, 1993.

[29] Friberg, S.E. and Yang, J., in *Emulsion and Emulsion Stability*, Surfactant Science Series, V.61, Ed: Sjoblom, J., New York, Marcel Dekker, Inc., pp. 1-40, 1996.

[30] Williams, D.H. and Fleming, I., *Spectroscopic Methods in Organic Chemistry*, 4th Edition, p.49, 1995.

[31] Williams, D.H. and Fleming, I., *Spectroscopic Methods in Organic Chemistry*, 4th Edition, p.60, 1995.

[32] Hepler, L. G. and Smith, R. G., in *AOSTRA Technical Publication*, Series #14, p. 129, Alberta Oil Sands Technology and Research Authority, Edmonton, Canada. 1994.

[33] Ali, L. H., *Fuel*, 57, 357(1978).

[34] Pouchert, C. J., *The Aldrich Library of FT-IR Spectra*, Edition 1, Aldrich Chemical Company, United State, 1985.

[35] Frost, R. L. and Vassallo, A. M., *Clays And Clay Minerals*, 44, 635(1996).

[36] Johnston, C.T, Agnew, S. F. and Bish, D. L., *Clays and Clay Minerals*, 38, 573(1990).

[37] Ignasiak, T.M., Kotlyar, L., Longstaffe, F.J., Stausz, O.P. and Montgomery, *Fuel*, 62, 353-362(1983).

---

[38] Van der Marel, H.W. and Beutelspacher, H., *Atlas of Infrared Spectroscopy of Clay Minerals and their Admixtures*, Elsevier, Scientific Publ. Co., 1976.

Chapter 7

Summary

Contents

7.1 Role of solid wettability on size of bubble generated at a rigid porous sparger

1. There is no effect of wettability of a porous rigid stainless steel sparger on the size of bubbles produced, at least under practical conditions (i.e., gas flowrate) for flotation. This may be attributed to the irregular pore shape and surface.
2. An equivalent pore diameter (D_e) can be estimated by trial-and–error back calculation using the Kumar and Kuloor model with D_e defined, bubble size is accurately predicted.

7.2 Role of fine solid wettability in froth treatment

1. The wettability of fine solids by water in bitumen froth increased with increasing heptane (paraffinic) content in the organic phase, resulting in an increased partition of solids into the interphase region. The change of interaction across the diluent/solid and diluent/water interfaces may be responsible.

2. The water wettability of fine solids changed little by washing with heptane, but increased significantly by toluene washing. An inversion of solid partition from organic to aqueous phase was observed in the latter case. The removal of absorbed organics by the strong dissolving power of toluene made the fine solids more water wettable.
3. A general correlation exists between wettability of fine solids and their partition among the three phases (organic, aqueous, and interphase). The key to improving the froth treatment process to produce bitumen free of solids and water is control of the wettability of the fine solids. This can be achieved by removing the organic substance from the solid surface and by increasing the paraffinic (heptane) content in the diluent. An ideal diluent should posses strong dissolving power for organic substances while exhibiting paraffinic property, a balance needs to be further established.
4. There appear two mechanisms to increase wettability of fine solids: remove organic coating by aromatic solvent, and change the interactions between the phases by increasing paraffinic (heptane) content in the diluent.

Chapter 8

Contribution to Knowledge and Future Work

Contents

8.1 Contribution to the Knowledge

8.1.1 Role of solid wettability on size of bubbles generated at a rigid porous sparger

1. Proved that there is no wettability effect on size of bubble produced at a stainless steel rigid porous spargers.
2. Confirmed that assuming contact angle is zero is adequate to solve for equivalent pore diameter of rigid porous sparger.

8.1.2 Role of fine solid wettability in froth treatment

1. Proved that the wettability of fine solids from the rag layer increases with increasing heptane content in diluent.
2. Showed that a toluene wash decreases the wettability of fine solids by removing the organic substance, whereas heptane does so by changing the interactions.

3. Identified that a diluent should have a paraffinic properties and ability to dissolve organic substances.

8.2 Suggested future work

8.2.1 Sparger wettability

1. Include gas momentum in a more rigorous treatment Kumar and Kuloor model.
2. Extend model to predict gas holdup and bubble surface area flux incorporating drift flux analysis.
3. Extend approach to non-rigid porous spargers (which are more widely used).

8.2.2 Fine solid wettability in froth treatment

1. Study contact angle and partition of fine solids in diluents of different composition, pH, electrolyte type and temperature, etc., to achieve the minimum water, and solid content in the organic phase.
2. Conduct demulsification experiments of water-in-oil emulsions stabilized by the fine solids from the rag layer washed by heptane and toluene under different conditions, such as pH, and electrolyte type, temperature, etc., to achieve the minimum water and solid content in the organic phase.
3. Correlate these studies with pilot scale tests.
4. Extend the findings to search other possible diluents.

Appendices

Kumar and Kuloor model for vertical orifices at constant flow

Single orifice

The Kumar and Kuloor model assumes that a bubble developed at a single orifice experiences two distinctive stages. An idealized sequence of bubble formation is illustrated at FigureA.1.

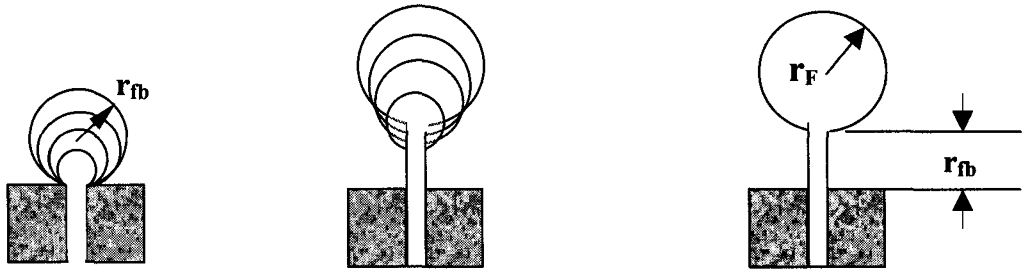

Figure A.1: - Idealized sequence of bubble formation: Two-stage

During the first stage, the bubble expands, a process that ends as soon as the upward forces overcome the downward forces. In the second stage, the bubble ascends while expanding, but remains connected to the orifice by a cylindrical neck. The second stage ends as soon as the distance that the vertical bubble base has moved reaches r_{fb}, the bubble radius from the first stage. The final volume is then

$$V_F = V_{fb} + Qt_F \tag{A1}$$

where V_{fb} is the volume of the bubble from the first stage, t_F the time that the bubble develops during second stage, and Qt_F the volume from the second stage.

a) First stage

When gas is fed through the orifice, a bubble forms and expands at a definite rate thereby increasing the inertial force and viscous drag force. Along with buoyancy and surface tension, these forces are

$$\textit{Buoyancy force}: F_b = V(\rho_l - \rho_g)g \tag{A2}$$

$$\textit{Viscous Drag}: F_{vis} = 6\pi r\mu v \tag{A3}$$

$$\textit{Surface tension force}: F_s = \pi D\gamma\cos\theta \tag{A4}$$

$$\textit{Inertial force}: F_i = \frac{d}{dt}(Mv) = \frac{Q^2(\rho_g + \frac{11}{16}\rho_l)}{12\pi(\frac{3}{4\pi})^{2/3}V^{2/3}} \tag{A5}$$

where v is the average velocity of the bubble center, D the pore diameter, and M the virtual mass of the bubble (i.e. the sum of the mass of the gas plus 11/16 of its volume of the surrounding liquid)

$$M = \left(\rho_g + \frac{11\rho_l}{16} \right) \bullet Qt \tag{A6}$$

and v is the rate of change of the bubble radius

$$v = \frac{dr}{dt} = \frac{Q}{4\pi r^2} \tag{A7}$$

From the force balance

$$F_b = F_{vis} + F_s + F_i \tag{A8}$$

one gets

$$V(\rho_l - \rho_g)g = 6\pi r \mu v + \pi D \gamma \cos\theta + \frac{Q^2(\rho_g + \frac{11}{16}\rho_l)}{12\pi(\frac{3}{4\pi})^{2/3} V^{2/3}} \tag{A9}$$

At the end of the first stage, $V = V_{fb}$, and rearranging Eq. (A9), yields

$$V_{fb}^{5/3} = \frac{11Q^2}{192\pi\left(\frac{3}{4\pi}\right)^{2/3} \cdot g} + \frac{3\mu Q V_{fb}^{1/3}}{2 \cdot \left(\frac{3}{4\pi}\right)^{1/3} \cdot g\rho_l} + \frac{\pi D \gamma \cos\theta V_{fb}^{2/3}}{g\rho_l} \tag{A10}$$

When rearranging the terms, Eq. (A10) becomes

$$V_{fb}^{5/3}-\frac{\pi D\gamma\cos\theta}{g\rho_l}V_{fb}^{2/3}-\frac{3\mu Q}{2\cdot\left(\frac{3}{4\pi}\right)^{1/3}\cdot g\rho_l}V_{fb}^{1/3}-\frac{11Q^2}{192\pi\left(\frac{3}{4\pi}\right)^{2/3}\cdot g}=0 \qquad \text{(A11)}$$

b) Second stage

The second stage begins at the moment the upward forces are larger than the downward forces. The bubble moves away from the orifice with a cylindrical neck forming to the orifice while it expands. It is assumed to detach when the moving distance covers r_{fb}, the radius from the first stage.

According to Newton's second law of motion, the bubble movement can be expressed as

$$\frac{d}{dt}\left(Mv'\right)=(V_{fb}+Qt)\rho_l g-6\pi r\mu v'-\pi D\gamma\cos\theta \qquad \text{(A12)}$$

where v' is the bubble velocity of the center in the second stage. It consists of two components: the velocity of expansion, $\frac{dr}{dt}$, and the velocity of bubble base movement, v, thus

$$v'=v+\frac{dr}{dt} \qquad \text{(A13)}$$

Substituting Eq. (A13) into (A12), and letting r_{fb} to be the radius of the bubble from the first stage and V_F the bubble volume of second stage, solving the differential equation, one obtains

$$r_{fb} = \frac{B}{2Q(A+1)}\left(V_F^2 - V_{fb}^2\right) - \frac{E}{AQ}\left(V_F - V_{fb}\right) - \frac{3C}{2Q(A-1/3)}\left(V_F^{2/3} - V_{fb}^{2/3}\right) \qquad \text{(A14)}$$

with

$$A = 1 + \frac{1.25 \cdot 6\pi \cdot \left(\frac{3}{4\pi}\right)^{1/3} V_{fb}^{1/3}\mu}{Q \cdot \left[\rho_g + \frac{11\rho_l}{16}\right]} \approx 1 + \frac{1.25 \cdot 96 \cdot \pi \cdot r_{fb}\mu}{11\rho_l \cdot Q} \qquad \text{(A15)}$$

$$B = \frac{\left(\rho_l - \rho_g\right) \cdot g}{Q \cdot \left[\rho_g + \frac{11\rho_l}{16}\right]} \approx \frac{16 \cdot g}{11 \cdot Q} \qquad \text{(A16)}$$

$$C = \frac{3\mu}{2 \cdot \left(\frac{3}{4 \cdot \pi}\right)^{1/3}\left[\rho_g + \frac{11\rho_l}{16}\right]} \qquad \text{(A17)}$$

$$E = \frac{\pi D\gamma \cos\theta}{Q \cdot \left[\rho_g + \frac{11\rho_l}{16}\right]} \approx \frac{16\pi D\gamma \cos\theta}{11Q\rho_l} \qquad \text{(A18)}$$

Since

$$r_{fb} = \left(\frac{3}{4\pi}V_{fb}\right)^{1/3} \tag{A19}$$

then, replacing r_{fb} in (A14), and expanding

$$\left(\frac{3}{4\pi}V_{fb}\right)^{1/3} = \frac{B}{2Q(A+1)}V_F^2 - \frac{B}{2Q(A+1)}V_{fb}^2 - \frac{E}{AQ}V_F + \frac{E}{AQ}V_{fb} - \frac{3C}{2Q(A-1/3)}V_F^{2/3} + \frac{3C}{2Q(A-1/3)}V_{fb}^{2/3} \tag{A20}$$

Rearranging the terms

$$\frac{B}{2Q(A+1)}V_F^{6/3} - \frac{E}{AQ}V_F^{3/3} - \frac{3C}{2Q(A-1/3)}V_F^{2/3} + \left(-\frac{B}{2Q(A+1)}V_{fb}^2 + \frac{E}{AQ}V_{fb} + \frac{3C}{2Q(A-1/3)}V_{fb}^{2/3} - \left(\frac{3}{4\pi}V_{fb}\right)^{1/3}\right) = 0 \tag{A.21}$$

Then the final bubble volume V_F can be obtained by Eqs. (A11) and (A21).

Multiple orifices

This model is an extension of the work on bubble formation at a single orifice. It estimates an average size of bubbles generated by a multiple orifice sparger based on the following assumptions[1]:

- The sparger has a large number of “potential sites”, but only some of them are “active sites” producing bubbles.

- The gas flow through the active pore sites is constant during bubble formation.
- The number of active pore sites decreases with an increase in gas flowrate.

The bubbles generated are assumed to be hexagonal packed in such a way that they contact each other (Figure A.2). The active pore sites per unit area *n* is,

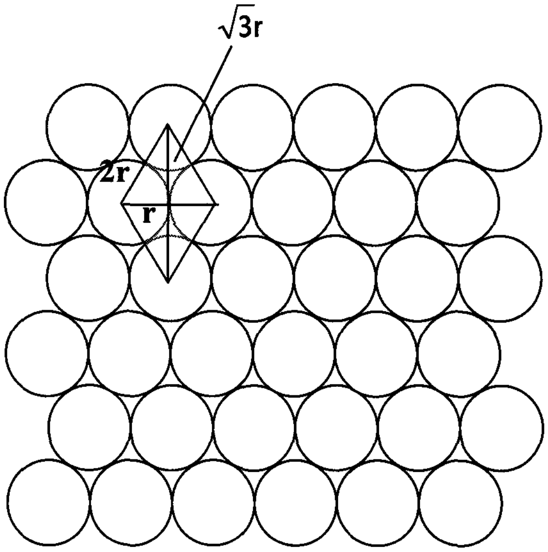

Figure A.2: - Close packing of bubbles.

$$n = \frac{(\frac{3}{4\pi}V_{F|Q})^{-2/3}}{2\sqrt{3}} = \frac{1}{2\sqrt{3}\cdot(\frac{3}{4\pi}V_{F|Q})^{2/3}} \qquad \text{(A22)}$$

Where $V_{F|Q}$ is the calculating final bubble size. Let A_s to be the external surface area of the porous media, then for each orifice, the gas flowrate is

$$Q = \frac{q}{nA_S} \tag{A23}$$

where q is the total gas flowrate, and Q the gas flowrate through a single orifice. The combination of Eqs. (A11), (A21), (A22) and (A23) can be used to estimate V_F or the average bubble diameter D_b. First, a value of n is assumed and the corresponding value of Q is calculated by Eq. (A23), then V_{fb} and V_F can be calculated by Eqs. (A11) and (A21), respectively. In turn, n is calculated by Eq. (A22). This n is compared to the previous n, and the iteration continues until these two n are equal.

Kumar and Kuloor model for horizontal orifices at constant flow

For constant air flowrate, this model again assumes that bubble formation is in two distinct stages. For the first stage, the bubble initially expands perpendicular to the orifice, but later, both the expansion and the movement are essentially in the vertical direction. As the bubble is formed at an angle to the vertical, a vertical component of the surface tension force will be operative during this stage. The first stage is assumed to end when the upward forces overcome the downward forces in vertical direction. Hence for the sparger operating at angle ϕ

$$V_{fb}^{5/3} - \frac{\pi D\gamma\cos\theta\cos\phi}{g\rho_l}V_{fb}^{2/3} - \frac{3\mu Q}{2\cdot\left(\frac{3}{4\pi}\right)^{1/3}\cdot g\rho_l}V_{fb}^{1/3} - \frac{11Q^2}{192\pi\left(\frac{3}{4\pi}\right)^{2/3}\cdot g} = 0 \tag{A24}$$

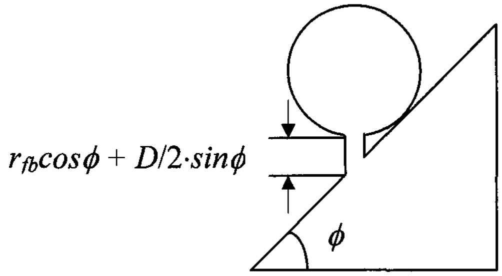

Figure A.3: - Condition of bubble detachment at oriented orifice

In the second stage, the characteristics in the present model are the same as the horizontal one, except the condition for detachment which occurs when the bubble has covered a distance equal to $r_{fb}\cos\phi+\frac{D}{2}\sin\phi$ (Figure A.3). Similar to the Eq. (A14), one obtains

$$r_{fb}\cos\phi+\frac{D}{2}\sin\phi=\frac{B}{2Q(A+1)}\left(V_F^2-V_{fb}^2\right)-\frac{E}{AQ}\left(V_F-V_{fb}\right)-\frac{3C}{2Q(A-1/3)}\left(V_F^{2/3}-V_{fb}^{2/3}\right)\text{(A25)}$$

If the sparger operates at 90°, the ϕ can only reach a maximum 60°, and remain constant afterwards. Therefore, Eq. (A25) is

$$\frac{1}{2}r_{fb}+\frac{\sqrt{3}}{2}\cdot\frac{D}{2}=\frac{B}{2Q(A+1)}\left(V_F^2-V_{fb}^2\right)-\frac{E}{AQ}\left(V_F-V_{fb}\right)-\frac{3C}{2Q(A-1/3)}\left(V_F^{2/3}-V_{fb}^{2/3}\right)\text{ (A26)}$$

$$\frac{B}{Q(A+1)}V_F^2 - \frac{2E}{AQ}V_F - \frac{3C}{Q(A-1/3)}V_F^{2/3} + \left(-\frac{B}{Q(A+1)}V_{fb}^2 + \frac{2E}{AQ}V_{fb} + \frac{3C}{Q(A-1/3)}V_{fb}^{2/3} - \left(\frac{3}{4\pi}\right)^{1/3}V_{fb}^{1/3} - \frac{\sqrt{3}}{2}D\right) = 0 \qquad \text{(A27)}$$

Where *A, B, C* have the same meaning as those in Eq. (A14). E is

$$E = \frac{\pi D\gamma\cos\theta\cos\phi}{Q\cdot\left[\rho_g + \frac{11\rho_l}{16}\right]} \approx \frac{16\cdot\pi D\gamma}{11\cdot Q\rho_l}\cos\theta\cos\phi \qquad \text{(A28)}$$

A similar procedure for the vertical orifice case can be used here to predict the bubble size.

For multiple horizontal orifices, the assumption for the vertical multiple orifices can be applied along with the equations for the single horizontal orifice. The bubble size can be predicted by the combination of Eqs. (A22), (A23), (A26) and (A27) with similar procedure in the case of vertical multiple orifices.

The simulation was performed by the combination of VC++ 6.0 and MATHLAB C++ Math Library 2.0. VC++ is from Microsoft, and the C++ Math Library from The MathWorks Inc., USA. VC++ was used as a framework, and the C++ Math Library as a tool to solve the equations.

---

[1] Kumar, R. and Kuloor, N. R., The Formation of Bubbles and Drops, in _Advanced in Chemical Engineering_, Volume 8, Ed: Drew, T. B., Cockelet, G. R., Hoopes, J. W. and Vermeulen, T., New York, Academic Press, pp. 255-368, 1970.

Surface tension of ethanol-water

Concentration of ethanol (V/V%)	0.1	0.5	3	10	15	20
Surface tension (mN/m)	71.62	70.46	62.13	50.25	46.15	41.67
Concentration of ethanol (V/V%)	25	30	35	40	45	50
Surface tension (mN/m)	38.37	35.95	33.91	32.35	30.93	29.86

Stainless steel sheet composition

Element	**C**	**Fe**	**P**	**S**	**Si**	**Ni**	**Cr**	**Mo**	**Cu**
Content (%)	0.054	1.53	0.066	<0.003	0.59	9.18	17.53	1.16	0.44

Water contact angle of stainless steel sheets

Heating temperature (^oC)	200	300	350	400	450	500	550
Water contact angle (^{o})	75.8	62	22.3	19.3	19.7	35.3	64.6

Water contact angle of sparger by ethanol-water mixture

Concentration of ethanol (V/V%)	20	25	30	35	40	45	50
Surface tension (mN/m)	89.7	87	73	63	51	33	14.6

Water contact angle of sparger by ethanol-water mixture (before and after 105°C heating)

Concentration of ethanol (V/V%)	20	25	30	35	40	45	50
Before	89.7	87	73	63	51	33	14.6
After	89.8	85	74.1	60	53	31	15

Pore structure integrity test

	Water flowrate (L/min)	0.00	2.00	3.00	4.00	5.00	7.00	8.00	10.00
Sparger 1	Pressure (PSI)	0.00	1.80	2.87	3.98	5.14	7.55	8.80	11.35
Sparger 2	Pressure (PSI)	0.00	1.70	2.73	3.82	4.97	7.37	8.62	11.20
Sparger 3	Pressure (PSI)	0.00	1.85	2.92	4.04	5.20	7.60	8.84	11.37

Pore structure integrity test

Pore structure subjected to modification

	Water flowrate (L/min)	0.00	2.00	3.00	4.00	5.00	7.00	8.00	10.00
Before	Pressure (PSI)	0.00	1.85	2.92	4.04	5.20	7.60	8.84	11.37
200°C	Pressure (PSI)	0.00	1.90	3.01	4.17	5.38	7.88	9.17	11.83
300°C	Pressure (PSI)	0.00	1.82	2.91	4.05	5.23	7.71	8.99	11.62

Surface tension of DOW 250C frother solution

Concentration (ppm)	0	2.5	5	10	15	20	30
Surface tension (mN/m)	72.01	70.07	68.03	66.01	63.96	62.24	62.0

Bubble size

Appendix B: Bubble data

CA=0			
0.776L/min	2.383L/min	4.034L/min	7.637L/min
0.41	0.45	1.01	1.28
0.41	0.52	0.81	0.9
0.43	0.52	0.84	1.88
0.45	0.52	0.94	1.47
0.45	0.52	0.89	1.72
0.45	0.52	0.71	1.32
0.45	0.52	0.69	0.73
0.45	0.52	1.19	0.64
0.45	0.52	0.94	1.86
0.45	0.52	0.99	1.73
0.45	0.59	1.1	1.15
0.45	0.59	0.81	0.64
0.46	0.59	0.75	0.71
0.47	0.59	0.89	1.04
0.47	0.59	1.35	1.23
0.47	0.59	0.79	1.92
0.48	0.59	0.81	1.28
0.48	0.59	0.89	1.63
0.48	0.59	0.89	1.6
0.49	0.61	1.02	1.55
0.49	0.61	1.07	1.03
0.49	0.61	0.99	0.73
0.5	0.61	0.71	0.73
0.5	0.61	1.1	1.83
0.5	0.61	0.75	0.73
0.5	0.61	0.81	1.52
0.51	0.61	1.1	0.71
0.51	0.61	0.81	2.03
0.51	0.61	0.89	0.96
0.51	0.61	0.69	1.52
0.52	0.64	0.69	1.12
0.52	0.64	1.21	0.73
0.53	0.64	1.39	1.54
0.53	0.64	1.47	0.71
0.53	0.64	0.79	0.83
0.53	0.64	1.38	1.23
0.53	0.64	1.4	0.91
0.53	0.64	1.4	1.6
0.53	0.64	0.89	0.71
0.54	0.64	0.79	0.91
0.54	0.64	0.69	1.41
0.54	0.64	0.69	1.35
0.54	0.64	1.01	1.62
0.54	0.64	0.79	1.21
0.54	0.64	0.88	1.52
0.54	0.64	0.81	1.18
0.54	0.64	0.89	2.05
0.54	0.64	0.89	1.22
0.54	0.64	0.79	0.77

Appendix B: Bubble data

0.55	0.64	0.89	0.83
0.55	0.64	0.88	0.64
0.56	0.64	1.19	1.47
0.56	0.64	1.2	1.18
0.56	0.64	1.01	0.52
0.56	0.64	0.81	1.47
0.56	0.64	1.07	1.28
0.56	0.64	1.1	0.91
0.56	0.64	0.99	1.12
0.56	0.64	1.01	0.71
0.56	0.64	1.1	2
0.56	0.64	0.89	1.43
0.56	0.64	1.13	1.15
0.56	0.64	0.89	0.86
0.56	0.64	1.2	2.43
0.56	0.64	0.99	1.74
0.56	0.64	1.26	1.72
0.56	0.64	0.69	1.6
0.56	0.67	0.79	2.12
0.56	0.67	0.94	1.32
0.56	0.67	0.79	1.35
0.57	0.67	1.01	1.14
0.57	0.68	1.01	1.09
0.57	0.69	1.41	1.52
0.57	0.71	0.94	1.67
0.57	0.71	0.69	1.01
0.57	0.71	1.3	1.09
0.57	0.71	1.1	1.15
0.57	0.71	1.16	1.12
0.57	0.71	1.21	0.96
0.57	0.71	1.1	1.46
0.57	0.71	1.1	1.44
0.58	0.71	1.01	0.81
0.58	0.71	1.13	1.01
0.58	0.71	1.02	1.32
0.58	0.71	0.81	1.86
0.58	0.71	1.19	1.03
0.58	0.71	0.94	1.14
0.58	0.71	0.99	0.96
0.58	0.71	1.1	0.52
0.58	0.71	1.13	0.64
0.59	0.71	0.75	1.72
0.59	0.71	0.75	0.91
0.59	0.71	0.71	0.96
0.59	0.71	0.94	1.12
0.59	0.71	1.16	1.23
0.6	0.71	0.81	1.12
0.6	0.71	0.81	0.86
0.6	0.71	0.94	1.52
0.6	0.71	0.89	0.77
0.6	0.71	0.81	1.01

0.6	0.71	1.1	1.03
0.6	0.71	1.1	1.32
0.6	0.71	0.94	1.18
0.6	0.71	0.81	1.12
0.6	0.71	1.07	1.03
0.6	0.71	0.69	1.23
0.61	0.71	0.88	0.71
0.61	0.71	1.2	1.15
0.61	0.71	1.2	1.52
0.61	0.71	0.81	1.83
0.61	0.71	1.07	1.21
0.61	0.71	0.75	1.12
0.61	0.71	0.89	1.32
0.61	0.71	1.07	1.12
0.61	0.71	0.99	0.71
0.61	0.71	0.69	0.81
0.61	0.71	0.69	1.86
0.61	0.71	0.69	0.83
0.62	0.71	0.99	0.91
0.62	0.71	0.85	0.81
0.62	0.71	0.81	0.81
0.62	0.71	1.1	1.22
0.62	0.71	0.75	1.49
0.62	0.71	0.57	1.01
0.62	0.71	0.88	0.81
0.62	0.71	0.75	1.18
0.62	0.71	0.99	1.21
0.62	0.71	0.5	1.22
0.62	0.71	0.85	1.41
0.62	0.71	0.81	1.28
0.62	0.71	1.34	0.83
0.63	0.71	0.89	1.04
0.63	0.72	0.62	0.91
0.63	0.72	0.79	1.63
0.63	0.73	1.13	1.32
0.63	0.73	0.69	0.81
0.63	0.73	0.88	0.71
0.63	0.73	0.88	2.24
0.63	0.73	0.81	0.87
0.63	0.73	0.69	0.91
0.63	0.73	0.5	0.45
0.63	0.73	0.62	1.52
0.63	0.73	0.89	1.63
0.632	0.73	0.88	1.01
0.64	0.73	0.79	1.44
0.64	0.73	0.84	0.59
0.64	0.73	1.01	0.71
0.64	0.73	1.3	1.32
0.64	0.73	1.01	0.83
0.64	0.73	0.57	0.9
0.64	0.73	0.71	1.15

0.64	0.73	0.62	0.52
0.65	0.73	0.99	0.71
0.65	0.73	0.89	0.77
0.65	0.73	1.52	1.01
0.65	0.73	0.81	2.18
0.65	0.73	0.81	1.44
0.65	0.73	0.75	1.21
0.65	0.73	1.41	1.21
0.65	0.73	1.01	1.03
0.65	0.74	0.69	1.28
0.65	0.74	1.01	0.83
0.65	0.74	0.62	0.81
0.65	0.74	0.79	0.64
0.65	0.74	0.69	0.57
0.65	0.74	0.5	1.28
0.65	0.75	1.39	1.32
0.66	0.75	1.39	1.23
0.66	0.75	0.99	0.59
0.66	0.75	0.99	1.15
0.66	0.76	1.02	0.64
0.66	0.76	0.88	1.23
0.66	0.76	0.85	1.03
0.66	0.76	0.62	0.96
0.66	0.76	0.62	1.03
0.66	0.76	0.85	0.96
0.66	0.76	1.13	1.32
0.66	0.76	1.13	1.15
0.67	0.76	1.13	0.81
0.67	0.76	1.13	1.6
0.67	0.76	0.88	1.23
0.67	0.76	0.81	1.41
0.67	0.76	0.57	1.03
0.67	0.76	0.81	1.03
0.67	0.76	0.5	1.23
0.67	0.76	0.88	0.96
0.67	0.76	1.18	1.15
0.67	0.76	0.41	1.28
0.67	0.77	0.69	0.96
0.67	0.77	1.01	1.62
0.67	0.77	0.62	0.77
0.67	0.77	1.21	1.23
0.67	0.77	0.94	1.21
0.67	0.77	1.21	1.21
0.67	0.77	1.07	1.01
0.67	0.77	0.75	0.71
0.67	0.77	1.33	0.64
0.67	0.77	1.2	1.09
0.67	0.77	1.1	1.15
0.67	0.77	1.1	1.03
0.67	0.77	1.01	0.91
0.68	0.77	1.41	1.41

0.68	0.77	1.21	1.36
0.68	0.77	1.01	1.32
0.68	0.77	0.99	0.91
0.68	0.77	1.1	1.74
0.68	0.77	1.13	0.64
0.68	0.77	0.94	1.12
0.68	0.77	0.99	1.21
0.68	0.77	0.71	1.14
0.69	0.77	1.16	1.01
0.69	0.77	1.24	0.64
0.69	0.77	1.24	0.59
0.69	0.77	0.69	1.09
0.69	0.77	1.19	1.73
0.69	0.77	0.75	0.77
0.7	0.77	0.69	1.21
0.7	0.77	0.69	1.55
0.7	0.77	1.02	0.64
0.7	0.77	0.89	1.92
0.7	0.77	0.99	2.03
0.7	0.77	1.13	1.15
0.7	0.77	0.81	0.45
0.7	0.78	0.85	0.81
0.71	0.78	0.75	0.77
0.71	0.78	0.57	0.77
0.71	0.78	0.69	0.77
0.71	0.78	1.07	1.15
0.71	0.78	1.19	0.9
0.71	0.78	0.69	0.86
0.71	0.78	1.58	0.9
0.71	0.78	0.69	1.14
0.71	0.78	0.85	1.15
0.71	0.78	1.16	1.14
0.71	0.78	0.69	0.86
0.71	0.78	0.69	1.22
0.71	0.78	0.94	1.28
0.71	0.78	1.19	1.32
0.71	0.78	1.36	1
0.71	0.78	0.94	1.49
0.71	0.79	1.3	1.09
0.71	0.79	1.34	1.21
0.71	0.79	0.71	1.09
0.71	0.79	0.94	1.29
0.71	0.79	1.02	1.46
0.71	0.79	0.71	0.81
0.71	0.79	0.89	0.61
0.71	0.79	1.52	0.83
0.71	0.79	1.02	1.18
0.71	0.8	1.07	1.01
0.71	0.8	1.44	1.04
0.71	0.8	0.57	1.15
0.71	0.8	1.39	1.23

0.71	0.8	0.99	0.91
0.71	0.8	1.33	0.77
0.71	0.8	0.89	0.86
0.71	0.8	1.07	0.73
0.71	0.81	0.99	0.83
0.72	0.81	1.01	0.71
0.72	0.81	1.07	0.83
0.72	0.81	0.69	1.03
0.72	0.81	1.02	1.09
0.72	0.81	0.62	0.86
0.72	0.81	0.88	1.23
0.72	0.81	0.88	1.18
0.72	0.81	0.94	1.18
0.72	0.81	0.94	1.18
0.72	0.81	0.94	1.12
0.72	0.81	0.75	1.32
0.72	0.81	0.85	1.35
0.72	0.81	1.07	1.01
0.72	0.81	0.94	1.28
0.72	0.81	0.94	1.77
0.72	0.81	0.84	1.72
0.72	0.81	0.88	0.45
0.72	0.81	0.81	0.91
0.72	0.81	1.02	1.6
0.72	0.81	0.62	1.6
0.73	0.81	0.69	1.6
0.73	0.81	0.62	1.43
0.73	0.81	0.81	0.64
0.73	0.81	0.71	1.41
0.73	0.81	1.2	1.23
0.73	0.81	0.85	1.36
0.73	0.82	0.88	1.49
0.73	0.82	0.89	1.32
0.73	0.82	0.81	1.21
0.73	0.82	0.75	1.47
0.73	0.82	1.1	1.54
0.73	0.83	0.99	1.04
0.73	0.83	1.13	1.54
0.73	0.83	1.07	1.23
0.73	0.83	0.89	1.55
0.73	0.83	1.16	1.32
0.73	0.83	1.16	1.52
0.73	0.83	0.99	0.71
0.73	0.83	0.89	0.9
0.73	0.83	1.21	1.28
0.73	0.83	0.99	1.72
0.73	0.83	0.88	1.54
0.73	0.83	0.75	1.09
0.73	0.83	0.89	1.73
0.73	0.83	0.89	1.41
0.74	0.83	0.89	1.47

0.74	0.83	0.89	0.96
0.74	0.83	0.79	0.52
0.74	0.83	0.69	0.71
0.74	0.83	0.89	1.28
0.74	0.83	1.19	1.41
0.74	0.83	1.19	1.12
0.74	0.83	1.19	1.52
0.74	0.83	1.19	0.9
0.74	0.83	1.19	1.67
0.74	0.83	1.19	1.63
0.74	0.83	1.19	1.12
0.74	0.83	1.19	1.63
0.74	0.83	0.99	1.32
0.74	0.83	1.27	1.43
0.74	0.83	1.39	1.23
0.75	0.83	1.41	1.15
0.75	0.83	0.99	1.43
0.75	0.83	0.99	0.83
0.75	0.83	0.88	1.79
0.75	0.83	1.13	1.63
0.75	0.83	1.19	1.03
0.75	0.83	1.1	1.04
0.75	0.83	0.89	1.12
0.75	0.83	1.01	0.96
0.75	0.83	0.99	1.44
0.75	0.83	1.02	1.41
0.75	0.83	1.34	1.52
0.75	0.83	0.75	1.92
0.75	0.84	0.88	1.32
0.75	0.84	1.5	1.14
0.75	0.84	1.01	1.32
0.75	0.84	1.2	0.9
0.75	0.84	0.55	0.32
0.75	0.84	0.79	0.81
0.75	0.84	0.79	0.91
0.75	0.85	0.94	1.04
0.75	0.85	1.07	1.01
0.75	0.85	0.69	1.21
0.75	0.85	0.98	1.09
0.75	0.85	0.59	0.9
0.75	0.85	0.99	0.59
0.75	0.85	0.57	0.71
0.76	0.85	0.89	1.43
0.76	0.85	0.81	1.55
0.76	0.86	0.55	1.32
0.76	0.86	1.1	1.21
0.76	0.86	1.07	0.83
0.76	0.86	1.21	1.15
0.76	0.86	1.02	1.58
0.76	0.86	1.33	0.9
0.76	0.86	1.26	1.35

Appendix B: Bubble data

0.76	0.86	0.89	1.21
0.76	0.87	0.69	1.15
0.76	0.87	0.98	1.03
0.76	0.87	0.99	0.91
0.76	0.87	1.1	0.87
0.76	0.87	0.85	1.46
0.76	0.87	1.33	1.94
0.76	0.87	0.81	1.47
0.76	0.87	0.85	1.72
0.77	0.87	1.1	1.41
0.77	0.87	0.94	1.28
0.77	0.87	1.13	1.46
0.77	0.87	1.07	0.71
0.77	0.87	1.12	1.43
0.77	0.87	0.69	1
0.77	0.87	0.75	0.87
0.77	0.87	1.07	0.52
0.77	0.87	0.71	1.41
0.77	0.87	0.55	1.04
0.77	0.87	0.85	1.41
0.77	0.88	0.81	1.32
0.77	0.88	0.69	1.47
0.77	0.88	0.81	1.01
0.77	0.88	0.84	1.18
0.78	0.88	1.47	0.64
0.78	0.88	0.84	0.64
0.78	0.88	0.55	0.83
0.78	0.88	0.85	0.52
0.78	0.88	0.5	0.87
0.78	0.88	0.88	0.61
0.78	0.89	0.88	0.77
0.78	0.89	0.88	0.81
0.78	0.89	0.88	1.32
0.78	0.89	1.2	1.52
0.78	0.89	0.89	1.62
0.78	0.89	1.41	1.52
0.78	0.89	0.85	0.96
0.78	0.89	1.3	0.9
0.78	0.9	0.57	1.21
0.78	0.9	0.81	0.83
0.78	0.9	0.94	0.83
0.78	0.9	1.21	0.83
0.78	0.9	1.3	0.71
0.78	0.9	0.89	0.91
0.78	0.9	0.57	0.9
0.78	0.9	0.57	0.87
0.78	0.9	0.62	1.15
0.78	0.9	0.81	1.15
0.79	0.91	1.1	0.96
0.79	0.91	0.88	0.91
0.79	0.91	1.26	0.83

0.79	0.91	1.2	0.91
0.79	0.91	0.94	0.77
0.79	0.91	1.02	1.12
0.8	0.91	0.99	0.9
0.8	0.91	1.1	0.81
0.8	0.91	0.99	0.91
0.8	0.91	0.79	1.09
0.8	0.91	0.79	1.21
0.8	0.91	0.79	1.23
0.8	0.91	0.89	0.96
0.81	0.91	0.69	1.22
0.81	0.91	0.69	1.29
0.81	0.91	0.62	1.46
0.81	0.91	0.38	1.41
0.81	0.91	0.69	1.23
0.81	0.91	0.85	1.12
0.81	0.91	0.69	0.91
0.81	0.91	0.62	0.96
0.81	0.91	0.75	1.47
0.81	0.91	0.71	1.23
0.81	0.91	0.81	1.43
0.82	0.91	0.89	1.15
0.82	0.91	1.13	0.64
0.82	0.91	0.94	1.18
0.82	0.91	1.3	1.32
0.82	0.91	1.2	1.44
0.82	0.92	1.34	1.09
0.82	0.93	1.1	1.01
0.82	0.93	0.85	0.83
0.83	0.93	0.94	0.64
0.83	0.93	1.1	1.52
0.83	0.94	0.79	1.03
0.83	0.94	0.89	0.96
0.83	0.95	0.88	1.23
0.83	0.95	0.99	0.81
0.84	0.95	0.84	1.15
0.84	0.95	1.1	0.64
0.84	0.95	0.99	0.77
0.85	0.96	0.89	0.87
0.85	0.96	0.81	0.71
0.85	0.96	1.41	0.77
0.85	0.96	0.99	0.83
0.85	0.96	1.02	1.43
0.85	0.96	0.84	1.03
0.85	0.96	1.19	1.15
0.85	0.96	1.21	1.28
0.86	0.96	1.1	1.04
0.86	0.96	0.62	0.96
0.86	0.97	0.81	1.32
0.87	0.97	0.89	0.96
0.87	0.97	0.99	0.91

Appendix B: Bubble data

0.87	0.98	0.99	1.09
0.88	0.98	1.13	1.12
0.88	0.98	0.69	1.01
0.89	0.98	0.89	0.91
0.89	0.99	0.69	1.28
0.89	0.99	1.02	0.87
0.89	1	0.81	0.73
0.9	1	1.01	1.35
0.9	1.01	1.3	
0.9	1.01	0.75	
0.9	1.01	0.79	
0.9	1.01	0.69	
0.9	1.01	0.89	
0.9	1.01	1.07	
0.9	1.01	0.69	
0.91	1.01	0.99	
0.91	1.02	0.99	
0.91	1.03	1.1	
0.91	1.03	1.21	
0.91	1.03	1.53	
0.91	1.03	1.1	
0.92	1.03	0.75	
0.92	1.03	1.01	
0.93	1.03	0.75	
0.93	1.04	0.75	
0.93	1.04	1.3	
0.93	1.04	1.26	
0.93	1.04	1.41	
0.93	1.04	1.21	
0.93	1.05	1.13	
0.94	1.05	1.53	
0.94	1.06	0.71	
0.97	1.06	0.94	
0.97	1.08	1.01	
0.97	1.1	1.07	
0.98	1.1	0.89	
0.98	1.12	1.01	
0.98	1.12	1.1	
0.98	1.12	1.13	
1.01	1.15	1.2	
1.01	1.15	1.41	
1.01	1.15	1.01	
1.02	1.18	1.1	
1.02		1.21	
1.02		0.79	
1.03		0.89	
1.03		0.94	
1.03		1.07	
1.03		0.79	
1.03		0.71	
1.05		0.71	

Appendix B: Bubble data

1.06	0.75
1.07	1.19
1.08	1.13
1.09	1.19
1.09	0.99
1.1	0.89
1.1	0.79
1.1	0.99
1.11	0.71
1.13	0.5
1.13	0.89
1.2	0.89
1.2	0.71
	0.75
	0.99
	0.88
	0.99
	0.94
	0.81
	1.19
	0.99
	1.16
	0.96

Appendix B: Bubble data

CA=41			
0.776L/min	2.383L/min	4.034L/min	7.637L/min
0.61	0.87	1.11	1.01
0.59	0.87	0.96	1.55
0.59	0.83	0.93	1.15
0.83	0.71	0.98	0.83
0.64	0.84	0.79	0.45
0.86	0.56	0.79	1.63
0.71	0.87	0.89	1.86
0.71	0.52	1.2	1.86
0.57	0.71	0.98	1.79
0.52	0.84	0.79	1.41
0.52	0.83	0.88	1.73
0.64	0.86	1.11	1.81
0.61	0.73	0.61	1.22
0.61	0.73	0.83	1.6
0.61	0.71	1.05	1.49
0.64	0.91	1.02	1.44
0.73	0.82	0.83	1.67
0.57	0.82	0.98	1.11
0.81	0.71	0.79	1.47
0.59	0.83	0.98	0.87
0.71	0.83	0.98	1.28
0.64	0.64	0.92	1.55
0.73	0.8	1.02	1.47
0.64	0.89	1.45	1.47
0.71	0.83	0.88	0.83
0.71	0.73	0.89	0.71
0.52	0.64	0.66	1.12
0.83	0.97	0.75	0.52
0.61	0.77	0.83	1.03
0.52	0.89	0.93	1.71
0.71	0.87	1.11	1.09
0.52	0.92	0.93	1.72
0.61	0.95	0.93	0.81
0.71	0.95	0.7	1.32
0.64	0.75	0.88	1.52
0.61	0.52	1.4	0.81
0.71	0.97	0.66	1.36
0.71	0.97	0.79	0.61
1.03	0.81	1.14	1.15
0.64	0.81	0.75	1.72
0.52	0.49	0.85	1.41
0.71	0.73	0.93	1.41
0.77	0.71	0.75	0.61
0.64	0.87	0.83	1.32
0.64	0.9	1.17	1.09
0.81	0.89	0.85	1.03
0.64	0.75	0.92	1.35
0.64	0.88	0.92	0.64
0.81	0.75	1.29	1.01
0.81	0.71	0.79	1.23

Appendix B: Bubble data

0.71	0.86	0.93	1.35
0.73	0.8	0.85	1.73
0.87	0.83	0.79	1.94
0.91	0.64	0.93	1.86
1.03	0.85	0.85	0.83
0.61	0.83	0.79	0.81
0.71	0.83	0.93	1.23
0.9	0.84	0.85	1.21
0.9	0.84	0.93	0.71
0.83	0.71	1.05	1.01
0.71	0.71	0.93	1.23
0.59	0.91	1.03	1.92
0.91	0.86	0.92	1.12
0.73	0.82	0.92	1.69
0.59	0.86	0.79	1.54
0.71	0.71	1.05	1.41
0.64	0.87	1.03	1
0.59	0.77	1.06	1.03
0.59	0.89	0.83	0.91
0.59	0.86	0.75	1.01
0.59	0.83	0.85	1.22
0.73	0.71	1.03	0.83
0.73	0.71	0.83	1.43
0.52	0.71	0.85	0.96
0.83	0.83	1.2	0.91
0.77	0.9	0.83	1.09
0.91	0.79	1.11	1.58
0.57	0.81	0.92	1.32
0.83	0.97	0.93	0.71
0.64	0.86	0.88	1.67
0.59	0.73	1.05	1.12
0.73	0.52	0.93	1.09
0.86	0.78	0.85	1.6
0.61	0.89	1.05	1.12
0.77	0.89	1.11	1.29
0.71	1.01	1.11	1.72
0.77	0.81	0.98	1.62
0.64	0.73	0.83	1.74
0.57	0.89	0.59	1.32
0.77	0.89	0.59	1.74
0.64	0.81	0.85	1.12
0.64	0.78	0.85	0.91
0.71	1.01	0.98	1.67
0.9	0.82	0.83	1.32
0.9	0.97	1.24	1.35
0.71	0.9	1.17	1.22
0.73	0.73	0.98	1.41
0.45	0.89	0.93	0.73
0.59	0.9	0.93	1.41
0.71	0.8	0.98	1.52
0.77	0.88	1.03	0.86
0.64	0.77	0.93	0.91

0.73	0.88	1.03	1.52
0.83	0.87	0.83	1.47
0.52	0.9	1.11	1.47
0.83	0.89	0.98	1.43
0.59	0.71	1.41	1.15
0.86	0.87	0.93	1.09
0.96	0.93	1.29	1.09
1.63	1.01	0.92	1.04
0.81	0.49	1.23	1.12
0.96	0.71	1.23	1.22
0.73	1.03	1.19	1.12
0.96	0.77	0.88	1.18
0.81	0.87	0.88	1.09
0.52	0.87	0.88	1.47
0.59	0.82	0.83	1.91
0.87	0.77	1.05	0.71
0.64	0.88	0.93	0.96
0.4	0.77	1.05	0.64
0.71	0.73	0.85	1.69
0.71	0.73	0.79	0.91
0.61	0.73	1.41	1.41
0.52	0.81	0.75	0.45
0.81	0.81	0.99	1.15
0.81	0.89	1.17	1.12
0.77	0.77	1.03	0.96
0.64	0.82	1.19	1.35
0.77	0.82	1.31	1.63
0.71	0.64	1.38	1.32
0.59	0.73	1.3	0.64
0.64	0.87	1.29	1.28
0.83	0.77	0.93	1.23
0.83	0.85	0.93	1.6
0.91	0.73	0.93	1.23
0.52	0.71	0.92	1.63
0.71	0.84	1.3	1.72
0.71	0.83	0.83	0.87
0.81	0.78	1.17	1.55
0.73	0.78	1.17	1.23
0.71	0.81	0.83	1.74
0.81	0.71	0.85	1.43
0.71	0.87	1.17	0.91
0.64	0.49	0.88	0.96
0.81	0.89	1.05	0.71
0.52	0.77	0.98	1.62
0.61	0.71	0.88	1.79
0.73	0.71	0.93	1.62
0.59	0.49	0.93	0.81
0.73	0.71	0.85	1.52
0.43	0.88	1.29	1.67
0.71	0.88	1.3	1.52
0.71	0.87	0.93	1.65
0.59	0.89	0.83	1.73

0.87	0.98	1.14	0.59
0.59	0.91	0.75	1.62
0.57	0.49	0.75	1.32
1.03	0.89	0.79	1.35
0.81	0.87	0.93	1.41
0.64	0.75	0.7	1.21
0.81	0.78	1.05	1.55
0.91	0.83	0.93	1.15
0.71	0.52	1.17	1.12
0.81	0.49	0.85	1.09
0.83	0.73	0.93	0.96
0.81	0.73	0.93	1.74
0.64	0.73	0.79	1.32
0.59	0.87	0.89	0.91
0.77	0.77	0.92	0.91
0.87	0.91	0.85	1.82
0.73	0.81	0.7	2.03
0.87	0.98	1.17	1.32
0.91	0.91	0.93	1.32
0.71	0.73	1.23	1.12
0.59	0.9	0.98	1.21
0.83	0.77	0.79	1.03
0.77	0.71	0.75	1.12
0.71	0.77	1.03	1.41
0.45	1	0.99	1.47
0.91	1.01	1.14	0.71
0.73	0.91	1.24	0.87
0.71	1.23	0.7	1.47
0.81	0.91	0.7	1.12
0.52	0.81	0.93	1.03
0.45	0.83	0.93	1.32
0.77	0.91	0.83	0.71
0.64	0.64	1.03	0.71
0.64	0.64	1.37	0.73
0.77	0.97	0.47	0.71
0.73	0.83	1.17	1.12
0.87	0.8	0.93	1.03
0.59	1.01	0.85	1.74
0.71	1.21	0.93	1.81
0.83	0.81	0.93	1.43
0.87	1.01	0.85	0.81
0.77	0.73	0.93	0.61
0.96	0.91	0.79	0.61
0.81	1.03	0.79	0.96
0.83	0.9	0.83	1.94
0.81	0.86	0.85	1.82
0.59	0.83	0.93	0.59
0.96	0.83	0.99	1.67
0.77	0.71	0.93	1.36
0.59	0.77	0.83	1.22
0.77	0.77	0.89	0.64
0.64	0.77	0.75	1.79

Appendix B: Bubble data

0.77	0.82	0.7	1.28
0.77	0.83	0.83	1.67
0.71	0.81	0.75	1.18
0.59	0.8	0.47	1.36
0.81	0.71	1.38	1.82
0.64	0.78	0.83	1.21
0.52	0.83	0.93	1.62
0.57	0.83	1.17	1.52
0.91	0.87	0.93	1.32
0.64	0.75	0.93	1.52
0.77	0.73	0.69	1.35
0.83	0.87	1.03	1.6
0.71	1.01	0.83	1
0.71	0.75	1.03	1.43
0.91	0.83	1.14	2.14
0.71	0.77	1.39	1.63
0.83	0.76	0.69	1.86
0.73	0.73	1.06	1.47
0.61	0.71	0.89	1.32
0.71	0.77	1.17	1.21
0.71	0.77	0.93	1.32
0.57	0.71	0.89	1.03
0.73	0.73	1.05	0.91
0.71	0.52	1.05	1.12
0.59	0.9	1.1	1.23
0.77	0.82	0.42	0.71
0.73	0.83	0.85	1.35
0.77	0.83	0.99	0.96
0.45	0.77	0.75	0.87
0.73	0.87	0.93	0.71
0.73	0.71	0.89	0.9
0.73	0.81	0.75	0.71
0.73	0.81	0.99	0.9
0.73	1.01	0.99	1.55
0.73	0.77	0.98	0.81
0.83	0.64	0.89	0.87
0.77	0.91	1.09	0.77
0.64	0.84	0.93	0.83
0.59	0.83	0.79	1.15
0.64	0.91	0.75	1.73
0.87	0.77	0.69	0.77
0.77	0.83	0.93	1.32
0.73	0.81	0.93	1.01
0.77	0.83	0.93	1.99
0.73	0.91	0.7	0.52
0.64	1.09	0.93	0.59
0.73	0.91	0.89	1.57
0.59	0.77	1.11	1.15
1.01	0.84	0.69	0.73
1.01	1.01	1.09	1.29
1.01	0.64	1.09	1.79
1.01	0.64	0.75	0.52

Appendix B: Bubble data

1.01	0.91	1.38	0.64
1.01	0.77	1.11	0.59
0.71	0.79	0.93	1.32
0.81	0.82	0.88	1.01
0.73	0.86	0.79	0.71
0.81	0.83	0.83	1.28
0.61	0.71	0.83	1.92
0.83	0.77	0.99	0.52
0.61	0.73	1.11	0.71
0.64	1.09	0.87	0.59
0.91	0.71	0.99	1.35
0.45	0.77	0.89	1.63
0.71	0.71	1.17	1.52
0.59	0.78	0.83	0.83
0.64	0.79	0.98	1.35
0.59	0.71	0.47	1.32
0.81	0.96	1.17	0.91
0.81	0.71	1.31	0.61
0.52	0.79	0.87	0.61
0.77	0.77	1.17	0.71
0.91	0.79	0.9	0.71
0.83	0.77	0.92	0.77
0.83	0.75	0.98	0.77
0.77	0.45	0.92	0.77
0.59	0.71	1.06	0.77
0.52	1.04	1.35	0.77
0.52	0.79	0.99	0.77
0.81	1.03	0.99	1.47
0.73	1.09	0.79	0.71
0.77	0.71	1.11	0.64
0.57	1.04	0.83	2.18
0.57	0.64	0.93	0.71
0.77	0.73	0.69	1.32
0.71	0.84	0.99	1.63
0.71	0.71	0.75	0.71
0.91	1.03	0.79	0.91
0.83	0.91	1.24	1.21
0.83	0.83	0.47	1.32
0.87	0.87	0.99	1.63
1.04	0.78	1.05	0.52
0.77	0.77	0.89	0.52
0.71	0.81	0.79	1.35
0.64	0.77	0.75	0.77
0.59	1.03	0.93	0.59
0.77	1.03	0.98	0.61
0.64	0.98	0.9	0.61
0.81	0.71	1.14	0.71
0.61	0.91	0.99	0.81
0.83	0.71	0.98	1
0.61	0.83	0.99	1.72
0.45	0.9	0.99	1.03
0.59	0.61	0.99	0.59

Appendix B: Bubble data

0.73	0.64	0.88	0.45
0.52	0.81	0.98	0.71
0.9	0.64	1.11	1.01
0.77	0.71	1.06	0.81
0.71	0.77	0.79	1.52
0.83	0.64	0.93	1.41
0.59	0.64	1.37	1.01
0.61	0.77	0.66	0.64
1.03	0.64	0.98	2.11
0.52	0.77	0.93	1.03
0.73	0.61	0.99	1.21
0.73	0.73	0.79	1.15
0.83	0.64	0.79	0.77
0.61	0.83	1.01	1.09
0.52	0.64	1.03	1.92
0.57	0.9	0.89	0.96
0.73	0.81	1.06	0.81
0.57	0.61	0.99	0.91
0.64	1.04	1.33	0.83
0.71	0.81	0.83	1.55
0.81	0.64	0.9	1.23
0.71	0.91	1.03	0.83
0.61	1.01	0.83	1.03
0.81	0.81	0.69	0.96
0.71	0.91	0.83	1.44
0.64	0.83	1.03	0.9
0.64	1.09	0.98	0.96
0.91	1.09	0.99	0.81
0.52	0.64	1.05	0.83
0.52	0.71	0.93	1.04
0.71	0.61	0.66	0.71
0.45	0.52	0.99	0.57
0.57	0.64	0.79	0.64
0.59	0.96	0.75	1.12
0.71	0.83	0.85	0.87
0.52	0.71	0.98	1.01
0.59	0.91	0.88	1.18
0.52	1.09	1.14	0.96
0.45	0.97	0.66	1.03
0.71	0.52	0.98	0.9
0.71	1.09	0.85	0.71
0.71	1.01	1.11	1.32
0.57	0.81	0.93	1.52
0.59	0.64	0.92	0.57
0.73	0.81	0.98	0.83
0.64	0.71	0.69	0.4
0.61	0.57	0.79	1.6
0.71	0.83	0.85	0.52
0.64	1.01	0.7	0.57
0.52	1.01	0.83	1.12
0.71	0.91	0.98	0.91
0.61	0.87	0.66	0.57

Appendix B: Bubble data

0.57	0.9	0.85	1.74
0.64	1.12	0.54	0.83
0.52	0.83	0.92	1.12
0.96	0.81	0.98	1.43
0.64	1.21	0.93	0.61
0.61	0.64	1.11	0.81
0.45	1.03	1.03	0.96
0.52	0.83	0.85	0.81
0.81	0.71	0.79	1.09
0.57	0.52	0.79	0.57
0.52	0.71	0.93	1.62
0.83	0.71	0.98	1.32
0.81	0.81	0.73	1.32
0.71	0.77	0.85	1.21
0.77	1.03	0.93	1.32
0.64	0.71	0.93	1.46
1.12	0.91	0.83	0.43
0.77	0.75	0.93	1.01
0.64	0.83	0.83	0.61
0.71	0.83	1.34	1.92
0.73	0.61	1.16	0.86
0.71	0.61	1.45	1.15
0.87	0.71	0.59	1.15
0.77	0.71	0.66	1.15
0.77	0.83	0.79	1.44
0.64	0.81	0.79	0.91
0.94	0.75	1.49	0.91
0.52	0.64	0.79	0.71
0.71	0.71	0.75	1.04
0.52	0.87	0.85	1.01
0.45	0.61	0.73	1.22
0.59	0.61	0.93	0.96
0.59	0.64	0.73	1.03
0.94	0.73	0.73	0.83
0.71	0.64	0.92	0.96
0.83	0.64	0.98	1.03
0.83	0.64	0.83	1.28
0.73	0.64	0.79	1.12
0.71	0.64	0.79	1.32
0.89	0.59	0.85	0.91
0.91	0.61	0.59	0.71
0.91	0.59	0.89	1.28
0.83	0.71	0.75	0.52
0.83	0.64	0.85	0.61
0.83	0.73	0.66	0.71
0.61	0.61	0.79	0.87
0.91	0.71	0.93	1.43
0.83	0.57	0.85	1.52
1.01	0.61	0.92	0.61
0.73	0.61	0.99	0.96
0.87	0.73	0.79	1.01
0.64	0.71	0.98	0.83

Appendix B: Bubble data

0.52	0.87	1.37	0.96
0.81	0.71	0.98	1.23
0.64	0.64	0.85	1.86
0.59	0.52	0.69	1.52
0.77	0.87	0.85	1.01
1.04	0.81	0.93	0.77
0.73	0.77	0.75	0.71
0.59	0.52	0.75	1.01
0.73	0.52	0.75	0.91
0.77	0.77	0.66	0.86
0.71	0.83	0.88	1.94
0.71	0.64	0.93	1.28
0.73	0.91	0.93	1.12
0.71	0.64	0.79	0.91
0.83	0.71	0.93	1.41
0.64	0.9	0.93	1.83
0.87	0.73	0.92	1.62
0.71	0.9	1.05	0.57
0.77	0.83	1.03	0.71
0.77	0.64	1.17	0.91
0.81	0.73	0.85	1.09
0.52	0.71	0.85	1
0.73	0.87	0.73	1.28
0.77	0.91	0.75	0.83
0.71	0.81	0.88	1.74
0.64	0.96	1.17	1.63
0.64	0.71	0.79	1.21
0.71	0.71	0.88	1.35
0.64	0.87	0.73	0.81
0.52	0.45	0.92	1.61
0.52	0.64	1.23	1.73
0.64	0.96	0.98	1.01
0.68	0.96	0.93	0.71
0.52	0.71	0.93	0.52
0.52	0.61	1.05	0.4
0.59	0.64	0.79	1.03
0.57	0.52	1.05	0.83
0.45	1.15	0.85	0.9
0.64	0.61	0.85	0.71
0.52	0.64	0.69	0.64
0.61	0.64	0.98	0.71
0.52	0.59	1.05	0.77
0.52	1.01	0.66	1.04
0.4	0.61	0.73	0.96
0.59	0.64	1.17	1.12
0.57	0.64	0.98	0.64
0.59	0.77	1.14	1.01
0.73	0.83	0.69	0.61
0.78	0.83	1.14	1.01
0.71	0.84	0.93	1.32
0.59	0.64	1.2	1.62
0.73	0.64	0.73	0.52

Appendix B: Bubble data

0.59	0.59	0.73	1.22
0.52	0.59	0.92	1.12
0.64	0.82	0.66	1.29
0.57	0.83	0.89	1.44
0.57	0.87	0.88	1.32
0.64	0.83	0.99	1.22
0.78	0.87	0.98	1.61
0.52	0.9	1.05	1.62
0.64	0.81	0.83	1.28
0.71	0.77	1.2	1.01
0.83	0.61	0.93	0.96
0.71	0.81	1.21	0.96
0.61	0.99	1.21	1.35
0.81	0.99	1.21	1.41
0.81	0.57	1.06	1.83
0.64	0.91	0.7	1.47
0.81	0.88	0.93	0.91
0.71	0.87	0.79	0.91
0.71	0.59	0.85	1.28
0.67	0.9	1.05	1.32
0.61	0.93	1.01	0.91
0.59	0.81	0.61	1.52
0.59	0.83	0.93	2.14
0.61	0.94	1.34	0.59
0.52	0.94	0.98	0.81
0.59	0.81	0.73	1.15
0.71	0.43	0.83	1.86
0.43	0.91	1.05	1.41
0.52	0.71	0.73	1
0.79	0.91	0.89	1.15
0.71	1	0.85	1.36
0.73	0.83	0.85	0.81
0.73	0.96	0.73	1.23
0.71	0.93	1.03	0.81
0.57	0.58	0.73	0.77
0.83	0.61	0.73	0.77
0.85	0.81	0.73	1.04
0.59	0.81	0.66	0.52
0.87	0.83	0.85	0.81
0.88	0.93	0.73	1.52
0.71	0.81	0.79	0.91
0.71	0.64	1.2	1.41
0.43	0.91	0.99	0.71
0.73	0.83	1.25	0.96
0.64	0.83	0.98	1.12
0.8	0.81	0.73	0.57
0.59	0.8	0.92	0.71
0.61	0.61	0.92	1.35
0.64	0.64	0.85	0.81
1.12	0.71	0.85	1.03
0.71	1.13	1.03	1.22
0.64	0.9	0.85	0.64

Appendix B: Bubble data

0.52	0.61	0.66	0.64
0.64	0.83	0.73	0.91
0.57	0.59	0.54	1.03
0.59	0.81	0.79	0.91
	0.81	0.88	0.96
	0.81	0.79	0.81
	0.83	1.2	0.96
	0.79	0.85	1.18
	0.77	0.79	0.81
	0.81	0.73	0.77
	0.91		0.71
	0.81		0.61
	0.83		1.63
	0.64		1.23
	0.77		1.32
	0.71		1.73
	0.71		1.32
	0.83		1.12
	0.87		1.41
	0.87		
	0.64		
	1.01		
	0.91		
	0.61		
	0.99		
	0.95		
	0.89		
	1.12		
	0.86		
	0.96		
	0.97		
	1.14		
	1.1		
	0.83		
	1.12		
	0.91		

Appendix B: Bubble data

CA=66			
0.776L/min	2.383L/min	4.034L/min	7.637L/min
0.93	0.45	0.83	0.83
0.65	0.79	0.73	1.12
0.69	0.79	0.73	0.64
0.95	0.42	0.83	0.57
0.95	0.33	1.20	0.64
1.04	0.73	0.99	0.40
0.74	0.79	1.27	0.77
0.73	0.80	0.90	0.96
0.80	0.91	0.90	1.09
0.75	0.77	1.00	0.40
0.72	0.83	0.81	0.71
0.80	0.91	0.73	0.90
0.69	0.78	0.99	1.23
1.02	0.96	0.90	1.41
0.78	0.82	0.65	1.09
1.01	1.00	0.48	1.35
0.92	0.83	0.63	0.43
0.93	0.93	0.94	1.03
0.66	0.79	1.31	0.83
0.65	0.87	0.88	0.61
0.76	0.90	0.81	1.60
0.62	0.93	0.70	1.12
0.61	0.90	0.93	0.96
0.80	0.87	0.83	0.87
0.71	0.84	0.85	1.09
0.68	0.74	0.88	0.96
0.54	0.86	0.69	1.77
0.57	0.80	1.00	0.57
0.69	0.83	1.38	0.81
0.59	0.95	1.27	1.18
0.46	0.86	1.14	1.35
0.80	0.91	1.00	1.12
0.82	0.77	0.63	0.71
0.99	0.91	0.81	0.96
0.85	0.77	0.81	0.91
1.00	0.76	0.90	0.83
0.88	0.93	1.00	0.96
0.96	0.91	1.00	1.09
0.80	0.91	0.83	0.71
0.65	0.79	0.63	1.28
0.58	0.84	0.85	1.44
0.61	1.01	0.90	0.32
0.70	0.90	0.90	0.71
0.90	0.54	0.81	0.83
0.93	0.91	0.48	0.43
0.83	0.85	1.10	0.57
0.77	0.84	0.80	1.15
0.61	0.84	0.69	0.77
0.69	0.77	0.73	0.64
0.60	0.76	0.81	1.00

0.90	0.77	1.16	1.28
0.59	0.83	1.20	1.12
0.72	0.91	0.63	1.12
0.52	0.79	0.93	0.90
0.61	0.80	0.90	1.15
0.66	0.88	0.69	1.01
0.84	0.89	0.69	1.52
0.71	0.91	0.83	1.23
0.76	0.77	0.73	1.15
0.68	0.80	0.90	1.36
0.62	0.91	1.00	0.73
0.67	0.73	1.04	1.23
0.59	0.93	0.90	1.46
0.75	0.79	0.93	1.21
0.54	0.77	1.07	1.41
0.54	0.93	1.00	1.92
0.61	0.73	0.85	0.91
0.78	0.97	0.73	0.96
0.89	0.94	0.71	1.12
0.98	0.99	0.85	1.12
0.91	0.89	0.93	1.23
0.43	0.98	1.00	0.91
0.53	0.61	0.90	0.96
0.67	0.81	0.85	1.15
0.62	0.92	0.88	1.03
0.71	0.95	0.81	1.28
0.69	0.91	0.94	1.63
0.42	0.91	1.00	1.52
0.51	0.95	1.06	0.96
0.69	0.97	1.00	1.32
0.54	0.87	1.29	1.18
0.54	1.00	1.17	1.28
0.74	0.97	0.88	1.82
0.54	0.79	0.71	0.87
0.54	0.84	0.94	1.12
0.48	0.69	0.98	1.01
0.46	0.74	0.94	1.47
0.60	0.87	0.73	0.90
0.58	0.61	0.69	0.81
0.70	0.87	0.90	0.71
0.48	0.87	1.18	0.81
0.38	0.69	0.69	1.03
0.88	1.14	0.69	1.83
0.69	0.61	0.69	1.35
0.37	0.69	0.69	1.12
0.58	0.92	0.83	1.72
0.54	0.92	0.73	1.86
0.54	0.50	0.99	1.28
0.54	0.87	0.92	1.03
0.52	0.85	1.04	1.03
0.80	0.98	0.98	1.22
1.00	0.89	0.69	0.91

Appendix B: Bubble data

1.02	0.97	0.83	1.09
0.59	0.85	0.69	0.83
0.73	0.96	0.77	0.90
0.84	0.65	1.31	1.44
0.62	0.79	0.81	0.81
0.74	0.60	0.93	1.09
0.74	0.80	0.85	1.23
0.71	0.83	1.04	1.03
0.93	0.82	1.04	1.01
0.98	0.86	0.90	0.87
0.91	0.65	0.90	1.23
0.71	0.87	1.07	1.23
0.71	0.61	1.04	0.61
0.74	0.81	0.88	0.77
0.71	0.92	0.88	1.28
0.75	1.02	1.25	1.09
0.53	0.81	0.98	0.64
0.56	0.78	1.06	1.83
0.95	0.79	0.83	1.15
0.69	0.78	0.98	1.41
0.45	0.65	1.04	1.09
0.46	0.65	0.81	0.90
0.59	0.65	1.10	1.15
0.59	0.73	0.98	0.96
0.69	0.85	0.81	1.12
0.65	0.79	0.90	0.96
0.75	0.77	0.98	1.12
0.74	0.77	0.71	0.81
0.67	0.71	0.81	0.91
0.80	0.48	0.69	1.04
0.67	0.97	0.85	1.91
0.57	0.65	0.69	0.59
0.69	0.62	1.01	0.71
0.75	0.61	0.99	0.64
0.83	0.79	0.90	0.71
0.78	1.02	1.01	1.43
0.54	0.99	0.81	1.43
0.56	0.50	0.81	1.60
0.53	0.48	0.90	0.71
0.66	0.50	0.81	1.43
0.46	0.43	0.94	0.77
0.62	0.65	0.90	0.83
0.54	0.77	1.06	1.22
0.69	0.77	1.38	1.32
0.59	0.77	0.90	0.86
0.59	0.77	0.71	1.12
0.60	0.77	1.31	1.12
0.93	0.67	0.85	2.58
0.75	0.85	0.83	1.09
0.71	0.81	0.99	0.45
0.83	0.92	0.81	0.43
0.69	0.84	1.18	0.29

0.45	0.61	0.69	0.83
0.45	0.77	1.06	1.41
0.64	0.69	0.71	0.91
0.59	0.62	0.99	0.77
0.69	0.74	0.90	0.59
0.61	0.85	0.85	0.71
0.59	0.69	0.73	3.01
0.59	0.85	1.01	0.64
0.83	0.80	0.92	0.90
0.92	0.69	1.04	1.12
0.57	0.50	0.71	1.23
0.43	0.59	0.73	1.15
0.69	0.50	1.01	0.57
0.69	0.73	0.88	1.28
0.56	0.79	0.92	1.23
0.57	0.85	1.01	1.04
0.57	0.65	0.73	1.14
0.54	0.81	1.01	1.15
0.73	0.73	0.61	0.96
0.64	0.61	1.01	0.64
0.61	0.65	0.73	1.15
0.75	0.79	0.63	0.64
0.65	0.73	0.48	1.52
0.51	0.79	0.85	1.04
0.54	0.69	0.92	0.83
0.59	0.77	0.94	1.22
0.54	0.85	0.92	0.64
0.60	0.91	1.27	1.35
0.74	0.73	1.06	0.81
0.62	0.88	1.01	1.32
0.60	0.73	0.71	1.23
0.65	0.60	0.73	1.41
0.56	0.67	0.98	0.73
0.75	0.69	1.27	0.77
0.54	0.60	0.73	1.12
0.71	0.61	0.83	0.71
0.64	0.73	0.92	0.61
0.62	0.48	0.73	0.71
0.64	0.65	0.81	0.96
0.52	0.77	1.01	0.61
0.57	0.87	1.01	1.32
0.69	0.85	1.01	0.64
0.53	0.84	0.71	1.28
0.51	0.35	1.20	1.28
0.37	0.85	0.79	0.64
0.38	0.61	1.20	1.03
0.75	0.74	0.93	0.87
0.59	0.71	0.44	1.03
0.46	0.60	0.99	1.35
0.95	0.96	0.63	0.77
0.48	0.87	0.81	0.87
0.88	0.69	0.81	0.61

0.92	0.87	0.94	1.03
0.84	0.92	1.27	0.71
0.61	0.54	0.73	1.15
0.59	0.81	1.25	0.91
0.65	0.79	0.83	0.52
0.66	0.81	0.85	1.03
0.54	0.79	1.04	1.09
0.93	0.65	0.83	0.64
0.48	0.43	0.83	0.83
0.83	0.57	0.71	1.67
0.73	1.14	0.81	2.39
0.58	0.81	1.27	1.72
0.54	0.79	0.85	1.29
0.77	0.81	0.92	1.03
0.58	0.97	0.41	0.64
0.61	0.69	0.79	1.63
0.54	0.80	0.61	2.43
0.61	0.69	0.83	2.36
0.72	0.54	0.73	1.28
0.73	0.91	0.79	1.09
0.80	0.69	0.61	1.55
0.78	0.87	1.20	2.38
0.85	0.88	1.05	1.32
0.37	0.92	1.14	1.83
0.57	0.66	0.73	1.28
0.51	0.85	0.41	1.46
0.65	0.85	0.88	1.52
0.71	0.58	0.61	1.01
0.37	0.69	0.73	1.03
0.71	0.75	0.55	1.94
0.73	0.66	0.80	1.23
0.84	0.53	0.85	1.01
0.77	0.60	0.80	1.03
0.73	0.60	0.90	0.83
0.91	0.60	0.73	1.03
0.82	0.53	0.81	1.21
0.45	0.60	1.20	0.71
0.59	0.73	0.63	1.01
0.75	0.73	0.80	1.12
0.81	0.98	0.61	1.01
0.73	0.93	0.55	0.91
0.71	0.87	0.81	1.67
0.83	0.83	0.81	1.09
0.85	0.86	0.85	1.36
0.87	0.93	0.80	1.47
0.87	0.73	0.80	1.73
0.90	0.87	0.81	2.31
0.95	0.91	0.55	0.71
0.84	0.89	0.64	1.82
0.73	0.79	0.83	1.63
0.72	0.93	0.65	2.06
0.80	0.93	0.65	1.03

0.91	0.53	0.54	1.22
0.80	0.75	0.61	1.43
0.74	0.93	0.83	0.71
0.70	0.73	0.52	1.41
0.67	0.62	0.85	1.63
0.86	0.60	0.80	1.47
0.83	0.65	0.80	1.01
0.77	0.89	0.73	1.03
0.75	0.93	0.61	0.61
0.75	0.93	0.83	1.43
0.70	0.89	0.54	0.64
0.75	0.94	0.94	0.83
0.80	0.93	0.71	1.18
0.69	0.73	1.61	1.43
0.81	0.95	0.71	0.77
0.69	0.77	0.90	1.01
0.53	0.78	0.94	1.58
0.93	0.85	0.83	1.35
0.73	0.83	1.27	1.98
0.92	0.73	0.41	1.32
0.76	0.83	0.99	0.96
0.93	0.66	0.85	1.03
0.68	0.79	0.61	0.90
0.80	0.93	0.85	1.22
0.59	0.79	0.61	0.83
0.81	0.89	0.83	1.01
0.64	0.75	0.69	1.49
0.77	0.73	0.69	1.01
0.81	0.93	0.61	1.23
0.79	0.86	0.90	1.32
0.79	0.91	1.06	1.47
0.73	0.92	1.25	1.09
0.80	0.73	0.71	1.09
0.72	0.73	0.80	0.91
0.75	0.66	1.25	0.81
0.53	0.66	0.85	0.52
0.51	0.78	1.25	0.64
0.69	0.66	0.90	1.23
0.61	0.73	0.79	1.72
0.83	0.89	1.04	0.83
0.70	0.92	0.69	0.77
0.84	0.93	1.21	1.15
0.65	0.79	0.79	0.71
0.70	1.07	1.27	0.91
0.66	0.85	0.83	1.15
0.73	0.98	1.25	0.73
0.28	0.66	1.27	0.64
0.70	0.80	0.85	1.22
0.70	0.85	0.90	1.67
0.74	1.03	1.06	1.15
0.73	0.69	1.18	0.73
0.59	0.65	1.32	1.15

Appendix B: Bubble data

0.77	1.15	0.85	0.96
0.60	0.93	1.31	1.35
0.62	0.77	1.68	1.09
0.75	1.18	0.71	1.01
0.74	0.83	0.73	1.01
0.86	0.83	0.46	0.90
0.82	1.15	1.10	1.01
0.81	0.93	0.83	0.90
0.93	1.12	0.79	1.15
0.80	0.78	0.85	0.91
0.71	0.76	0.79	0.71
0.69	0.89	0.90	0.86
0.88	0.88	1.04	0.96
0.66	0.73	0.85	2.03
0.62	0.93	1.04	1.35
0.67	0.89	1.33	1.01
0.62	0.83	1.04	0.73
0.73	0.80	0.73	1.44
0.60	0.92	1.06	1.15
0.51	0.66	1.21	1.44
0.83	0.80	0.85	0.96
0.68	0.91	0.85	1.04
0.68	0.98	0.80	1.60
0.86	0.83	0.79	1.14
0.71	0.92	1.18	0.81
0.77	0.85	1.06	1.23
0.73	0.92	0.99	0.83
0.69	0.73	1.25	1.03
0.66	0.73	1.31	1.01
0.62	0.93	0.99	1.43
0.76	0.93	1.07	1.54
0.83	0.79	0.92	1.04
0.75	0.85	1.20	1.35
0.74	0.83	1.20	0.71
0.78	0.92	0.61	1.35
0.75	0.79	1.03	0.77
0.59	0.69	0.61	1.29
0.79	0.79	1.03	1.29
0.60	0.80	1.27	1.15
0.61	0.78	1.40	0.77
0.93	0.79	1.22	1.62
0.69	0.81	1.04	1.92
0.67	0.80	0.80	1.01
0.80	0.83	0.94	0.96
0.80	0.92	0.94	0.87
0.87	0.83	0.94	1.54
0.83	0.79	0.71	1.35
0.71	1.18	0.71	0.91
0.79	0.79	0.63	1.01
0.71	1.07	0.63	0.96
0.73	1.18	0.83	0.90
0.71	1.06	1.18	2.89

Appendix B: Bubble data

0.78	0.75	0.90	0.73
0.54	0.62	1.03	0.59
0.54	0.85	1.22	1.92
0.58	0.78	1.31	1.15
0.58	0.78	0.94	1.41
0.46	1.24	1.06	0.77
0.52	0.89	1.20	1.03
0.52	0.81	0.73	0.91
0.54	0.73	1.31	1.81
0.52	1.03	1.36	1.47
0.46	1.06	1.18	1.41
0.58	1.15	1.20	1.32
0.77	0.76	1.07	1.29
0.69	0.69	1.06	1.60
0.62	0.83	1.12	0.86
0.77	0.73	1.26	1.46
0.50	0.62	0.63	1.58
0.74	0.73	0.73	1.32
0.50	0.65	1.61	1.22
0.61	0.79	0.99	1.15
0.54	1.26	0.69	1.04
0.67	0.85	0.79	1.60
0.54	0.75	1.72	0.91
0.61	0.73	1.27	1.03
0.54	0.73	0.79	0.91
0.54	0.75	1.18	1.44
0.65	0.88	0.73	0.91
0.77	0.75	0.85	0.77
0.62	0.93	1.18	1.62
0.48	0.80	1.14	1.12
0.63	0.73	0.61	1.12
0.61	0.89	0.99	0.96
0.69	0.92	0.80	0.96
0.58	0.98	0.69	1.09
0.73	0.75	0.92	0.81
0.62	0.89	1.38	0.71
0.71	0.80	0.90	1.79
0.63	0.73	0.88	0.81
0.50	0.75	0.92	1.03
0.54	0.80	1.10	0.91
0.52	0.85	1.18	1.57
0.54	0.91	1.55	2.02
0.46	0.75	0.63	0.91
0.62	0.73	0.63	0.87
0.50	0.85	0.93	1.41
0.77	0.93	1.29	1.28
0.67	0.91	0.73	1.03
0.58	0.62	1.55	1.04
0.62	0.88	0.99	1.60
0.50	0.83	0.90	0.64
0.43	0.66	1.18	1.62
0.54	0.79	1.18	0.61

Appendix B: Bubble data

0.54	0.88	1.18	0.61
0.61	0.65	1.12	1.18
0.61	0.89	0.85	1.55
0.50	0.65	0.85	0.59
0.54	0.66	0.92	1.21
0.73	0.66	0.99	1.43
0.79	0.79	0.90	0.96
0.67	0.62	1.39	1.04
0.62	1.31	1.37	1.21
0.91	0.88	0.69	1.15
0.73	0.73	0.69	0.71
0.50	0.79	1.18	0.71
0.36	0.62	1.25	1.29
0.38	0.66	1.25	1.60
0.67	0.62	1.25	0.59
0.50	0.65	1.51	0.87
0.77	0.66	1.06	1.23
0.69	0.81	1.04	1.01
0.69	0.89	0.69	1.12
0.50	0.89	0.61	1.43
0.62	0.62	0.73	1.32
0.54	0.65	0.92	1.43
0.43	0.65	1.03	1.01
0.69	0.65	1.18	1.12
0.61	0.79	1.27	0.96
0.54	0.62	0.99	1.54
0.63	0.60	0.80	1.01
0.43	0.46	0.70	0.71
0.69	0.73	0.83	1.09
0.43	0.73	1.26	1.15
0.65	0.79	0.99	1.09
0.81	0.73	0.73	1.22
0.54	0.73	0.63	1.09
0.48	0.91	0.90	0.83
0.35	0.79	0.73	1.09
0.74	0.99	0.61	1.32
0.50	0.76	1.72	1.36
0.58	0.66	0.85	1.35
0.51	0.78	1.03	1.43
0.85	0.85	0.63	2.33
0.80	0.73	0.90	0.91
0.69	0.79	0.70	1.01
0.85	0.66	1.04	1.72
0.99	0.75	1.18	1.09
0.80	0.92	1.49	0.91
0.69	0.77	0.90	1.67
0.89	1.37	1.06	0.61
0.79	0.62	1.07	1.35
0.94	0.73	1.25	1.92
0.94	0.66	1.25	1.35
0.94	0.73	0.61	1.60
0.94	0.62	0.90	1.12

0.73	0.73	1.38	1.03
0.97	0.73	1.39	1.86
0.92	0.79	1.18	1.43
0.80	0.76	0.46	1.73
0.94	0.83	0.88	1.98
0.99	0.75	0.71	1.03
0.85	0.92	0.90	0.91
0.85	0.78	0.80	1.92
0.85	0.92	0.71	0.90
0.79	0.73	0.93	1.04
0.83	0.85	0.90	1.14
0.73	0.78	1.06	1.36
0.66	0.89	1.04	0.77
0.94	0.89	0.73	0.96
0.97	0.78	1.06	1.09
0.94	0.73	0.73	1.04
0.67	0.93	0.41	1.36
0.44	0.62	1.31	1.18
0.94	0.89	0.83	0.71
0.75	0.62	0.83	1.15
0.73	0.80	0.83	2.00
0.73	0.89	1.12	0.59
0.80	0.80	0.83	1.04
0.73	0.83	0.73	1.01
0.80	0.83	1.12	0.96
1.03	0.73	0.88	0.91
0.99	0.53	0.99	0.83
0.94	0.91	0.99	1.43
0.79	0.41	1.21	1.03
0.85	0.89	0.90	0.64
0.66	0.62	1.07	1.01
0.76	0.78	0.54	0.71
0.73	0.89	1.38	1.74
0.89	0.53	1.12	1.09
0.77	0.92	0.79	1.15
0.73	0.89	0.93	1.32
0.89	1.24	0.99	1.47
0.96	0.75	1.06	2.58
0.96	0.73	0.73	1.21
0.73	0.73	0.59	1.01
0.75	0.89	0.92	1.32
0.88	0.80	1.06	1.43
0.99	0.93	1.12	0.91
0.46	0.99	0.90	1.43
0.53	0.85	0.94	1.03
0.66	0.88	0.85	0.91
0.46	0.89	1.06	1.79
0.73	0.76	0.85	0.71
0.75	0.73	0.79	1.47
0.85	0.75	1.12	1.94
0.53	0.73	1.06	1.72
0.66	0.75	0.93	1.21

Appendix B: Bubble data

0.94	0.83	0.83	1.23
0.83	0.76	1.31	1.23
0.69	0.85	0.94	1.23
0.66	0.89	0.94	0.96
0.94	0.80	0.94	1.41
0.69		0.94	1.62
0.94		0.94	1.55
0.94		0.90	1.62
0.94		0.90	1.09
0.77		1.26	1.43
0.94		1.72	0.71
0.80		0.79	1.74
0.83		0.79	1.94
0.94		0.79	1.12
0.88		0.93	0.81
0.44		0.85	0.59
0.92		1.32	1.32
0.92		1.27	1.12
0.46		0.90	0.73
0.92		0.85	0.81
0.92		0.63	1.63
0.79		0.73	1.35
0.75		1.16	1.15
0.75		1.04	1.15
0.79		0.85	1.52
0.89		1.27	1.12
0.92		0.73	2.26
0.85		1.32	0.71
0.92		0.85	1.15
0.61		0.94	1.52
0.89		0.79	1.12
0.89		0.94	1.23
0.66		0.93	1.12
0.46		1.12	1.12
0.89		0.75	1.21
0.75		1.17	1.22
0.73		1.18	1.21
0.73		0.75	0.64
0.73		0.90	1.28
0.53		0.73	0.81
0.82		0.99	1.03
0.53		1.06	1.62
0.33		1.27	
0.46		1.33	
0.89		1.06	
0.82		1.04	
0.69		1.06	
0.78		1.27	
0.94		1.12	
0.59		1.04	
0.53		0.99	
0.66		1.10	

Appendix B: Bubble data

0.69	0.55
0.79	0.73
0.69	0.75
1.03	0.66
0.75	0.83
0.79	0.75
0.79	0.94
0.63	0.66
0.75	0.75
0.73	0.73
0.80	0.79
0.73	0.54
0.73	1.49
0.53	1.49
0.53	0.70
0.53	1.49
0.53	0.99
0.66	0.85
0.83	0.75
0.66	0.75
0.66	1.18
0.66	1.04
0.66	1.12
0.73	1.12
0.99	0.79
0.66	0.94
0.73	0.93
0.94	0.54
1.01	1.12
0.73	1.06
0.73	0.93
0.74	0.61
0.89	1.12
0.89	0.66
0.71	0.63
0.53	0.90
0.73	1.32
0.94	0.79
0.83	1.04
0.66	0.85
0.94	1.27
0.83	
0.94	
0.83	
0.83	
0.73	
0.85	
0.94	
0.94	
0.83	
0.99	
0.53	

Appendix B: Bubble data

0.73
0.73
0.66
0.91
0.91
0.79
0.73
0.73
0.99
0.61
0.83
0.79
0.73
0.59

The surface tension and interfacial tension of heptane-toluene mixtures, and with water

Heptane	*Surface tension*	*Interfacial tension with water*
mole	**mN/m**	**mN/m**
0.000	28.22	36.01
0.074	26.8	36.61
0.153	25.71	37.12
0.243	24.39	38.01
0.325	23.64	38.55
0.419	22.33	39.16
0.517	21.96	40.55
0.628	21.23	42.28
0.746	20.86	44.95
0.867	20.72	47.1
1.000	20.04	50.9

The water contact angle of fine solids before washed (degree)

Heptane in diluent (mole)	0	0.15	0.32	0.52	0.74	1
Wet	50	45	43	38	30	25
Dried			158	155	152	150

The water contact angle of fine solids after heptane washed (degree)

Heptane in diluent (mole)	0	0.15	0.32	0.52	0.74	1
Wet	51	47	43	40	35	25
Dried	151	145	141	137	135	130

The water contact angle of fine solids after toluene washed (degree)

Heptane in diluent (mole)	0	0.15	0.32	0.52	0.74	1
Wet	<10	<10	<10	<10	<10	<10
Dried	83	70	52	47	32	20

The solid contents among various phases in partition with heptane-toluene/water system (weight%), before washed, wet

Heptane in diluent (mole)	0	0.15	0.32	0.52	0.74	1
Organic	19	33	57	53	48	95
Interphase	81	67	43	47	52	5
aqueous	<5	<5	<5	<5	<5	<5

The solid contents among various phases in partition with heptane-toluene/water system (weight%), before washed, dried

Heptane in diluent (mole)	0	0.15	0.32	0.52	0.74	1
Organic	30	31	33	32	34	51
Interphase	70	64	59	67	65	48
aqueous	<5	5	8	<5	<5	<5

The solid contents among various phases in partition with heptane-toluene/water system (weight%), after heptane washed, wet

Heptane in diluent (mole)	0	0.15	0.32	0.52	0.74	1
Organic	13	14	22	67	63	73
Interphase	79	59	46	32	35	25
aqueous	8	10	10	<5	<5	<5

. The solid contents among various phases in partition with heptane-toluene/water system (weight%), after toluene washed, wet

Heptane in diluent (mole)	0	0.15	0.32	0.52	0.74	1
Organic	<5	<5	<5	<5	<5	<5
Interphase	42	38	35	24	24	13
aqueous	58	62	65	76	76	87

Water content correction procedure for the partition

W_{wet}: weight of wet sample used to correct

W_{dried}: weight of dried sample used to correct

W_{wetp}: weight of wet sample used to partition

W_{driedp}: weight of dried sample used to partition

W_{phase}: weight of dried sample partition in specific phase

$$\frac{W_{dried}}{W_{wet}} = \frac{W_{driedp}}{W_{wetp}}$$

then

$$W_{driedp} = \frac{W_{dried} \times W_{wetp}}{W_{wet}}$$

the percentage of solids in the specific phase is

$$Solids\ percentage = \frac{W_{phase}}{W_{driedp}} \times 100$$